DPPT

Beryllium-10 in the Taylor Dome Ice Core:
Applications to Antarctic Glaciology and Paleoclimatology

by

Eric J. Steig

A dissertation submitted in partial fulfillment
of the requirements for the degree of

Doctor of Philosophy

University of Washington

1996

Approved by 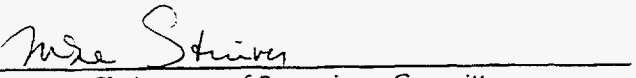
Chairperson of Supervisory Committee

Program Authorized
to Offer Degree Geological Sciences

Date March 6, 1996

DISCLAIMER

UMI
300 North Zeeb Road
Ann Arbor, MI 48103

In presenting this dissertation in partial fulfillment of the requirements for the Doctoral degree at the University of Washington, I agree that the Library shall make its copies freely available for inspection. I further agree that extensive copying of this dissertation is allowable only for scholarly purposes, consistent with "fair use" as prescribed in the U.S. Copyright Law. Requests for copying or reproduction of this dissertation may be referred to University Microfilms, 1490 Eisenhower Place, P.O. Box 975, Ann Arbor, MI 48106, to whom the author has granted "the right to reproduce and sell (a) copies of the manuscript in microform and/or printed copies of the manuscript made from microform."

Signature Eric J. Stein

Date 3/6/96

University of Washington

Abstract

Beryllium-10 in the Taylor Dome Ice Core: Applications to Antarctic Glaciology and Paleoclimatology

by Eric J. Steig

Chairperson of the Supervisory Committee: Professor Minze Stuiver
Department of Geological Sciences

An ice core was drilled at Taylor Dome, East Antarctica, reaching to bedrock at 554 meters. Oxygen-isotope measurements reveal climatic fluctuations through the last interglacial period. To facilitate comparison of the Taylor Dome paleoclimate record with geologic data and results from other deep ice cores, several glaciological issues need to be addressed. In particular, accumulation data are necessary as input for numerical ice-flow-models, for determining the flux of chemical constituents from measured concentrations, and for calculation of the offset in age between ice and trapped air in the core.

The analysis of cosmogenic beryllium-10 provides a geochemical method for constraining the accumulation-rate history at Taylor Dome. High-resolution measurements were made in shallow firn cores and snow pits to determine the relationship among beryllium-10 concentrations, wet and dry deposition mechanisms, and snow-accumulation rates. Comparison between theoretical and measured variations in deposition over the last 75 years constrains the relationship between beryllium-10 deposition and global average production rates. The results indicate that

variations in geomagnetically-modulated production-rate do not strongly influence beryllium-10 deposition at Taylor Dome. Although solar modulation of production rate is important for time scales of years to centuries, snow-accumulation rate is the dominant control on ice-core beryllium-10 concentrations for longer periods.

A continuous profile of beryllium-10 obtained for the 554-meter core is used to establish an accumulation-rate history at Taylor Dome, taking into account remaining uncertainties in production rates, deposition mechanisms, and atmospheric mixing processes. A preliminary interpretation of the accumulation-rate record indicates that climate conditions at Taylor Dome are strongly influenced by conditions in the Ross Sea, particularly the configuration of the Ross Ice Shelf. These results show that the Taylor Dome core can be used to provide new constraints on regional climate over the last 130,000 years, complementing the terrestrial and marine geologic record from the Dry Valleys, Transantarctic Mountains and western Ross Sea.

TABLE OF CONTENTS

Page

List of Figures ii

List of Tables iv

Chapter 1 Introduction 1

Chapter 2 Geochemical and Geophysical Studies at Taylor Dome 6

Chapter 3 Extraction and analysis of ^{10}Be in polar ice 27

Chapter 4 Can we use ^{10}Be to solve the inverse problem in ice-core paleoclimatology? 50

Chapter 5 Estimation of the stratospheric fraction of ^{10}Be in the polar troposphere. 80

Chapter 6 On the relationship between ^{10}Be concentrations and ice accumulation rates 96

Chapter 7 On the use of ^{10}Be to determine annual-layer thicknesses in ice cores 115

Chapter 8 A preliminary paleoclimatic interpretation of the ^{10}Be record at Taylor Dome 139

References Cited 150

LIST OF FIGURES

Number		*Page*
2.1	Map of the Antarctic continent	7
2.2	Map of the Taylor Dome area	10
2.3	Stable isotope profiles in snow pits at Taylor Dome	14
2.4	Automatic weather station data at Taylor Dome	15
2.5	Profiles of $\delta^{18}O$, NO_3 and ^{10}Be in the Taylor Dome deep core	18
2.6	Profiles of ECM, $\delta^{18}O$ of O_2, and CH_4 in the Taylor Dome deep core	19
2.7	Depth-age scale for the Taylor Dome deep core	22
2.8	Stable isotope profiles at Taylor Dome and Vostok	23
3.1	Elution patterns for beryllium and boron	31
4.1	Star production rate as a function of latitude and altitude	60
4.2	Estimated temporal variations in isotope production rates	62
4.3	Schematic model of atmospheric mixing with respect to ^{10}Be	65
4.4	Calculated ^{10}Be concentration in the polar stratosphere	70
4.5	Calculated ^{10}Be concentration in the polar troposphere	73
5.1	$\delta^{18}O$ and β radiation profiles at Taylor Dome	82
5.2	^{10}Be concentrations at Taylor Dome, 1920 - 1994	83
5.3	^{10}Be at Taylor Dome and Dye 3, 9 – 13 year bandpass filtered	87
5.4	Comparison of predicted and measured ^{10}Be production	89

5.5 Sensitivity of the ^{10}Be flux to changes in the cosmic ray flux 92

6.1 δD and ^{10}Be at Vostok 98

6.2 $\delta^{18}O$ and ^{10}Be at Taylor Dome 99

6.3 ^{10}Be flux at Taylor Dome versus accumulation rate 104

6.4 Accumulation rates at Taylor Dome for different values of W 108

6.5 Maximum and minimum estimates of accumulation rates at Taylor Dome 112

7.1 High-resolution ^{10}Be data from firn and ice cores at Taylor Dome 121

7.2 Frequency spectrum of the surface (0 - 10 meter) ^{10}Be data 123

7.3 Wave number for the ^{10}Be data in Figure 7.1 122

7.4 Annual layer thickness as a function of depth in the Taylor Dome core 125

7.5 Frequency spectra for ^{10}Be and ECM at Taylor Dome 127

7.6 Schematic representation of Dansgaard-Johnsen flow model 130

7.7 Refined layer thickness estimates at Taylor Dome 133

7.8 Layer thicknesses at Taylor Dome, corrected for accumulation rate 136

8.1 Accumulation rates at Vostok compared with Dry Valleys glacial-geologic history 141

8.2 $\delta^{18}O$ and accumulation rate at Taylor Dome, 0 - 130 ka 143

8.3 ^{10}Be at Taylor Dome and Vostok, compared with the SPECMAP global ice-volume/sea-level curve 145

LIST OF TABLES

Number		*Page*
2.1	Modern accumulation rates at Taylor Dome	12
2.2	Matches between Taylor Dome and Vostok used in constructing the standard timescale	21
3.1	^{10}Be data from the Taylor Dome 1993 – 1994 deep core	35
3.2	High-resolution ^{10}Be data at Taylor Dome	42
3.3	Miscellaneous snow pit and core data at Taylor Dome	48
6.1	Comparison of accumulation rates and ^{10}Be concentrations at Taylor Dome	103

ACKNOWLEDGMENTS

I wish to express my gratitude to the members of the supervisory committee—Minze Stuiver, Pieter Grootes, Alan Gillespie, Steve Porter and Ed Waddington—for their support and constructive criticism, and for giving me the opportunity to work in the polar regions. Special thanks are due Alan for his thorough review of the manuscript.

Many thanks are due my friends and colleagues at the University of Washington, especially Juliet Crider, Paul Bierman, Christine Massey, Doug Clark, Yann Merrand and Bruce Weertman.

Travis Saling, Paula Reimer and Phil Wilkinson of the Quaternary Isotope Lab provided a generous atmosphere and important technical advice and support. I learned much from Pratigya Polissar (Hampshire College) who provided excellent support as an undergraduate supervisee in the fall of 1994.

On behalf of myself and Pieter Grootes, I want particularly to thank Ed Waddington and David Morse, who were responsible for geophysical aspects of the Taylor Dome project, for their hard work and enthusiasm in the field. Without their efforts, and that of countless military and civilian Antarctic support personnel and the staff of the Polar Ice Coring Office, this project would not have been possible.

Thanks to Robert Finkel at Lawrence Livermore National Laboratory and to Susan Harder, University of Washington, for getting me started on the sample preparation for ^{10}Be, and to John Southon, Mark Caffee, Tom Brown and Lennox Harris for enjoyable night-watches together at the CAMS accelerator.

Finally, I wish to thank my undergraduate advisors at Hampshire College, John Reid and Herbert Bernstein, for their continuing support and interest in my work.

This thesis was supported by a grant through the Office of Polar Programs at the National Science Foundation and by a Department of Energy Pre-Doctoral Fellowship in Global Change.

This thesis is dedicated to my parents: to my mother, Katharine, for holding back the tide of destruction and development which threatens the wilderness places where I gained the inspiration to become an earth scientist; and to my father, Michael, for his undying support and for instilling in me a passion for intellectual inquiry.

Chapter 1
INTRODUCTION

Cosmogenic isotopes—those elements produced in nature by cosmic radiation—have become one of the most important tools in the earth sciences in the last few decades. Applications range from the dating of geomorphic surfaces and the study of soil development and erosion, to the study of geomagnetic field variations and the relationship between solar activity and climate. Virtually all of these applications require some knowledge of the time-dependent production rate of cosmogenic isotopes, which varies with changes in solar activity and geomagnetic field strength.

Most of what we know about the variation of cosmogenic isotope production over time comes from the measurement of ^{14}C concentrations in the atmosphere, oceans and biosphere. Though often excluded from discussions of cosmogenic isotopes, radiocarbon (^{14}C) was actually the first such isotope to be detected (Libby, 1946; Anderson et al., 1947), and it continues to be the most widely used. Of particular importance is the tree-ring record of atmospheric ^{14}C variations (e.g. Pearson et al., 1986; Pearson and Stuiver, 1986; Stuiver and Pearson, 1986) which shows ± 10 % variation over the last 15 ka, generally interpreted to reflect changes in global production rates resulting from changes in the geomagnetic dipole moment (Olson, 1970; Damon, 1988; Stuiver et al., 1991).

As a proxy for isotope production, the radiocarbon record is complicated by two factors. First, because ^{14}C is globally mixed in the

atmosphere, the ^{14}C record contains no information about the latitude dependence of production-rate variations. The ^{14}C record cannot be used to distinguish changes in geomagnetic field strength, which have the greatest effect at the equator, from changes in solar activity, which have the greatest effect at the poles. Second, much of the atmospheric ^{14}C record does not reflect changes in production, but rather indicates exchange of ^{14}C from different carbon reservoirs in response to changes in climate.

It was these difficulties with the use of ^{14}C to determine production-rate variations which in part motivated the measurement of ^{10}Be in marine sediment cores and in ice cores from polar regions. Unlike ^{14}C, which exists in the atmosphere primarily as $^{14}CO_2$, ^{10}Be becomes attached to aerosol species such as sulfate and is rapidly removed from the atmosphere. There is no rapid exchange of ^{10}Be among different reservoirs such as the ocean and biosphere. The record of cosmogenic isotope production in ^{10}Be deposited at the earth's surface is therefore less attenuated than that of ^{14}C in tree rings or similar media.

The earliest measurements of ^{10}Be in polar ice were made by McCorkell et al. (1967) in Greenland in the late 1960's, and the first long records were obtained by Raisbeck et al. (1981) from an ice core at the Soviet Antarctic station, Vostok. From this work, it quickly became apparent that incomplete knowledge of atmospheric circulation patterns and aerosol deposition mechanisms, as well as glaciological questions such as the accurate dating of ice-cores, precluded a simple relationship between ^{10}Be concentrations in ice cores and production rates in the atmosphere.

Somewhat ironically (given the original motivations for the research) it is now recognized that "the observed variations in ^{10}Be concentrations in ice cores are primarily due to climatic changes and not to changes in production rate."[1] Indeed, a defensible argument can be made that at present our knowledge of solar and geomagnetic variation (from, for example, the ^{14}C record) is *more* robust than our understanding of ice-core chemistry. This is the point of view taken in this dissertation. My purpose is to explore the relationship between the concentration of cosmogenic isotopes in ice cores and their production in the atmosphere and, in doing so, to contribute not only to the discipline of cosmogenic isotope research, but also to glaciology, the atmospheric sciences, and paleoclimatology.

In the chapters which follow, I present data on ^{10}Be variations in a series of firn and ice cores drilled at Taylor Dome, East Antarctica, as part of a glaciology/paleoclimatology project which began in 1990. The deep core to bedrock (at a depth of 554 meters), completed in January, 1994 (Grootes et al., 1994), reaches through the penultimate glacial period which began about 125,000 year ago.[2] In Chapter 2, I discuss the scientific background which motivated an ice-core drilling effort at Taylor Dome, and describe preliminary geophysical and geochemical results, including relevant data from other researchers who have been involved with the Taylor Dome project. Chapter 3 details the sample selection, preparation and analysis methods used and developed in the course of my dissertation work and summarizes the cosmogenic isotope data obtained. In the remaining chapters I seek to establish a framework for the use of ^{10}Be as tool in

glaciology and paleoclimate research. In Chapter 4, I develop and use a simple conceptual model to evaluate the effect of variations in production-rate and of atmospheric circulation on the net input of ^{10}Be to the Antarctic polar atmosphere. Chapter 5 addresses empirically one of the problems brought up in Chapter 4—determining the transport of ^{10}Be from the low-latitude stratosphere to the polar troposphere—by taking advantage of the latitude-dependence of solar modulation on ^{10}Be production rates. In Chapter 6, I discuss the relationship between ^{10}Be concentrations and snow accumulation rates and determine a best-estimate of accumulation rates at Taylor Dome over the last 130,000 years. Chapter 7 presents a novel approach to the determination of layer thickness in ice cores, using the ^{10}Be 11-year solar modulation cycle as a stratigraphic tool. Finally, Chapter 8 combines the results of the preceding chapters to develop a preliminary paleoclimatic interpretation of the Taylor Dome ice core.

Notes to Chapter 1

1. Lal (1987) p. 785.

2. Because the core has turned out to be three to four times older than we had first anticipated (Waddington et al., 1993), many more ^{10}Be measurements were made than originally expected and the ^{36}Cl work planned in our 1994 NSF proposal in still in progress. A preliminary discussion may be found in Steig et al. (1995); P. J. Polissar, an undergraduate at Hampshire College who did his senior thesis work (Polissar, 1995) with me deserves substantial credit for the ^{36}Cl work and many of the ^{10}Be analyses.

> The original impetus [of *The Last Great Ice Sheets*] was to present a straightforward ice-sheet reconstruction in three dimensions ... as input for a family of numerical modeling experiments of the ice-age atmosphere in global circulation models. However, it soon became evident that a unique reconstruction cannot now be made because the areal extent and paleoglaciology of these ice sheets is not well understood, despite more than a century of research....
>
> —Denton and Hughes (1981, p. vii)

Chapter 2

GEOCHEMICAL AND GEOPHYSICAL STUDIES AT TAYLOR DOME

2.1 Introduction

First identified by Drewry (1980; 1982), Taylor Dome[3] is actually a narrow ridge, about 80 km long by 20 km wide, just inland of the Transantarctic Mountains in East Antarctica (Figure 2.1). The ridge lies at an elevation of 2400 meters, and is separated from the main East Antarctic ice sheet by a depression about 100 meters lower; local accumulation at Taylor Dome supplies ice to Taylor Glacier to the northeast and the Skelton Neve to the southeast.

The idea for drilling an ice core at Taylor Dome arose out of the research of Denton, Stuiver and others, who had been interpreting the Quaternary glacial-stratigraphic history of McMurdo Sound and the Dry Valleys. Much of this work was published in the volume, *The Last Great Ice Sheets* (Denton and Hughes, 1981) and several papers in a special issue of *Quaternary Research* (Bockheim et al., 1989; Denton et al., 1989a, b). The radiocarbon-dated glacial geologic evidence showed that, during the last glacial maximum—prior to about 13,000 radiocarbon years before present—the Ross Ice Shelf expanded to fill much of the present-day Ross

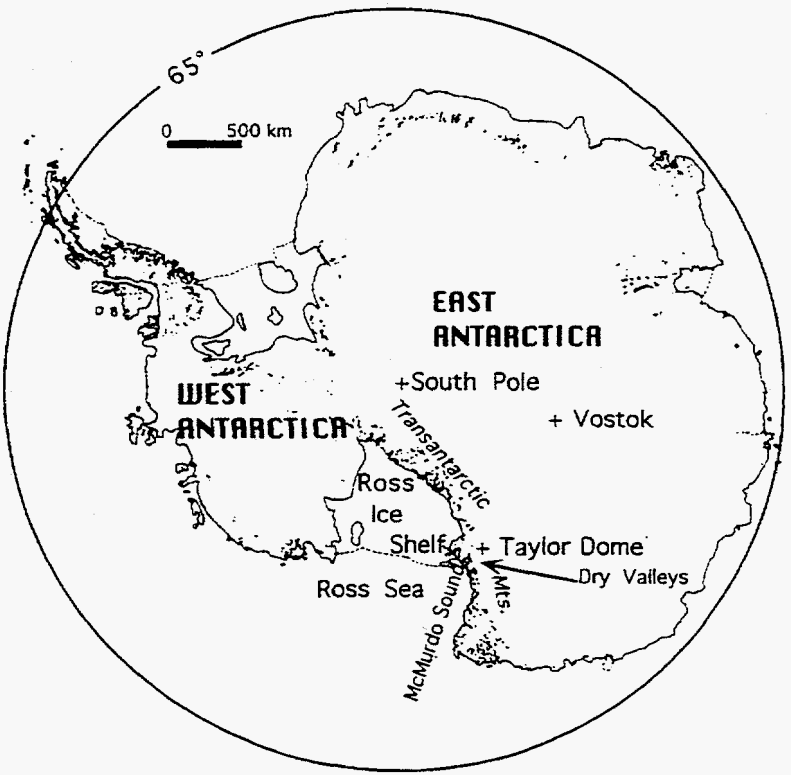

Figure 2.1 Map of the Antarctic continent, showing location of Taylor Dome, the Dry Valleys, and other geographic terms referred to in the text. Stippled marks show location of ice-free bedrock.

Sea, grounding in McMurdo Sound as the Ross Ice Sheet and invading the lower portions of the Dry Valleys. At the same time, the large outlet glaciers which drain the East Antarctic ice sheet through the Transantarctic Mountains into the Dry Valleys, as well as small alpine glaciers, were in retreat. The implication of this out-of-phase relationship is that, while lower sea level during the last glacial maximum (LGM, or marine isotope stage 2) permitted expansion of ice onto newly-exposed continental shelf, the cold, dry ice-age climate also meant reduced accumulation rates, possibly resulting in ice sheet thinning in the interior of the continent.[4]

In spite of the cold conditions, meltwater production in the Dry Valleys may have been greater during isotope stage 2 than it is today. From numerous radiocarbon dates on lake shorelines and deltas in Taylor Valley, Stuiver et al. (1981) showed that Glacial Lake Washburn (present-day Lake Bonney), dammed by the expanded Ross Ice Shelf ice, reached a high-stand at or near the LGM. Recent work shows that Lake Vanda (in Wright Valley) also expanded, with a high-stand near 10,000 radiocarbon years B.P. (B. Hall, personal communication), near the time of the northern-hemisphere Younger Dryas (Nilsson, 1961; Alley et al., 1993). This seeming inconsistency has been attributed to the insulating effect of fresh, high-albedo snowfall, which may limit ablation of ice-surfaces in the Dry Valleys. If greater aridity at the LGM led to dirty low-albedo surfaces, susceptibility to melting during the brief austral summer may have increased (Denton et al., 1989a). This explanation, however, is somewhat

ad hoc and is representative of the kind of problem for which independent climate records may be useful.

A major advance for Antarctic glaciology was the recovery and analysis of deep ice cores from the Antarctic interior. Results from these cores[5] confirmed many of the paleoclimate inferences made from glacial-geologic data, including the generally lower accumulation rates during isotope stage 2 (Jouzel et al., 1989). These cores, however, are from well inland on the polar plateau, and relate only indirectly to paleoclimate in coastal regions. The complex glacial geologic history in the Ross ice drainage system suggested the need for a local record of climate. Taylor Dome was a natural choice both for its proximity to McMurdo Sound and because of the potential for relating geophysical measurements at Taylor Dome with the glacial-geologic record of terminal and marginal positions of Taylor Glacier (Stuiver et al., 1981; Denton et al., 1989a; Marchant et al., 1994).

2.2 Selection of a drilling site at Taylor Dome.

Selection of the drilling site at Taylor Dome (Figure 2.2) was based on a variety of considerations. In our first two field seasons (1990-91, 1991-92), we[6] set up a strain net, oriented along the 80 × 20 km ridge that defines the ice divide. The strain net provided a convenient coordinate system, within which we conducted ice-penetrating radar profiles, snow-pit and shallow firn-core chemistry, and meteorological observations. The center line (C)

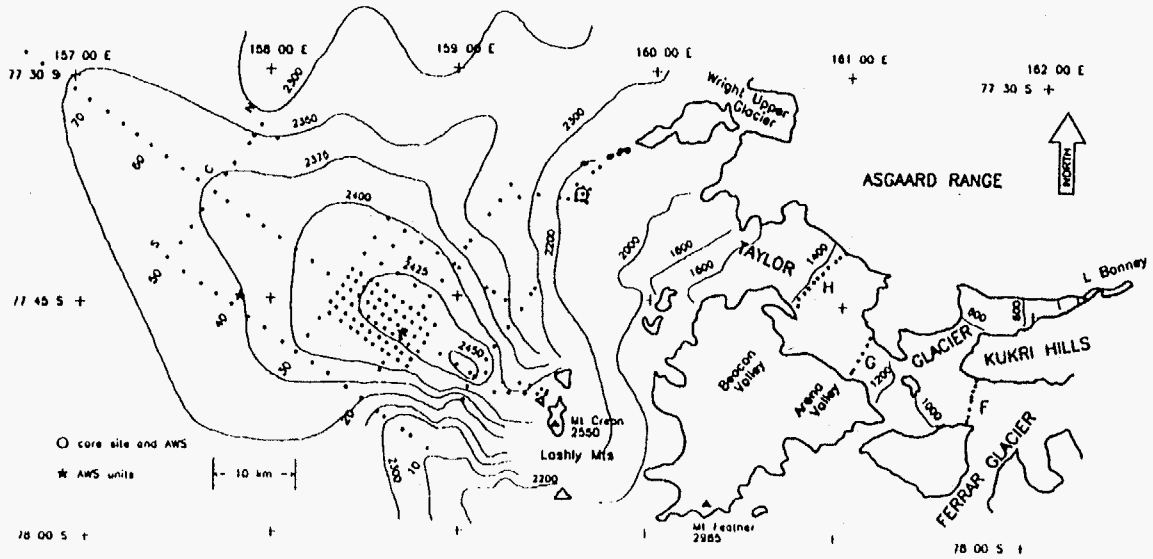

Figure 2.2 Map of the Taylor Dome area, showing coordinate system (N, C, S and 10, 20 ... 70) referred to in the text. Locations of drilling sites are: deep core near AWS at 20C (★), firn cores near AWS at 40S (★) and upper Taylor Glacier (O). Contour interval is 25 m. Dots show location of survey poles. Skelton Neve is beyond the lower left corner of the map.

runs from the ice saddle identified by Drewry (1982) to a small nunatak in the Lashly Mountains. Two parallel lines, *N* and *S* respectively, run along the Taylor and Skelton sides of the ice divide, at a spacing of 10 km. Four main cross-lines, also at 10 km spacing, run perpendicular to these lines. Locations on the net are denoted by their direction with respect to *N*, *C* and *S*, and their nominal distance from a fixed bedrock point in the Lashly Mountains. The Taylor Dome deep ice core was drilled near *20C* .

2.2.1 *Ice Penetrating Radar (IPR)*

Preliminary radar work at Taylor Dome showed that the ice-divide was centered on a bedrock high, with an average ice thickness of about 750 meters (Drewry, 1982). Drewry's radar observations suggested the presence of subglacial lakes within a few ice-thicknesses of the ice-divide, indicating potential limitations to recovery of a long paleoclimate record. Subsequent geophysical studies, including more detailed radar work and borehole thermometry, show that the ice at Taylor Dome is frozen to its bed. The 'lakes' identified by Drewry are probably just particulary strong radar reflectors, possibly volcanic ash layers (Morse, pers. comm. 1994).

The IPR survey was largely the responsibility of D. Morse, and is discussed at length in his dissertation (Morse, 1996). The results show that the sub-glacial relief is significant, with the distance-to-bedrock varying from more than 1000 meters to less than 500 meters. In part because of the complex deformation apparent in radar-reflecting layers in the thicker sections, we chose to drill at a relatively shallow location. The

disadvantages of the more-compressed record in a shallow location should be offset by the greater simplicity of flow, simplifying calculation of the age-depth relationship.

2.2.2 *Spatial variability in surface conditions at Taylor Dome*

During six field seasons at Taylor Dome, we dug snow-pits and collected a series of shallow firn cores for analysis of a variety of parameters, including stable isotopes ($\delta^{18}O$), ^{10}Be, and soluble ions.[7] On many of the cores, J. Dibb (University of New Hampshire) conducted β radiation analyses to identify the 1964 and 1954 bomb-radioactivity horizons.[8] Combined with detailed density measurements, the β profiles allow us to estimate the spatial variability of accumulation rate at Taylor Dome. Table 2.1 shows preliminary results from these calculations.[9]

Table 2.1 Preliminary determinations of modern accumulation rate for locations at Taylor Dome shown in Figure 2.2.

Location	Mean accumulation rate ($g\ cm^{-2}\ a^{-1}$)
20C	6.7
upper Taylor Glacier	2.3
10C	3.2
20N	1.2
20S	7.9
40S	8.2
30C	3.3
30S	2.8
10S	15.0
Drill Site	7.6

As a comparison between Table 2.1 and Figure 2.2 indicates, there is a strong gradient in surface conditions at Taylor Dome, with the greatest accumulation on the south side, decreasing towards the upper part of Taylor Glacier to the north and northeast. Stable isotope ratios (i.e. $\delta^{18}O$) and soluble-ion concentrations increase towards the southeast; lower isotope ratios in the areas having low accumulation rates may reflect isotope enrichment through vapor loss, as evidenced by lower firn densities (Grootes and Steig, 1992). Figure 2.3 shows example $\delta^{18}O$ results.

To complement the survey of surface conditions, we set up automatic weather stations (AWS) at upper Taylor Glacier, 40S, 20C, and west of 50S to establish a multi-year record of meteorological conditions at Taylor Dome. Except for a brief period during the coldest months, the AWS ran continuously. An example of the results from 1991 at 40S is shown in Figure 2.4; these and more recent AWS results are presented in more detail by Morse (1996). In general, wind patterns at Taylor Dome reflect two main components; the dominant vector is from the west to southwest, corresponding to katabatic winds off the East Antarctic interior. The secondary component is approximately south to southeast, and tends to be associated with clouds and higher temperatures, suggesting the influx of moist maritime air across the Ross Ice Shelf and along the axis of the Transantarctic Mountains. This general picture of air mass movement in the area of Taylor Dome is consistent with the large scale pattern of cyclonic and katabatic wind activity in Antarctica (Thompson and Mosley-

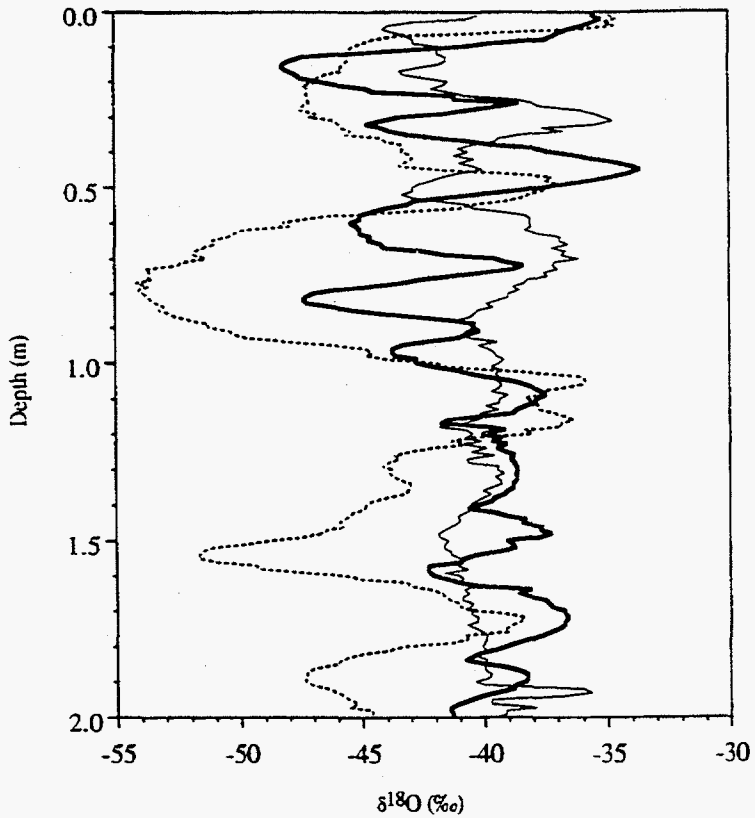

Figure 2.3 Stable isotope profiles at Taylor Dome for snow pits collected in 1991 at locations 20S (thin line), 10N (dashed) and 30C (bold). Sample interval is 1 cm.

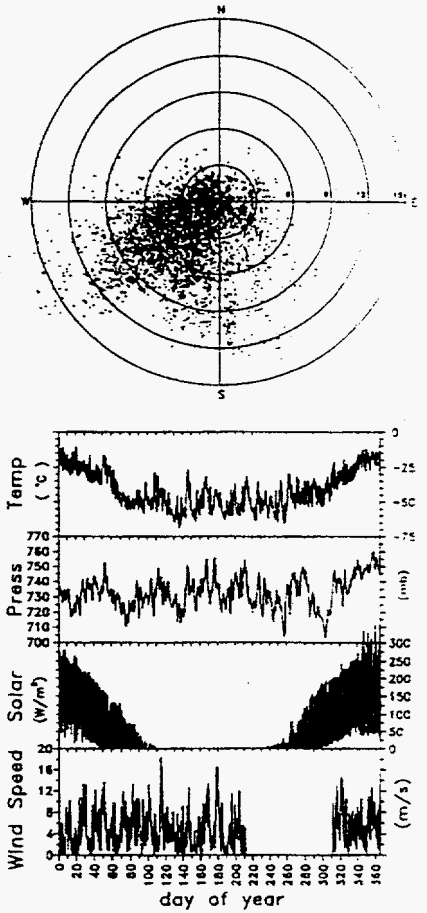

Figure 2.4 Automatic weather station (AWS) data for 1991. Top graph shows wind direction (e.g. S = wind from south) and speed (m s^{-1}). After Morse and Waddington (1992).

Thompson, 1982; Bromwich and Stearns, 1993). The dominance of marine air in the southeasterlies, compared with the drier continental air in the southwesterlies, is also consistent with the pattern of accumulation at Taylor Dome, with greater accumulation both expected and observed towards the southeast.

The survey of surface isotopes, meteorology, and chemistry showed that careful selection of a drilling site was essential if a useful paleoclimate record was to be obtained at Taylor Dome. In particular, low (and even negative) accumulation towards Taylor Glacier, and evidence of significant metamorphosis in the upper few meters of firn, suggested that we avoid drilling towards the northeast. Fortunately, the observation of relatively undisturbed stratigraphy in a snow-pit at 20C coincided with the independent observation of planar radar-reflection layers in the same general area. Ultimately, we chose to drill within 1.5 km of 20C, slightly towards the Skelton Neve side of the Taylor Dome ice divide (see Figure 2.2).

2.2.3 *Results from the deep drilling*

Stable isotope measurements were conducted at the Quaternary Isotope Laboratory (QIL), University of Washington, by T. Saling under the direction of M. Stuiver and P. Grootes. I did sample preparation for the ^{10}Be analyses at QIL, and analyses at Lawrence Livermore National Laboratories, as described in more detail in Chapter 3. Analytical precision (1σ) of the $\delta^{18}O$ analyses is ±0.2 ‰; for ^{10}Be measurements it is ±5 % ($1\ \sigma$).

Many other investigators have conducted analyses on the Taylor Dome core, which include measurements of cosmogenic ^{14}C (D. Lal), methane, total gas, and $\delta^{18}O$ of O_2 concentrations (M. Bender, E. Brook, C. Sucher), visual stratigraphy (J. Fitzpatrick), soluble ions (P. Mayewski, P-Y Whung, E. Saltzman) electrical conductivity (K. Taylor), diatoms (D. Kellogg) and dust concentrations (E. Mosley-Thompson). These analyses are still in progress, and it is beyond the scope of this dissertation to include all these data. However, it is useful to consider the general features of these other ice-core properties in the context of the ^{10}Be and $\delta^{18}O$ records.

Sampling of the Taylor Dome core was conducted primarily at the National Ice Core Laboratory (NICL) in Denver, Colorado. Gas analyses were conducted on discrete 10 cm sections of the core because of the large amount of ice (>500 g) required per analyis. Most other properties were measured continuously in 25 to 100 cm sections. Electrical conductivity (ECM) and conductance (DEP) measurements were made at 5 mm intervals. Figures 2.5 and 2.6 show several of these properties versus depth in the Taylor Dome core. As expected from previous ice-core analyses, all properties show parallel or inverse-parallel trends, with ^{10}Be, ECM and soluble-ion concentrations increasing as $\delta^{18}O$ and greenhouse gas concentrations decrease. This familiar pattern suggests that the Taylor Dome core can be interpreted in the same context as other long ice cores from around the world; that is, low $\delta^{18}O$ and gas concentrations generally reflect periods of cooling, lower accumulation rates, and increased

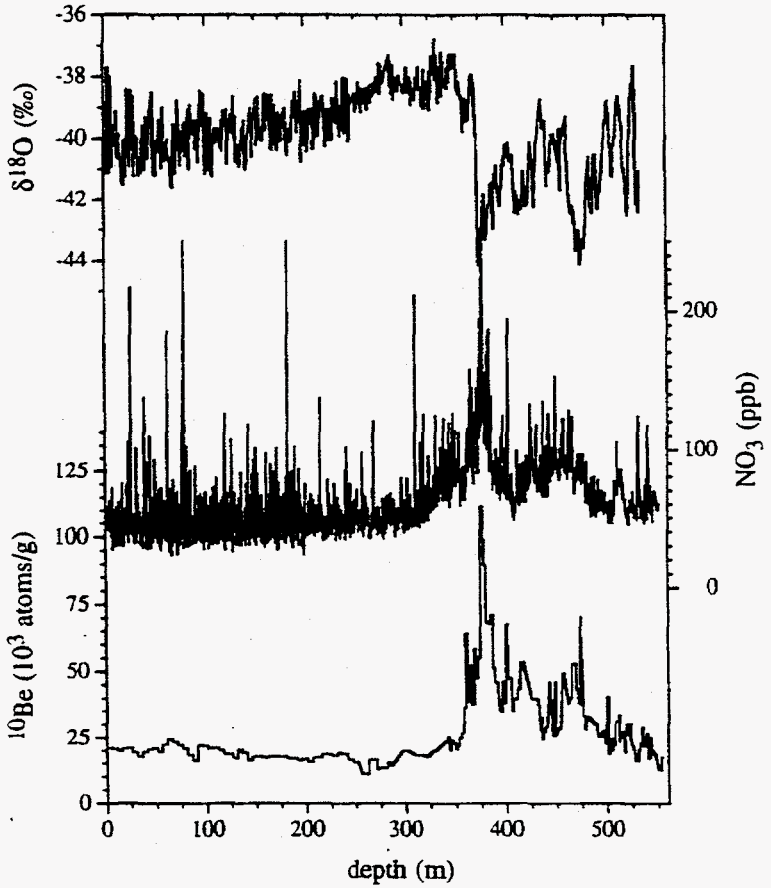

Figure 2.5 Profiles of $\delta^{18}O$, NO_3 (P. Mayewski, pers. comm.) and ^{10}Be in the Taylor Dome ice core.

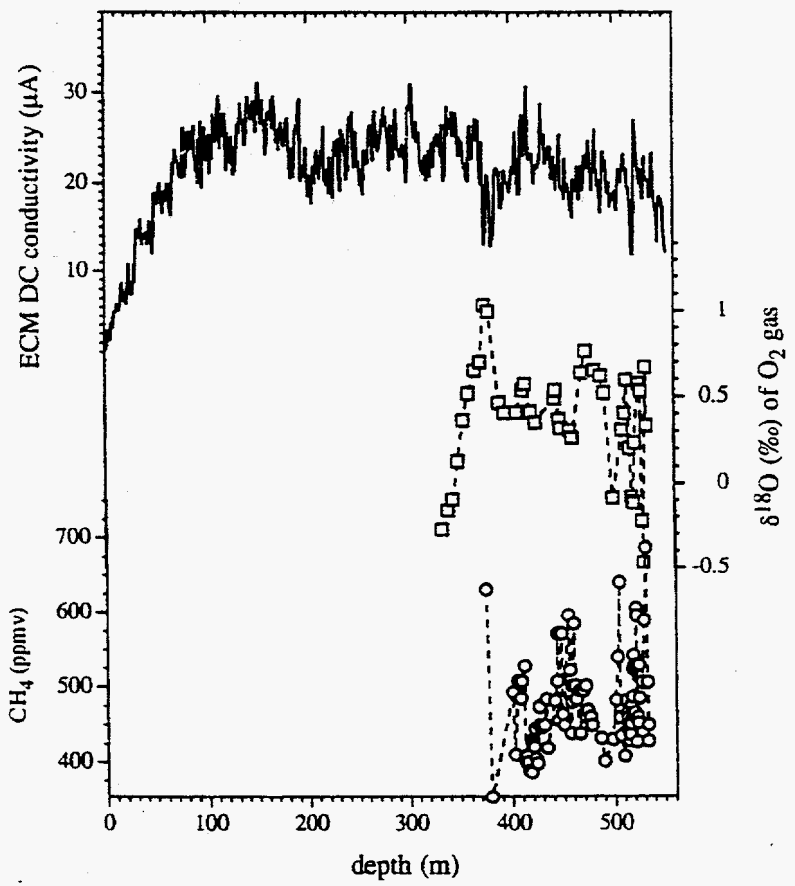

Figure 2.6 Profiles of ECM (K. Taylor, pers. comm.), $\delta^{18}O$ of O_2 and methane (E.J. Brook, pers. comm.) in the Taylor Dome core.

dustiness and windiness leading to higher concentrations of soluble ions, ^{10}Be and dust.

2.3 The Taylor Dome "Standard Timescale"

The $\delta^{18}O$ data at Taylor Dome shows several features which are directly comparable with features in the δD record at Vostok (Jouzel et al., 1987). To obtain a preliminary timescale (i.e. depth-age relationship) for the Taylor Dome core, I assume that climate events recorded in both records were synchronous. We matched the mid-points of major shifts in isotope values, including what is taken to be the transition from the penultimate glaciation (marine isotope stage 6) to the last interglaciation (isotope stage 5e), and the transition from the last glacial maximum (LGM, isotope stage 2) to the Holocene. Table 2.2 shows the matches and the age as determined from the most up-to-date Vostok timescale (Jouzel, et al., 1993). For the timescale since about 14 ka, there are few features which can be used to match the $\delta^{18}O$ at Taylor Dome with the δD at Vostok. For the Holocene portion of the core, I instead used a simple ice-flow model (Dansgaard-Johnsen type flow, with h = 220 meters; see Chapter 7), combined with ^{10}Be as a proxy for accumulation rates (W = 260; see Chapter 6). The resulting depth-age relationship is plotted in Figure 2.7 and is referred to as the Std_Time_9507 (July, 1995 standard timescale).

Table 2.2 Matches between Taylor Dome and Vostok used in constructing Std_Time_9507.

Taylor Dome Depth (meters)	Vostok Depth (meters)	Vostok Age (EGT Timescale, ka)
374.00	336.50	14800
395.50	585.50	34892
410.87	678.50	42100
448.00	830.50	54458
464.47	865.50	57100
482.00	1002.15	69362
488.94	1046.50	73100
492.89	1075.50	75493
497.73	1127.50	79700
507.21	1233.50	87065
518.30	1446.80	102900
521.28	1501.65	107089
525.24	1597.00	115300
531.40	1906.50	135068

Figure 2.8 shows $\delta^{18}O$ on the Std_Time_9507 timescale, compared with the Vostok record. While Std_Time_9507 is not definitive, preliminary results from correlation between methane and $\delta^{18}O$ of O_2 profiles at Taylor Dome and Vostok, and at GISP2 in central Greenland (E. J. Brook, personal communication) show that the timescale is reasonable, and is probably not in error by more than 10% (assuming that the GISP2 and Vostok records timescales are valid). Ongoing analysis of radar data, gas analyses, and the use of ^{10}Be as a proxy for accumulation rate and layer thickness (see

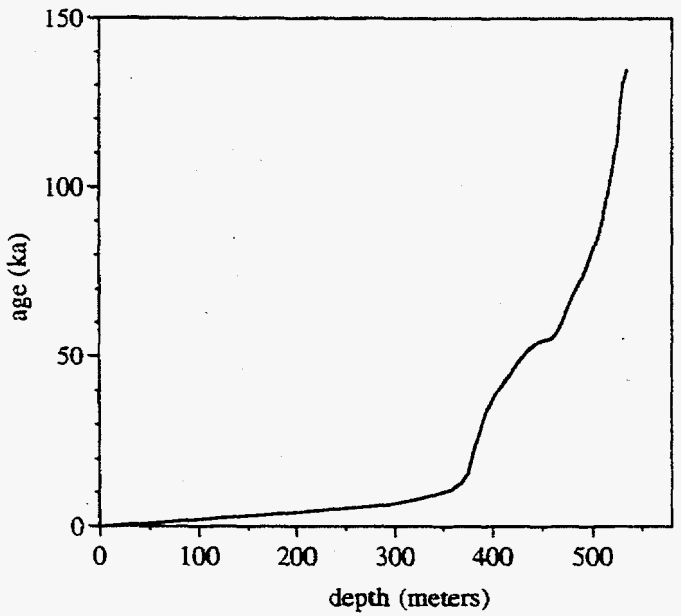

Figure 2.7 Depth-age scale for the Taylor Dome core, as determined from $\delta^{18}O$ matching with the Vostok δD record. Prior to 14 ka, the depth-age scale combines a Dansgaard-Johnsen-type flow pattern (h = 220 meters) with accumulation rates determined from ^{10}Be concentrations.

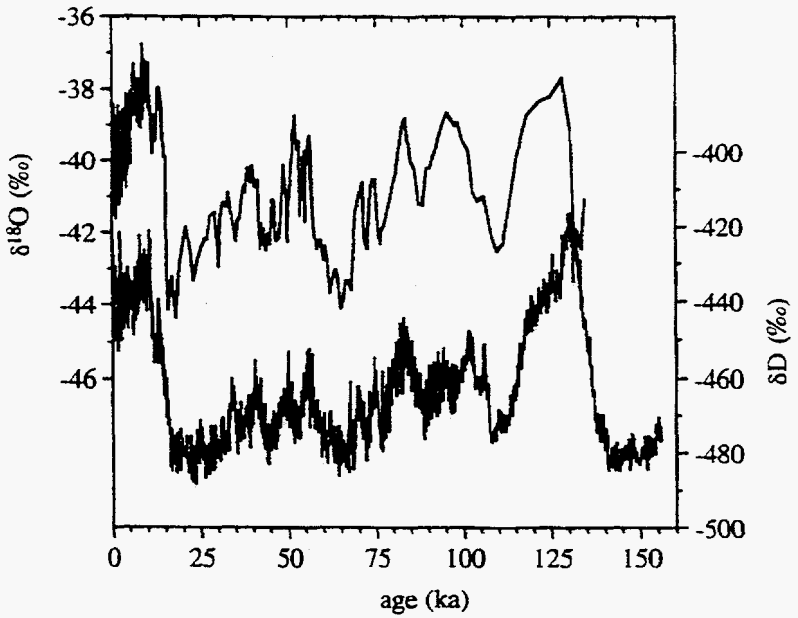

Figure 2.8 Stable isotope profiles from deep ice cores in East Antarctica. Top: $\delta^{18}O$ at Taylor Dome on the Std_Time_9507 timescale. Bottom: δD at Vostok (Jouzel et al., 1987) on the "extended glaciological timescale" (EGT) of Jouzel et al. (1993).

Chapters 6 and 7) will allow for further refinement of the timescale. At present, it provides a common framework within which to compare the Taylor Dome data with other paleoclimate records. Plausible errors in the Std_Time_9507 timescale are not large enough to affect the conclusions drawn in subsequent chapters of this dissertation.

Notes to Chapter 2

3. Taylor Dome has also been referred to as McMurdo Dome (e.g. Denton et al., 1989a). The name Taylor Dome has now been approved by the Advisory Committee on Antarctic names of the U.S. Board on Geographic Names.

4. The marine isotope stage numbers refer to climatic divisions defined by the deep-sea $\delta^{18}O$ record. In general, even numbers refer to warm (interstadial or interglacial) periods and odd numbers refer to cold (stadial, glacial) periods (Shackleton and Opdyke, 1973).

5. This work is summarized by Lorius et al. (1989). More up-to-date references include those of Jouzel et al. (1993; 1995) and Raisbeck et al. (1992).

6. By "we", I mean myself and P.M. Grootes from the Geology Department and Quaternary Isotope Laboratory and E.D. Waddington and D.L. Morse from the Geophyics Program, all at the University of Washington.

7. The notation $\delta^{18}O$ refers to the isotopic ratio $^{18}O/^{16}O$ normalized with respect to a standard. In this dissertation, all $\delta^{18}O$ measurements have been normalized to V-SMOW (Vienna Standard Mean Ocean Water):

$$\delta^{18}O = \frac{\left(^{18}O/^{16}O\right)_{sample} - \left(^{18}O/^{16}O\right)_{V-SMOW}}{\left(^{18}O/^{16}O\right)_{V-SMOW}} \times 1000‰$$

8. According to methods described in Dibb et al. (1990).

9. Thanks are due H.P. Marshall, Geophysics Program, University of Washington, for working out the details.

Chapter 3

EXTRACTION AND ANALYSIS OF ^{10}BE IN POLAR ICE

3.1 Introduction

The earliest measurements of ^{10}Be in ice were conducted by the traditional radioactive counting method which, because of the long half-life of ^{10}Be (1.5 Ma: Middleton et al., 1993), required several thousand kg of ice. Today, accelerator mass spectrometry (AMS) allows us to measure as few as 10^3 to 10^5 atoms of ^{10}Be, which typically amounts to a required sample size of only a few hundred grams of ice. Raisbeck et al. (1978) conducted the first such analyses at the cyclotron in Orsay, France. All measurements discussed in this dissertation were made at the Center for Accelerator Mass Spectrometry (CAMS) at Lawrence Livermore National Laboratory (LLNL), Livermore, California.

In this chapter, I describe the techniques used in the preparation of ^{10}Be for measurement by AMS. The methods used here build on the work of various other researchers, and are presented here primarily for completeness. I have made some refinements to optimize efficiency for the extraction of ^{10}Be from polar ice. ^{10}Be data obtained during the course of this dissertation work are tabulated at the end of this chapter.

3.2 Extraction of ^{10}Be from polar ice

3.2.1 *Standard Procedure*

To prepare ice sample for ^{10}Be analysis, I began with the standard cation-exchange chromatography procedure used by the CAMS group at LLNL. (R.C. Finkel, pers. comm., 1993). The chief purpose of the cation-exchange procedure is to isolate ^{10}Be from other elements that we may wish to analyze separately and that interfere with the efficiency of ionization at the accelerator source, or that are isobars of ^{10}Be. The removal of the isobar ^{10}B is of particular concern because it is present in polar ice in concentrations several orders of magnitude higher than ^{10}Be, and is also a common element in the laboratory environment.

Because virtually all the beryllium in polar ice is ^{10}Be and is in extremely low concentrations ($\sim 10^{4}$ atoms/g ice) we use isotope dilution to obtain a manageable sample. Isotope dilution consists of adding a known amount of "carrier" ^{9}Be to the sample, allowing for measurement of the ^{10}Be / ^{9}Be ratio by AMS. From the measured ratio, normalized against a known standard, we calculate the original ^{10}Be concentration by multiplying by the known amount of carrier ^{9}Be added. To a typical 500 g ice sample, 0.5 mg of nearly pure ^{9}Be ($^{10}Be/^{9}Be \sim 10^{-14}$) in a 1 ml solution of 0.01 M HNO_3 is added, along with 1 ml/liter of 1 M HNO_3 to ensure that all Be remains in solution. The ice sample is then melted, filtered to remove contaminating particulates, and evaporated to dryness in a teflon beaker. Once dry, the sample is re-dissolved and dried again to ensure that

there is no loss of Be to the sides of the container, and finally re-dissolved in a 0.1 M HCl solution and transferred by pipette to a cation-exchange resin.

The cation-exchange procedure uses a commercially available synthetic resin (I use BioRad® AG 50W-X8 100-200 mesh, hydrogen form resin) and takes advantage of the higher affinity of Be^{2+} ions relative to B^{+} for the sulfonyl group ($R\text{-}SO_3^-$) cation-exchange sites, and the even higher affinity of H^+. By adjusting pH and total H^+ abundance, we can selectively remove B and Be from the column. Experimentally, a 10 ml column of resin rinsed with ten 10 ml fractions of 1 M HCl yields a narrowly defined Be peak in the 4th to 6th fraction, while B is almost entirely eliminated in the first 3 fractions. Details of the procedure are given below, and a typical example elution curve is shown in Figure 3.1.

Standard ^{10}Be sample preparation and analysis procedure

1) Weigh dry, acid-washed beaker

2) Place ice sample in beaker of known mass; weigh

3) Add 0.500 mg of pure ^{9}Be in 1 ml of a 0.1 M HNO_3 carrier solution to the sample. Add 1 ml of 1 M HNO_3.

4) Filter sample through 0.45 µm pore-size filters by vacuum filtration.

5) Transfer filtered sample to teflon beaker and evaporate to dryness.

6) Redissolve precipitated $Be(OH)_2$ in 1 ml of 1 M HCl. Re-evaporate.

7) Redissolve precipitated $Be(OH)_2$ in 1 ml of 0.1 M HCl and transfer to top of cation column by pipette.

8) Rinse cation column with 20 ml of deionized ultrapure water.

9) Rinse cation column with ten 10 ml solutions of 1 M HCl, collecting the eluent from each fraction separately.

10) Regenerate column with ten column volumes of 6 M HCl, to completely replace all cation sites with H+. Rinse column with 20 ml ultrapure water.

11) Take 1 ml aliquots of each fraction and measure B and Be concentrations with atomic emission or absorption spectrometer.

12) Combine three or four fractions centered on Be peak in small teflon beaker; evaporate to dryness. Discard other fractions.

13) Dissolve precipitated $Be(OH)_2$ in 1 ml of 1 M HCl and transfer to centrifuge tube.

14) Precipitate $BE(OH)_2$ with 1 ml 15 % NH_4OH, centrifuge, discard supernate, redissolve in HCl, and repeat.

15) Rinse precipitated $Be(OH)_2$ in 1-2 ml of ultrapure water, centrifuge, and transfer to quartz crucible for drying.

16) Once dry, flame quartz crucible or place in oven at 900 °C to oxidize to BeO.

17) Mix BeO with equal amount Ag powder and load into target.

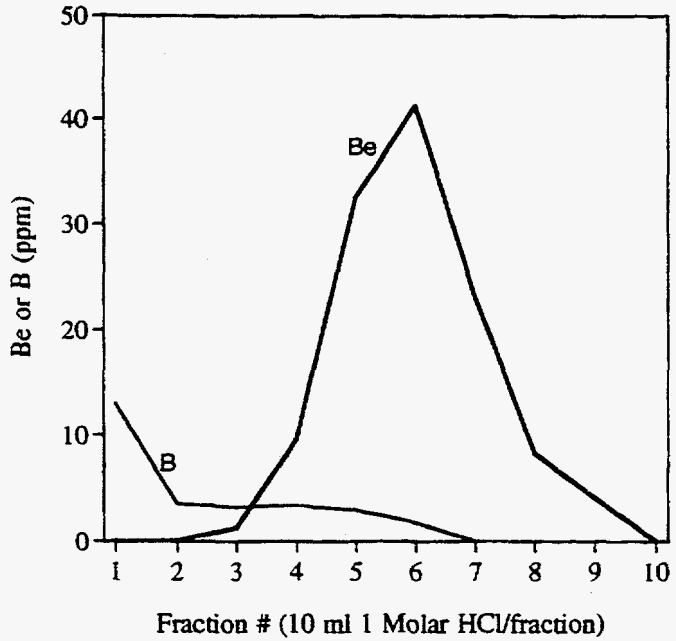

Figure 3.1 Typical elution patterns for beryllium (Be) and boron (B). Ten equal fractions of 10 ml 1 mol/liter HCl were used in the elutions. Recovery is >90% of the 0.5 mg of ^{9}Be carrier added to the sample. More than 50% of the B is removed from the solution by the second fraction.

3.2.2 *Refinements*

Two changes to the procedure described above were used in the processing of most samples:

1) Elimination of evaporation step (#5).

Because no other cation besides ^{10}Be was analyzed, it was found to be unnecessary to evaporate the samples to small volumes. Instead, the entire melted ice sample was poured through the column, followed by 3 column-volumes of 1 M HCl to eliminate B. Finally, 60 ml of 1.5 M HCl was used to elute Be. This procedure yields a broadened Be peak in the elution, but does not affect the total yield of Be.

2) Filter size

Samples were generally filtered through 5 μm filters (rather than 0.45 μm) to reduce the likelihood that ^{10}Be adsorbed to particulate matter in the ice core caused significant loss of ^{10}Be; more than 95% of the dust at Taylor Dome is below 2 μm in size. This potential problem was recogized recently by interlaboratory comparison of measurements made on the GRIP (central Greenland) ice core. It is probably not a concern for Antarctic ice , which has an order-of-magnitude less dust than Greenland ice. However, further testing of Taylor Dome samples is necessary to ensure this. Some samples were filtered at 0.45 μm to collect diatoms for D. Kellogg, and do not show any consistent offset in concentration from adjacent samples filtered at 5 μm.

3.3 Measurement of ^{10}Be at CAMS

The CAMS facility (Davis et al., 1990; Southon et al., 1990) is built around an FN tandem accelerator previously used for nuclear research at

the University of Washington. Ionization of the target element is achieved through bombardment with Cs ions from an ion sputter source operating at ~8 keV. For ^{10}Be, targets are made by mixing the prepared BeO powder with a roughly equal amount amount of Ag powder. The mixture is pounded into a ~1 mm hole drilled into a steel sample holder. Although as much ^{10}B as possible has been removed by the cation-exchange procedure, a detectable amount will remain in the sample, and must be separated from ^{10}Be in the acclerator.

In brief, analysis of ^{10}Be at the CAMS facility is as follows: Extraction of BeO^- ions from the ion source into the accelerator is achieved by electro-static acceleration between the source and a positively charged plate maintained at 8.3 MV. Both $^{10}BeO^-$ and $^{9}BeO^-$ are injected simultaneously into the accelerator proper, where they travel towards a high-voltage anode. The ion beams pass through a carbon foil where they are stripped of some of their electrons. Among other charge states, $^{10}Be^{4+}$ and $^{9}Be^{4+}$ ions are produced, as well as a non-negligible amount of $^{10}B^{4+}$. The $^{9}Be^{4+}$ ions are focussed through a series of magnets to reach a Faraday cup, where they gain electrons: the current generated at the Faraday cup is proportional to the number of $^{9}Be^{4+}$ ions. The $^{10}Be^{4+}$ / $^{10}B^{4+}$ ion beam, now travelling along a separate trajectory from the $^{9}Be^{4+}$ beam, reaches an argon-filled gas-ionization detector where the separate detection of $^{10}Be^{4+}$ and $^{10}B^{4+}$ is achieved by the differing energy loss properties of each element. A plot of total energy (E) versus energy loss (ΔE) between two detecting chambers produces a characteristic pattern that allows

discrimination of the $^{10}Be^{4+}$ and $^{10}Be^{4+}$ ion abundances. Because there is overlap between the Be and B fields on the $\Delta E/E$ plot, a ^{10}Be window must be determined empirically through comparison of clean (low B) and dirty (high B) blanks.

3.4 Summary of ^{10}Be analyses

Tables 3.1, 3.2 and 3.3 summarize all ^{10}Be analyses described in this dissertation. All analyses were normalized against a group of standards prepared at CAMS, and corrected for sample blanks prepared with ultrapure water by the procedures described above. The combined sample blank plus instrument blank is generally 50×10^{-15} ($^{10}Be/^{9}Be$); a typical Taylor Dome ice sample has a $^{10}Be/^{9}Be$ ratio of 500×10^{-15}.

Table 3.1 ^{10}Be Data from the Taylor Dome 1993-1994 Deep Core (Core M3C1)

Notes: 1) UW = University of Washington, UNH = University of New Hampshire
McMurdo = Crary Lab, McMurdo Station, Antarctica

2) Samples marked UNH are "waste" melt samples from the UNH ion-extraction system. These samples were stored in acid-rinsed Nalgene containors and processed at UW.

3) Only UNH samples were filtered with 0.45 μm filters. All others were filtered at 5 μm.

top depth (meters)	bottom depth (meters)	location processed (see notes above)	mass (grams)	background-corrected ^{10}Be/^{9}Be ratio (×10^{15})	^{9}Be concentration (10^{3} atoms/g)	1σ precision
1.17	6.17	McMurdo	1178	742.2	21.07	1.19
6.17	11.17	McMurdo	1355	839.2	20.72	0.97
11.17	16.17	McMurdo	1288	774.6	20.11	1.05
16.17	21.17	McMurdo	1131	713.4	21.09	0.94
21.17	26.17	McMurdo	1202	756.8	21.05	0.99
26.17	31.17	McMurdo	1099	639.8	19.47	0.90
31.17	36.17	McMurdo	1297	687.2	17.72	0.90
36.17	41.17	McMurdo	1110	652.3	19.65	1.06
41.17	46.17	McMurdo	1987	1236.0	20.80	0.97
46.17	51.00	McMurdo	1087	682.4	20.99	0.86
51.00	56.00	McMurdo	2126	1248.0	19.63	0.81
56.00	61.00	McMurdo	1374	919.3	22.37	1.16
61.00	66.00	McMurdo	1316	963.9	24.50	1.21
66.00	71.00	McMurdo	1387	976.3	23.55	1.22

Table 3.1 *Continued*

top depth (meters)	bottom depth (meters)	location processed (see notes above)	mass (grams)	background-corrected $^{10}Be/^{9}Be$ ratio ($\times 10^{-15}$)	^{0}Be concentration (10^{3} atoms/g)	1σ precision
71.00	76.00	McMurdo	2177	1436.0	22.06	1.08
76.00	81.00	McMurdo	1176	726.3	20.65	0.95
81.00	86.12	McMurdo	2203	1207.0	18.32	0.73
86.12	91.12	McMurdo	2144	1031.0	16.08	0.81
91.12	96.12	McMurdo	2832	1868.0	22.06	1.25
96.12	101.00	McMurdo	1273	835.0	21.94	0.97
101.00	101.12	McMurdo	3050	1892.0	20.75	0.86
101.12	112.06	McMurdo	1191	752.7	21.14	0.96
112.06	117.06	McMurdo	1016	611.2	20.11	1.06
117.06	126.12	McMurdo	1139	637.7	18.72	0.77
126.12	131.12	McMurdo	1994	1018.0	17.07	0.77
131.12	136.12	McMurdo	1994	1160.0	19.46	0.91
131.12	136.12	McMurdo	1987	1224.0	20.60	0.93
136.12	141.12	McMurdo	1113	638.6	19.19	1.09
141.12	146.12	McMurdo	3035	1480.0	16.31	0.76
146.12	156.23	McMurdo	1071	566.6	17.69	0.77
156.23	161.12	McMurdo	2210	1146.0	17.34	0.86
161.12	181.12	McMurdo	1037	545.4	17.59	0.98
181.12	186.12	McMurdo	2279	1158.0	16.99	0.93
186.12	186.10	McMurdo	1386	721.8	17.42	0.87
191.30	196.30	McMurdo	1330	646.2	16.25	0.74
196.30	201.30	McMurdo	1040	521.8	16.78	0.77
201.30	206.30	McMurdo	2360	1096.0	15.53	0.86
206.30	210.30	McMurdo	1385	716.2	17.29	0.78
210.30	215.32	McMurdo	1228	632.7	17.23	0.92

Table 3.1 *Continued*

top depth (meters)	bottom depth (meters)	location processed (see notes above)	mass (grams)	background-corrected $^{10}Be/^{9}Be$ ratio ($\times 10^{-15}$)	^{10}Be concentration (10^3 atoms/g)	1σ precision
215.32	221.30	McMurdo	1373	767.1	18.68	0.98
227.00	231.40	UNH	2930	1595.0	18.21	0.93
231.40	234.60	McMurdo	1259	727.1	19.32	0.90
234.60	241.14	McMurdo	1343	756.9	18.84	0.77
241.14	242.00	UW	3250	1670.0	17.19	0.80
242.00	247.40	UNH	3225	1582.0	16.41	0.86
247.40	252.30	UW	1317	603.3	15.33	0.66
256.20	263.20	UNH	3007	999.8	11.12	0.48
263.20	271.00	UW	1291	629.9	16.33	0.82
271.00	273.00	UW	2733	1045.2	12.79	0.60
273.00	282.10	UW	1151	455.2	13.23	0.61
282.10	285.20	UW	1349	614.6	15.24	0.77
285.20	287.05	UW	1358	578.1	14.24	0.77
297.05	302.05	UW	1385	831.8	20.09	0.97
310.00	320.00	UW	2733	1487.1	18.20	0.85
320.00	322.00	UW	2733	1427.1	17.46	0.82
328.00	330.00	UW	2733	1645.1	20.13	1.05
340.50	341.54	UW	1105	785.5	23.77	1.31
341.54	343.50	UW	807	611.6	25.35	1.31
343.50	345.50	UW	901	551.0	20.45	1.06
345.50	347.50	UW	984	705.7	23.99	1.10
347.50	350.00	UW	976	667.8	22.88	1.02
350.00	352.00	UW	918	567.1	20.66	0.97
352.00	354.00	UW	896	590.9	22.06	1.25
354.00	356.00	UW	917	687.7	25.08	1.07

Table 3.1 *Continued*

top depth (meters)	bottom depth (meters)	location processed (see notes above)	mass (grams)	background-corrected $^{10}Be/^{9}Be$ ratio ($\times 10^{-15}$)	^{9}Be concentration (10^{3} atoms/g)	1σ precision
356.00	358.00	UW	908	732.5	26.98	1.29
358.00	360.00	UW	938	1021.0	36.40	1.70
360.00	361.50	UW	435	831.2	63.91	3.57
361.50	364.00	UW	1107	1293.0	39.06	1.74
364.00	365.50	UW	623	972.6	52.21	2.36
366.00	368.00	UW	866	977.2	37.74	2.01
368.00	370.00	UW	507	885.6	58.42	2.89
370.00	372.00	UW	836	1188.0	47.53	2.39
372.00	374.00	UW	901	1487.0	55.20	2.28
374.00	376.00	UW	891	2965.0	111.29	5.74
376.00	378.00	UW	922	2730.0	99.03	4.28
378.00	380.00	UW	1005	2695.0	89.68	4.09
380.00	382.00	UW	710	1453.0	68.44	2.79
382.00	385.00	UW	899	1826.0	67.93	3.30
385.00	387.00	UW	859	1820.0	70.86	2.92
387.00	389.00	UW	998	1527.0	51.17	2.41
389.00	391.50	UW	901	1229.0	45.62	1.87
393.50	395.00	UW	910	953.3	35.04	1.89
395.00	396.50	UW	886	920.4	34.74	1.49
396.50	398.53	UW	880	1213.0	46.10	2.55
398.53	400.03	UW	919	1054.0	38.36	1.61
400.03	401.50	UW	619	1248.0	67.43	3.07
401.50	402.60	UW	853	1504.5	58.98	3.20
402.60	405.58	UW	820	1158.5	47.23	2.38
405.58	407.42	UNH	952	996.1	34.99	1.42

Table 3.1 *Continued*

top depth (meters)	bottom depth (meters)	location processed (see notes above)	mass (grams)	background-corrected $^{10}Be/^{9}Be$ ratio ($\times 10^{-15}$)	^{10}Be concentration (10^3 atoms/g)	1σ precision
407.42	411.80	UW	679	810.5	39.91	1.98
411.80	413.40	UNH	1013	1317.0	43.48	1.74
415.03	417.40	UNH	1035	1646.0	53.21	2.64
425.20	431.20	UNH	1057	1260.0	39.88	1.74
431.20	432.80	UNH	971	1092.0	37.63	1.80
432.80	435.40	UNH	1035	1011.0	32.66	1.43
435.00	437.00	UW	783	644.7	27.54	1.24
435.40	437.40	UNH	1035	757.1	24.46	1.11
437.40	439.20	UNH	967	795.0	27.51	1.41
439.20	441.00	UNH	967	844.5	29.22	1.33
443.00	448.82	UNH	1028	1412.0	45.93	1.93
448.82	446.80	UNH	977	754.6	25.84	1.18
452.40	454.20	UNH	990	854.2	28.87	1.36
456.20	457.80	UNH	1018	1501.0	49.32	2.68
459.80	461.60	UNH	1071	1219.0	38.08	1.60
463.80	465.60	UNH	1013	1222.0	40.34	1.93
465.60	467.43	UNH	1029	1624.0	52.77	2.82
467.43	469.60	UNH	1003	1592.0	53.09	2.14
469.60	471.40	UNH	1026	1331.0	43.37	2.36
471.51	473.60	UNH	1033	1182.0	38.29	1.78
473.60	474.00	UNH	895	1884.0	70.40	3.43
474.00	474.50	UW	631	1171.8	62.12	2.89
474.00	475.50	UW	515	579.5	37.63	1.79
475.50	477.50	UW	635	628.1	33.10	1.43
477.50	479.50	UW	940	797.6	28.38	1.46

Table 3.1 *Continued*

top depth (meters)	bottom depth (meters)	location processed (see notes above)	mass (grams)	background-corrected $^{10}Be/^{9}Be$ ratio ($\times 10^{-15}$)	^{0}Be concentration (10^{3} atoms/g)	1σ precision
479.50	481.00	UW	582	569.0	32.70	1.62
487.50	489.50	UW	994	897.7	30.20	1.35
491.65	493.65	UW	685	518.2	25.30	1.11
496.33	497.23	UW	625	519.5	27.80	1.30
497.73	499.29	UNH	752	511.4	22.74	1.17
499.70	500.80	UW	976	1185.0	40.61	1.94
501.28	502.72	UW	621	349.9	18.84	0.87
502.72	505.63	UW	1144	844.0	24.67	1.21
504.66	505.63	UW	882	531.4	20.15	0.97
505.63	506.65	UW	1013	668.0	22.06	0.89
506.65	508.21	UW	795	526.4	22.14	1.22
508.21	510.75	UW	1177	1090.4	30.98	1.39
510.75	512.50	UW	642	638.4	33.26	1.72
512.50	513.30	UW	435	305.3	23.47	1.30
513.30	514.80	UW	660	496.9	25.18	1.12
515.80	517.30	UW	620	505.5	27.27	1.19
517.30	518.30	UW	577	335.2	19.43	0.87
518.30	519.77	UW	1057	838.3	26.52	1.43
520.28	522.88	UW	956	861.0	30.12	1.65
522.28	522.78	UW	865	682.0	26.37	1.20
522.78	523.39	UW	798	575.3	24.11	1.01
523.39	523.78	UW	918	662.3	24.13	1.25
523.78	524.78	UW	856	580.4	22.68	0.92
526.28	527.33	UW	668	407.7	20.41	0.91
527.33	528.33	UW	865	409.2	15.82	0.87

Table 3.1 *Continued*

top depth (meters)	bottom depth (meters)	location processed (see notes above)	mass (grams)	background-corrected $^{10}Be/^{9}Be$ ratio ($\times 10^{-15}$)	^{10}Be concentration (10^{3} atoms/g)	1σ precision
528.33	530.98	UW	985	472.0	16.03	1.32
530.98	532.39	UW	1234	750.9	20.35	0.98
532.39	533.92	UW	965	662.3	22.95	1.10
533.92	535.25	UW	436	378.7	29.05	1.40
536.15	537.23	UW	423	275.6	21.79	0.93
537.23	538.66	UW	672	440.3	21.91	1.11
538.66	539.39	UW	694	474.4	22.86	1.19
539.39	540.20	UW	623	496.0	26.63	1.14
540.20	541.18	UW	568	288.1	16.96	0.77
541.18	542.22	UW	665	344.5	17.33	0.71
542.18	542.68	UW	732	542.5	24.79	1.27
543.68	545.70	UW	753	451.6	20.06	1.11
545.70	547.20	UW	568	320.1	18.85	0.76
550.22	553.12	UW	495	185.4	12.53	0.66
553.12	554.12	UW	724	374.1	17.28	0.76

Table 3.2 High-resolution ^{10}Be data at Taylor Dome

Core name and location	top depth (meters)	bottom depth (meters)	location processed	mass (grams)	Background-corrected ^{10}Be/^{9}Be ratio ($\times 10^{-15}$)	^{10}Be concentration (10^{3} atoms/g)	1σ precision
Core M1C3	0.00	0.33	UW	880	472.6	17.95	0.96
(40S)	0.33	0.67	UW	802	624.7	26.04	1.28
Collected	0.67	1.00	UW	884	514.8	19.47	0.92
1992	1.00	1.33	UW	835	475.3	19.05	1.05
	1.33	1.67	UW	697	374.2	17.95	0.73
	1.67	2.00	UW	499	214.0	14.34	0.65
	2.00	2.33	UW	525	147.4	9.40	0.44
	2.33	2.67	UW	806	410.3	17.03	0.86
	2.67	3.00	UW	906	635.0	23.44	1.32
	3.00	3.33	UW	749	661.2	29.52	1.22
	3.33	3.67	UW	801	541.7	22.60	1.06
	3.67	4.00	UW	439	218.3	16.65	0.74
	4.00	4.33	UW	795	492.7	20.72	0.89
	4.33	4.67	UW	676	177.0	8.76	0.39
	4.67	5.00	UW	435	197.6	15.20	0.65
	5.00	5.33	UW	884	332.9	12.59	0.66
	5.33	5.67	UW	535	220.2	13.76	0.62
	5.67	6.00	UW	748	446.7	19.97	0.84
	6.00	6.33	UW	640	354.6	18.53	0.89
	6.33	6.67	UW	564	374.2	22.19	1.09
	6.67	7.00	UW	969	539.8	18.64	0.80
	7.00	7.33	UW	600	295.4	16.47	0.68
	7.33	7.67	UW	669	303.3	15.17	0.64
	7.67	8.00	UW	615	315.3	17.15	0.71
	8.00	8.33	UW	648	360.1	18.58	0.77

Table 3.2 *Continued*

Core name and location	top depth (meters)	bottom depth (meters)	location processed	mass (grams)	Background-corrected ^{10}Be concentration $^{10}Be/^{9}Be$ ratio ($\times 10^{-15}$)	(10^{3} atoms/g)	1σ precision
Core M1C3	8.33	8.67	UW	925	515.9	18.65	0.93
(*continued*)	8.67	9.00	UW	885	435.7	16.47	0.78
	9.00	9.33	UW	889	299.5	11.26	0.60
	9.33	9.67	UW	866	589.1	22.76	1.26
	9.67	10.00	UW	675	468.8	23.23	1.25
	10.00	10.25	UW	781	255.6	10.95	0.59
	10.25	10.50	UW	564	272.1	16.12	0.73
	10.50	10.75	UW	606	151.2	8.34	0.43
	10.75	11.00	UW	498	263.0	17.66	0.84
	11.00	11.25	UW	845	552.3	21.86	1.11
Deep Core	49.21	49.31	UW	542	332.5	20.50	1.14
(M3C1)	49.31	49.41	UW	661	414.2	20.96	0.97
Collected	49.41	49.51	UW	407	272.8	22.41	0.95
1994	49.51	49.61	UW	756	518.3	22.94	1.20
	49.61	49.71	UW	721	566.3	26.29	1.17
	49.71	49.81	UW	476	246.1	17.28	0.96
	49.81	49.91	UW	473	218.6	15.45	0.86
	49.91	50.01	UW	481	214.2	14.89	0.78
	50.01	50.11	UW	817	420.8	17.22	0.86
	50.11	50.21	UW	676	432.6	21.41	0.86
	50.21	50.31	UW	999	602.9	20.19	1.07
	50.31	50.41	UW	862	545.5	21.16	1.01
	50.41	50.51	UW	965	712.2	24.68	1.37
	50.51	50.61	UW	432	394.9	30.54	1.48

Table 3.2 *Continued*

Core name and location	top depth (meters)	bottom depth (meters)	location processed	mass (grams)	Background-corrected ^{10}Be concentration $^{10}Be/^{9}Be$ ratio ($\times 10^{-15}$)	(10^3 atoms/g)	1σ precision
Core M3C1	50.61	50.71	UW	932	610.4	**21.91**	1.04
(continued)	50.71	50.81	UW	824	434.6	**17.64**	0.89
	50.81	50.91	UW	406	189.4	**15.60**	0.66
	50.91	51.01	UW	972	436.7	**15.02**	0.72
	298.60	298.70	UW	859	391.9	**15.25**	0.77
	298.70	298.80	UW	495	339.4	**22.94**	1.04
	298.80	298.90	UW	698	346.1	**16.58**	0.91
	298.90	299.00	UW	982	696.1	**23.71**	1.08
	299.00	299.10	UW	581	363.0	**20.88**	1.04
	299.10	299.20	UW	408	252.5	**20.71**	0.85
	299.20	299.30	UW	804	518.6	**21.56**	1.21
	299.30	299.40	UW	474	266.3	**18.78**	0.90
	299.40	299.50	UW	512	395.7	**25.86**	1.19
	299.50	299.60	UW	898	564.3	**21.01**	0.95
	299.60	299.70	UW	976	699.8	**23.98**	1.30
	299.70	299.80	UW	968	520.8	**18.00**	0.80
	299.80	299.90	UW	437	234.1	**17.91**	1.00
	299.90	300.00	UW	940	471.4	**16.77**	0.83
	300.00	300.10	UW	779	627.0	**26.91**	1.48
	300.10	300.20	UW	991	520.4	**17.56**	0.78
	300.20	300.30	UW	536	353.4	**22.05**	0.93
	300.30	300.40	UW	854	378.7	**14.83**	0.63
	300.40	300.50	UW	418	204.8	**16.38**	0.68
	340.54	340.61	UW	564	441.4	**26.19**	1.37
	340.61	340.68	UW	898	671.7	**25.01**	1.30

Table 3.2 *Continued*

Core name and location	top depth (meters)	bottom depth (meters)	location processed	mass (grams)	Background-corrected $^{10}Be/^{9}Be$ ratio ($\times 10^{-15}$)	^{10}Be concentration (10^3 atoms/g)	1σ precision
Core M3C1	340.68	340.73	UW	927	692.9	**25.01**	1.28
(*continued*)	340.73	340.78	UW	601	262.6	**14.62**	0.80
	340.78	340.83	UW	469	307.2	**21.92**	1.17
	340.83	340.88	UW	820	550.8	**22.46**	1.11
	340.88	340.93	UW	423	278.4	**22.00**	0.94
	340.93	340.98	UW	572	377.0	**22.06**	1.02
	340.98	341.03	UW	932	483.9	**17.37**	0.70
	341.03	341.08	UW	687	406.1	**19.76**	0.81
	341.08	341.13	UW	687	544.9	**26.53**	1.38
	341.13	341.18	UW	694	518.8	**25.00**	1.11
	341.18	341.23	UW	495	211.4	**14.28**	0.66
	341.23	341.28	UW	787	482.7	**20.51**	0.97
	341.28	341.33	UW	827	615.3	**24.87**	1.33
	341.33	341.38	UW	495	294.5	**19.88**	1.03
	341.38	341.43	UW	599	588.1	**32.86**	1.85
	341.43	341.48	UW	441	264.2	**20.05**	0.90
	341.48	341.53	UW	811	730.5	**30.14**	1.36
	341.53	341.60	UW	951	797.6	**28.04**	1.27
Snow pit	0.00	0.10	McMurdo	1103	750.0	**22.67**	1.26
at deep	0.10	0.20	McMurdo	923	430.9	**15.56**	0.68
core drill	0.20	0.30	McMurdo	829	437.0	**17.57**	0.82
site	0.30	0.40	McMurdo	1313	460.9	**11.70**	0.54
Collected	0.40	0.50	McMurdo	1107	281.3	**8.47**	0.43
1994	0.50	0.60	McMurdo	1381	542.0	**13.08**	0.60

Table 3.2 *Continued*

Core name and location	top depth (meters)	bottom depth (meters)	location processed	mass (grams)	Background-corrected $^{10}Be/^{9}Be$ ratio ($\times 10^{-15}$)	^{10}Be concentration (10^3 atoms/g)	1σ precision
snow pit	0.60	0.70	McMurdo	1263	534.7	14.11	0.60
(*continued*)	0.70	0.80	McMurdo	1285	741.9	19.25	0.83
	0.80	0.90	McMurdo	1028	386.8	12.54	0.51
	0.90	1.00	McMurdo	1178	695.0	19.67	1.04
	1.00	1.10	McMurdo	1145	697.1	20.29	0.86
	1.10	1.20	McMurdo	1174	686.3	19.49	1.05
	1.20	1.30	McMurdo	1192	1041.1	29.11	1.58
	1.30	1.40	McMurdo	907	406.6	14.94	0.66
	1.40	1.50	McMurdo	748	429.8	19.15	0.88
	1.50	1.60	McMurdo	1292	983.4	25.37	1.21
	1.60	1.70	McMurdo	1015	555.4	18.24	0.79
	1.70	1.80	McMurdo	1074	603.0	18.72	1.05
	1.80	1.90	McMurdo	1000	576.1	19.20	0.96
	1.90	2.00	McMurdo	1030	341.6	11.06	0.61
	2.00	2.10	McMurdo	809	409.4	16.87	0.83
	2.10	2.20	McMurdo	1429	610.8	14.25	0.72
	2.20	2.30	McMurdo	916	418.2	15.22	0.84
	2.30	2.40	McMurdo	1152	599.4	17.34	0.93
	2.40	2.50	McMurdo	850	280.7	11.01	0.52
	2.50	2.60	McMurdo	1108	452.5	13.61	0.73
	2.60	2.70	McMurdo	1026	446.9	14.52	0.64
	2.70	2.80	McMurdo	1343	883.1	21.92	1.08
	2.80	2.90	McMurdo	746	487.8	21.79	0.90
	2.90	3.00	McMurdo	1340	863.0	21.47	1.01
	3.00	3.10	McMurdo	965	485.8	16.78	0.92

Table 3.2 *Continued*

Core name and location	top depth (meters)	bottom depth (meters)	location processed	mass (grams)	Background-corrected ^{10}Be concentration $^{10}Be/^{9}Be$ ratio ($\times 10^{-15}$)	10^{3} atoms/g)	1σ precision
snow pit	3.10	3.20	McMurdo	907	440.8	**16.20**	0.82
(*continued*)	3.20	3.30	McMurdo	779	462.8	**19.80**	1.07
	3.30	3.40	McMurdo	1298	643.2	**16.52**	0.89
	3.40	3.50	McMurdo	1080	936.4	**28.90**	1.44
	3.50	3.60	McMurdo	1160	634.8	**18.24**	0.91
	3.60	3.70	McMurdo	779	893.6	**38.24**	1.69
	3.70	3.80	McMurdo	1358	525.0	**12.89**	0.66
	3.80	3.90	McMurdo	1130	614.0	**18.11**	0.83
	3.90	4.00	McMurdo	1050	434.9	**13.81**	0.71

Table 3.3 Miscellaneous snow pit and core data at Taylor Dome

Core or snow pit location	top depth (meters)	bottom depth (meters)	location processed	mass (grams)	Background-corrected $^{10}Be/^{9}Be$ ratio ($\times 10^{-15}$)	^{10}Be concentration (10^3 atoms/g)	1σ precision
Misc. Snow Pits (collected 1994)							
Taylor/Ferrar	0	0.1	McMurdo	7300	2161	9.90	0.7
20N	0	10	McMurdo	4001	9105	152.20	8.9
20S	0	10	McMurdo	2175	1706	26.23	0.5
10C	0	0.02	UW	892	845.2	31.69	1.1
(collected 1993)	0.02	0.04	UW	996	764	25.65	2.2
	0.04	0.06	UW	876	833	31.80	1.0
	0.06	0.08	UW	1004	816	27.18	1.4
	0.08	0.1	UW	933	704	25.24	1.0
	0.1	0.12	UW	1053	734.4	23.33	2.1
	0.12	0.14	UW	1051	988.5	31.46	0.7
	0.14	0.16	UW	919	937.1	34.10	1.0
	0.16	0.18	UW	1179	1174	33.32	0.4
	0.18	0.2	UW	1030	1289	41.86	0.3
	0.2	0.22	UW	909	985	36.24	1.0
	0.22	0.24	UW	1097	1009	30.77	0.7
	0.24	0.26	UW	913	1145	41.93	0.5
	0.26	0.28	UW	936	982.4	35.10	3.1

Table 3.3 *Continued*

Core or snow pit location	top depth (meters)	bottom depth (meters)	location processed	mass (grams)	Background-corrected $^{10}Be/^{9}Be$ ratio ($\times 10^{-15}$)	^{10}Be concentration (10^3 atoms/g)	1σ precision
10S	0	0.1	UW	802	293.6	12.24	0.6
(collected 1993)	0.1	0.2	UW	1154	594.3	17.22	1.3
	0.2	0.3	UW	937	432.4	15.44	1.2
	0.3	0.4	UW	1571	699.7	14.90	0.4
	0.4	0.5	UW	949	431.5	15.20	1.0
Upper Taylor	0.00	0.33	Livermore	453	450.6	33.27	2.6
Glacier	0.33	0.67	Livermore	569	578.8	34.04	2.3
Core M3C1	0.67	1.00	Livermore	556	443.1	26.67	1.3
(collected 1992)	1.00	1.33	Livermore	571	455.2	26.68	2.0
	1.33	1.67	Livermore	550	495	30.09	0.5
	1.67	2.00	Livermore	559	413.4	24.74	0.2
	2.00	2.33	Livermore	549	647.6	39.43	1.9
	2.33	2.67	Livermore	497	398.7	26.85	1.5
	2.67	3.00	Livermore	545	542.7	33.30	2.3
	3.00	3.33	Livermore	461	313.7	22.73	1.1
	3.33	3.67	Livermore	576	373	21.67	0.3
	3.67	4.00	Livermore	456	248.7	18.23	1.1
	4.00	4.33	Livermore	508	504.2	33.16	2.8
	4.33	4.67	Livermore	513	459.5	29.98	0.9
	4.67	5.00	Livermore	562	425.5	25.31	0.3

Transfer of chemical constituents in both directions across the tropopause is clearly of great importance. ... Exactly how the transfer takes place remains unclear.

— R.P. Wayne, Chemistry of Atmospheres, 1991, pp. 64-5.

Chapter 4

CAN WE USE ^{10}BE TO SOLVE THE INVERSE PROBLEM IN ICE-CORE PALEOCLIMATOLOGY?

4.1 Introduction

The concentrations of aerosol species in polar ice cores provide some of the most remarkable records available of the chemical makeup of the ancient atmosphere. Yet, while it seems evident that ice-core data give an accurate *qualitative* view of the paleo-atmosphere, a quantitative reconstruction requires that we fully understand the relationship between ice-core chemistry and aerosol concentrations in the atmosphere.

A particularly promising approach is the use of cosmogenic isotopes such as ^{10}Be, ^{36}Cl and ^{26}Al as tracers of aerosol behavior. The value of cosmogenic isotopes is that their production in the atmosphere is independent of climate, making them fundamentally different from other chemical or isotopic species. Within certain limits, we can specify *a priori* the atmospheric distribution of cosmogenic isotopes. For example, Raisbeck and co-workers (Raisbeck et al., 1981; Yiou et al., 1985) suggested that the ^{10}Be flux could be considered approximately constant in Antarctica, and used ^{10}Be to estimate paleo snow-accumulation rates in the Vostok ice core. Similarly, Alley et al. (1996) used the assumption of a constant ^{10}Be flux as a

test for the validity of a simple model for aerosol deposition on the Greenland ice sheet.

Essentially, the degree to which cosmogenic isotopes are useful for atmospheric studies depends on our ability to quantify their atmospheric distribution. A quantitative assessment of the uncertainties associated with this approach is lacking in the literature, making it difficult to interpret the significance of relevant paleoclimatic interpretations (e.g. Alley et al. 1996, Raisbeck et al., 1987). In this chapter, I discuss the current status of cosmogenic isotope research in the context of a simple inverse problem: the determination of original aerosol concentrations from measured concentrations in ice cores. By considering the major influences on isotope distributions—in particular the influence of changes in atmospheric circulation and production rate on the concentration of cosmogenic isotopes in the polar troposphere—I hope to provide a useful conceptual framework for the application of cosmogenic isotopes to the solution of the inverse problem. In general, I refer to ^{10}Be; most of my comments, however, apply also to other less commonly measured cosmogenic isotopes.

4.2 The ice core-paleoclimate inverse problem: why ^{10}Be is important

In principle, the governing equations which describe the transfer of aerosols from air to snow under modern conditions can be determined empirically. In applying these transfer functions to paleoclimate, however, a

major obstacle arises: the transfer of aerosols from air to snow is dependent not only on conservative properties, such as snow-accumulation rate, which in favorable cases may be known independently, but also on such variables as wind speed and surface roughness. Such *non-conservative* variables may be difficult (or impossible) to determine from the ice core record.

Waddington (1996) suggests that the problem should be formalized in terms of geophysical inverse theory. We might express it as a system of linear equations:

$$\mathbf{Fm} = \mathbf{d} \tag{1}$$

where **d** is a vector of measured variables, **m** represents the atmospheric concentrations of interest, and **F** is a matrix of transfer functions. For example, consider the linear inverse problem

$$\begin{bmatrix} \frac{W}{\rho_{ice}} + \frac{v_d}{\dot{b}} & 0 \\ 0 & \frac{W}{\rho_{ice}} + \frac{v_d}{\dot{b}} \end{bmatrix} \cdot \begin{bmatrix} \chi_{SO_4} \\ \chi_{^{10}Be} \end{bmatrix} = \begin{bmatrix} [SO_4] \\ [^{10}Be] \end{bmatrix} \tag{2}$$

having the same form as Equation 1. Equation 2 states that the measured ice-core concentrations of SO_4 and ^{10}Be depend on their original concentrations in air (χ), the snow accumulation rate ($\dot{b}$), the wet-deposition scavenging ratio (W), and the dry-deposition velocity (v_d).[10] The density of ice is

denoted by ρ_{ice}. A unique solution for $\chi_{^{10}Be}$ and χ_{SO_4} requires that the parameters W, υ_d and $\dot{b}$ are known.

Although modern values of W and υ_d can in principle be determined accurately from surface snow and atmospheric measurements, these parameters may have changed substantially in the past. As discussed by Cunningham and Waddington (1993), and as confirmed by empirical data (Harder et al., 1996), the dry-deposition velocity, υ_d, increases with wind speed, an effect that could be important enough to account entirely for the large changes in ^{10}Be and SO_4 concentrations that are associated with the major climate shifts recorded in ice cores. Because wind-speed is non-conservative, that is, not directly recoverable from ice-core analysis, even the simple system represented by Equation 2 cannot be solved without additional information.

As a working model for aerosols in the GISP2 core, central Greenland, Alley et al. (1996) assume that the concentrations of various chemical species can be described as in Equation 2, where W and υ_d remain constant and where (in this particular case) $\dot{b}$ is known independently. They test their model against the assumption that the ^{10}Be concentration in the polar troposphere remains within relatively narrow bounds over the time interval considered (14 ka to 11 ka). Effectively, Alley et al. (1996) solve the inverse problem by assuming *a priori* knowledge of one of the unknowns ($\chi_{^{10}Be}$), and treating the terms χ_{SO_4}, χ_{NO_3} ... χ_{n-1} and $\left(\upsilon_d + \frac{W}{\rho}\dot{b}\right)$ as the n unknowns in a system of n equations. While Alley et al's (1996) work

requires some unproven assumptions (in particular, the the values of v_d and W for ^{10}Be can be translated to the relavent parameters for other chemical species), it illustrates how ^{10}Be (or other cosmogenic isotopes) can be used in ice-core paleoclimate research.

In our simple example, the determination of χ_{SO_4}, the primary variable of interest, is dependent *only* on how well $\chi_{^{10}Be}$ is known. Although the 'real' inverse problem is much more complex, the philosophy is the same: in the context of Equation 1, a unique solution becomes more likely if we are able to specify some of the elements in the solution vector, **m**, as well as some of those in **d** and **F**. For polar ice-core work in particular, we want to be able to specify the concentration of ^{10}Be in the polar troposphere. To do so, we need to consider both 1) the production rate of ^{10}Be and 2) the transport of ^{10}Be from other parts of the atmosphere.

4.3 Production of cosmogenic isotopes in the atmosphere

The production rate of cosmogenic isotopes in the atmosphere increases with altitude and with geomagnetic latitude. The vertical gradient in production is essentially an exponential function of atmospheric depth (column-integrated mass of the atmosphere) while the horizontal (i.e. meridional) gradient reflects the configuration of the earth's magnetic field. High-frequency changes in production result from the cyclic modulation effect of solar activity, with the strongest periodicities at 11 years and 88

years; empirically, times of high solar activity (high sunspot numbers) are strongly anti-correlated with isotope production. There is also a quasi-periodic variability corresponding to the Maunder and Spörer-type sunspot minima, during which production rates are generally high. Low frequency variations in production result from the secular change in geomagnetic field strength, which is quasi-periodic at about 10,000 years. In general, production rate variations associated with geomagnetic field changes are greatest at the equator and negligible at the poles; the opposite is true as regards solar modulation. The magnitude of all production-rate variations increases with altitude. Because ^{10}Be is incompletely mixed in the atmosphere, its distribution partly reflects the gradients in production. To calculate the net source (production + transport) of ^{10}Be to the polar troposphere, it is therefore an over-simplification to use the global average production rate; instead, both the temporal and spatial distribution of production must be taken into account.

4.3.1 *Spatial distribution of ^{10}Be: zonal-mean[11] star-production rates*

The production of cosmogenic isotopes in the atmosphere is relatively well understood from both a theoretical and empirical standpoint. Libby (1946) made the earliest measurement of natural ^{14}C, following Montgomery's (1939) recognition of the importance of secondary cosmic ray neutrons in the production of radiocarbon (^{14}C), via thermal[12] neutron capture:

$$^{14}N(n,p)^{14}C \qquad (3)$$

Secondary neutrons are produced by the bombardment of atoms in the upper atmosphere by the high-energy protons which comprise the primary galactic cosmic ray flux. While these reactions create secondary protons as well as neutrons, the neutrons become increasingly important with depth in the atmosphere as the charged protons lose energy during ionizing reactions with atoms in the atmosphere. Like radiocarbon, most cosmogenic isotopes of interest are produced by secondary neutrons, but the main production pathway is spallation rather than capture and much higher energy neutrons (rather than 'thermal' neutrons') are involved; for example:

$$^{14}N,^{16}O + n \xrightarrow{spallation} {}^{10}Be + \gamma + n, p, etc. \qquad (4)$$

Collectively, the spallation reactions which create cosmogenic isotopes are referred to as 'stars' because of their appearance on the photographic plates originally used in their detection. The importance of neutrons in star production is a consequence of the balance between the proton/neutron ratio (which increases with altitude) and the availability of target atoms (which decreases with altitude) in the atmosphere. For the lower atmosphere (below about 12.5 km) the neutron energy distribution is nearly invariant with latitude and altitude (Lal and Peters, 1967) and is in equilibrium with the star production rate. Consequently, the distribution of

star production in the lower atmosphere can be determined from the thermal neutron distribution, which has been measured in detail (Simpson and Fagot, 1953; Soberman, 1953; Meyer and Simpson, 1955). Lal and Peters (1967) used this approach to determine cosmogenic isotope inventories for the lower atmosphere as a function of latitude and altitude. It is noted that the neutron half-life is so short (~12 minutes) that the distribution of neutrons is independent of atmospheric dynamics.

In the stratosphere, where spallation energies are higher and where the majority (about 70%) of cosmogenic production occurs, the neutron distributions alone are not adequate for determining star-production distributions, in part because there is neutron leakage out of the atmosphere. Lal and Peters (1967) used measured star-production data to determine the relationship between the neutron distribution in the lower atmosphere and star-production rates at high altitudes, allowing the low-altitude thermal neutron distribution to be used as an index of isotope production at any altitude and latitude.

An alternative to the largely empirical approach of Lal and others (Lal and Peters, 1962; Lal and Peters, 1967; Castagnoli and Lal, 1980; Lal, 1988) is to calculate the distribution of star production from first principles. The so-called "hadronic cascade" calculation uses experimentally-determined reaction cross sections for target atoms in the atmosphere, the measured energy spectra of the cosmic ray flux, and the known configuration of the earth's magnetic field to follow the propagation of high-energy particles and their spallation products through the atmosphere. The hadronic cascade

calculation essentially involves numerical solution of the Boltzmann equation describing the kinetic behavior of particles at low pressure. One of the earliest such calculations applied to cosmogenic isotopes was described by Benioff (1956); a more recent and complete analysis has been made by O'Brien et al. (1979; 1991). Although there are significant discrepancies in the calculated production rates for radiocarbon, O'Brien's calculations for star-production agree well with those of Lal, both in terms of global averages and for latitudinal and vertical distribution. The accuracy of the empirical approach depends primarily on how representative of the spatial and temporal averages were the particular data used. At present we must rely on measurements made during the 1950's and 1960's. For the cascade calculations, the chief uncertainty is in the accuracy of cross-section measurements. The favorable comparison between the quasi-empirical and hadronic-cascade calculations suggests that in general, the distributions of star production are known quite well, probably to within a few percent in the vertical direction. For the latitude-dependence of star production, the discrepancy between the two approaches is somewhat larger; Lal (pers. comm. 1993) estimates that the meridional variation in production is known to a precision of about 20%.[13] The star production calculations of O'Brien et al. (1991) are shown in Figure 4.1.

To calculate ^{10}Be production rates from star production rates, we need to know the probability distribution for spallation as a function of the neutron energy spectrum, a relationship that can be determined empirically. Because the energy spectrum for neutrons varies little with altitude and

latitude, the probability distribution is usually expressed as a "yield-per-star", $y_{^{10}Be}$, and assumed to be constant;[14] this assumption imparts an error of about 10% (Yasyulenis et al., 1974; O'Brien, 1979). Another source of error in the yield function is the dependence of the spallation cross section on the composition of the atmosphere, but this is negligible for isotopes such as ^{10}Be, which are derived from abundant atmospheric constituents (N, O, Ar). It may be important for isotopes of $z > 18$ such as $^{81}_{36}Kr$, whose parent nuclei ($z \geq 36$) are not distributed uniformly throughout the atmosphere.

At present, the chief uncertainty in the yield functions for cosmogenic isotopes in the atmosphere lies in the degree to which we can accurately measure cross sections. For the cosmic-ray energy distribution and atmospheric composition of the lower atmosphere, $y_{^{10}Be}$ is known from experiments within about a factor of three (between 5.0×10^{-3} (Silberberg and Tsao, 1973) and 1.4×10^{-2} (Rudstam, 1966)). Independent estimates of the global average production rate of ^{10}Be (Somayajulu et al., 1984; Monaghan et al., 1985) appear to favor an intermediate value of $y_{^{10}Be} = 2.5 \times 10^{-2}$ (Lal and Peters, 1967; Lal, 1988), suggesting that ±50% is a conservative estimate for the precision of $y_{^{10}Be}$.

4.3.2 *Temporal variations in production rate*

For our purposes, the flux of cosmic rays outside the magnetosphere can be considered constant,[15] but the distribution of cosmic rays which reach the earth's atmosphere depends both on the intensity and configuration of the magnetic field, and on the strength of solar activity.

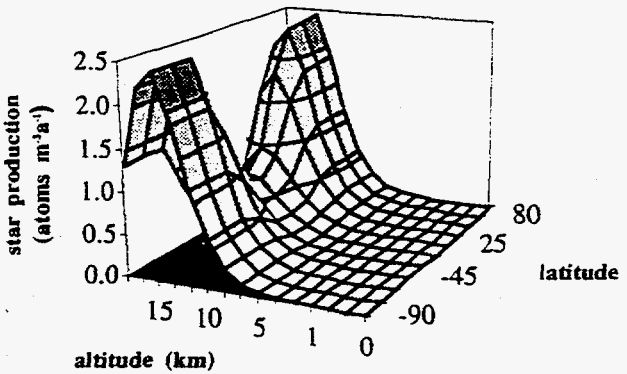

Figure 4.1 Star production rates for typical solar modulation parameter (ϕ = 600 MV) and today's geomagnetic field strength (M = 1), according to the calculations of O'Brien et al. (1991).

At present, the high-frequency periodic variations in solar activity are fairly well understood, and do not greatly concern us for most paleoclimate studies, since their effect on ^{10}Be production can be removed from the data with an appropriate low-pass filter.[16] The available evidence suggests that long-term variations (>200 years) are probably minimal, though their importance cannot be ruled out. Of greater importance is the secular variation in geomagnetic field strength.

A reasonable proxy for geomagnetic field strength as function of time is the marine-core record of remnant magnetism. Although there is some controversy as to the validity of such records (Raisbeck et al., 1994), the coherence of data from several ocean basins suggests that their general features are reliable (Weeks et al., 1995). I use the natural remnant magnetism (NRM) records of Tric et al. (1992) and Weeks et al. (1995), combined with O'Brien et al.'s (1991) calculations of ^{10}Be production rates, to estimate the time-dependent variation of ^{10}Be production over the last 140 ka. Figure 4.2 shows the calculated ^{10}Be production normalized to modern rates averaged over 1) the global atmosphere and 2) the polar atmosphere only.[17]

Figure 4.2 shows that significant variation in the global average production rate of ^{10}Be can be expected on millennial timescales. Additionally, Figure 4.2 illustrates the importance of atmospheric mixing processes. The production rate in polar regions is virtually insensitive to geomagnetic field variations; the sensitivity of the ice-core ^{10}Be record

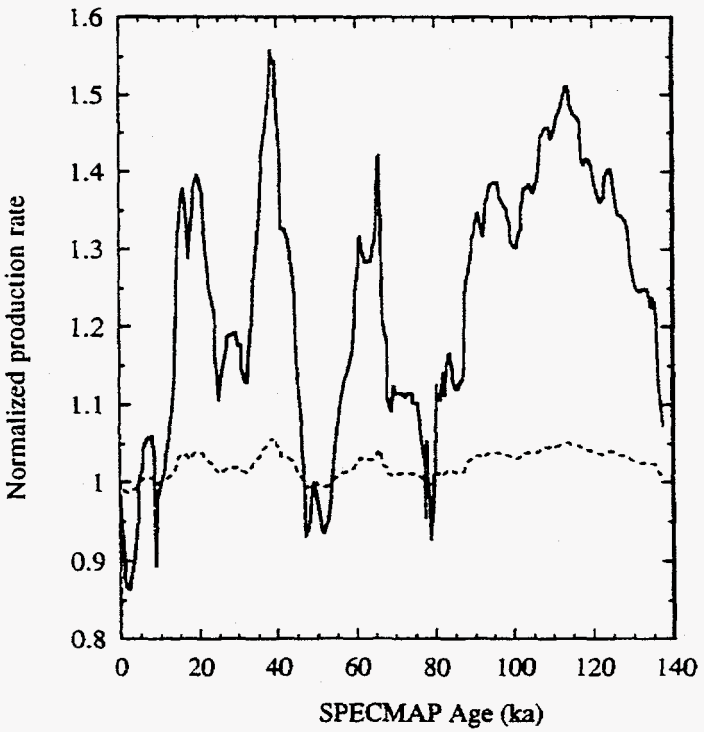

Figure 4.2 Cosmogenic isotope production rates estimated from the geomagnetic data of Tric et al. (1992) and Weeks et al. (1995). Estimates are shown normalized to a modern value = 1 for the global average (—) and the polar atmosphere only (–).

depends, therefore, on how much of the ^{10}Be in the polar troposphere is produced at low latitudes, where the geomagnetic influence is strong. As I address in Chapter 5, this fraction is poorly known, with estimates for the southern polar troposphere ranging from less than 35% (Steig et al., 1996) to about 75% (Mazaud et al., 1994). Note that for the last 10 ka, production rates almost certainly varied by less than 10%, as assumed by Alley et al. (1996). Prior to that time production rate variations could be important depending on the low-latitude fraction involved. Until that fraction can be determined with more certainty, the two curves in Figure 4.2 should be treated as upper and lower bounds on the variations in production rate which affect the polar ^{10}Be record.

4.4 Atmospheric mixing

As a consequence of the vertical and meridional gradients in ^{10}Be production, atmospheric circulation patterns influence the ^{10}Be concentration in the polar troposphere. Examination of Figure 4.1 suggests that meridional mixing within the troposphere itself is not particularly important; the total gradient in production, equator to pole, is less than a factor of two,[18] so that the total variation in local concentrations that can result from tropospheric mixing alone is at most about ±30%. Also, ^{10}Be produced in or transported to the troposphere is removed by precipitation scavenging within a few weeks (Raisbeck and Yiou, 1981, 1985; Harder, pers.

comm., 1995), substantially more rapidly than the characteristic mixing times (~months) for the troposphere. Between the stratosphere and troposphere, on the other hand, and within the stratosphere, the gradients in ^{10}Be production are strong enough that transport and mixing of equatorial, temperate, and polar air masses, as well as stratosphere-troposphere exchange processes, may be important.

Figure 4.3 shows a conceptual model, used in subsequent sections of this chapter, which describes the concentration of ^{10}Be in the polar troposphere as a function of meridional mixing in the stratosphere and stratosphere-troposphere exchange. The model considers only the southern hemisphere, and is comprised of four atmospheric reservoirs: the polar (PT) and non-polar troposphere (NT) and the polar (PS) and non-polar stratosphere (NS). Concentrations (atoms $^{10}Be/g_{air}$) in each reservoir are denoted by χ^{NS}, χ^{PS} etc. and represent a balance of atmospheric dynamics, ^{10}Be production, and removal from the atmosphere by deposition at the earth's surface. The production rate of ^{10}Be in each reservoir is integrated over the appropriate ranges of longitude, latitude, and altitude. Production is denoted by P^{NS}, P^{NT}, P^{PS} and P^{PT}. For consistency with the production rate calculations of Lal (1988), I use the same standard reference atmosphere (Lal, 1988), to define the vertical density distribution and the height of the tropopause. Transfer of ^{10}Be between reservoirs can occur via diffusion across boundaries, or by advective mixing. The degree of mixing is dependent on the relative magnitudes of the time-constants for atmospheric dynamics (τ_{dyn}) and the residence time of ^{10}Be in each reservoir (τ^{NS}, etc.).

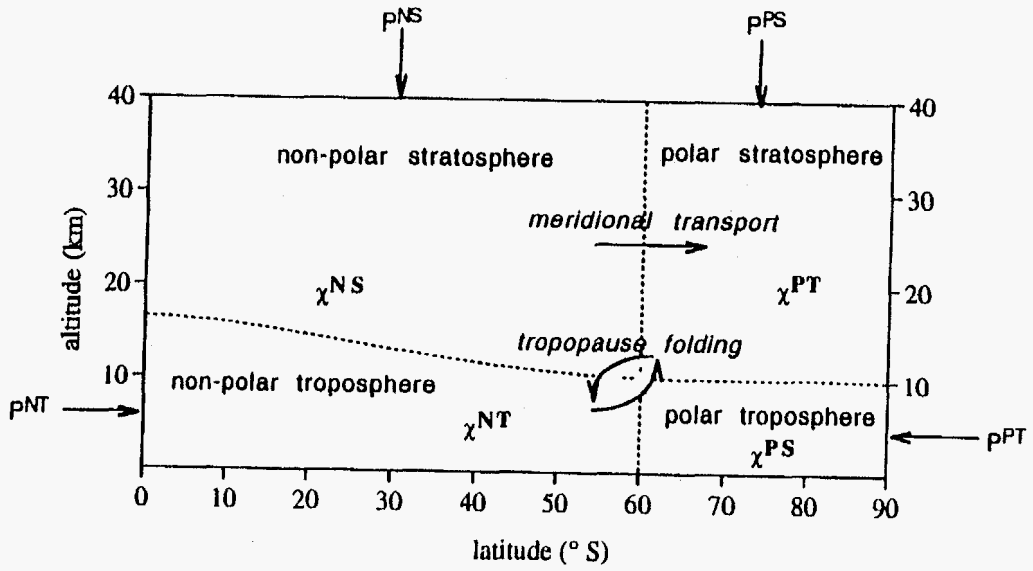

Figure 4.3 Schematic model of atmospheric mixing with respect to ^{10}Be.
P denotes production, χ denotes mixing ratio (atmospheric concentration).

4.3.1 Meridional mixing in the stratosphere

The concentration of a chemical or isotopic species at any given location in the atmosphere is described by

$$\frac{\partial \chi_i}{\partial t} = Q_i - S_i + \mathbf{v} \cdot \nabla \chi_i + \mathbf{k} \nabla^2 \chi_i \qquad (5)$$

in which **k** is the diffusion coefficient, **v** is the advection coefficient, which describes the mean wind field, Q_i is the production rate, and S_i is the loss rate by chemical or other non-dynamical processes. Lal and Peters (1967) discuss the application of Equation 5 to cosmogenic nuclides with relatively short half-lives, such as ^{7}Be (half-life = 53 days). In that case the radioactive decay constant λ_i is the dominant component of the sink term, S_i. For ^{10}Be, radioactive decay is negligible (half-life = 1.5×10^6 years), and $S_{^{10}Be}$ is dominated by the loss of ^{10}Be from the atmosphere by deposition at the earth's surface.

In the stratosphere, the source term, Q, for ^{10}Be is simply the stratospheric production rate (P_S). The loss term is

$$S\ (\text{atoms g}^{-1}\text{a}^{-1}) = f\chi \qquad (6)$$

where f is the fraction (per year) of ^{10}Be lost to the troposphere. The coefficients **k** and **v** (Equation 5) describe diffusion and advection within the stratosphere; S therefore includes both advection and diffusion across the

tropopause. Because the residence time (τ_{trop}) of ^{10}Be in the troposphere is very short (~weeks (Raisbeck and Yiou, 1981, 1985)) compared with the time constant (> 1 year) for air-mass exchange with the stratosphere, the source of tropospheric ^{10}Be to the stratosphere can be considered negligible.

Equation 5, a three-dimensional model, can be reduced to one dimension by averaging over longitude and altitude. Zonal averaging (along latitude bands) is reasonable because the time scale for the stratospheric zonal winds is a matter of days, compared with months to years for the meridional winds. In addition, advection is much more important than diffusion (Garcia and Solomon, 1983); it is a reasonable as a first-order approximation to ignore **k**. Making these simplifications, and combining Equations 5 and 6 yields:

$$\frac{\partial \chi}{\partial t} = P - v\frac{\partial \chi}{\partial y} - f\chi \qquad (7)$$

A further simplification can be made by recognizing that, especially in the southern hemisphere, the stratospheric polar vortex (at about 60°S) is a significant barrier to meridional mixing. For example, based on ozone profiles during the late austral winter, Hartmann (1990) shows that the effective diffusivity of mass across the vortex is two to three orders of magnitude smaller than typical estimates of the global average value (e.g. Garcia and Solomon, 1983). Although the breakup of the vortex during the spring allows for some exchange between polar and non-polar reservoirs,

the time-constant for complete meridional mixing is probably somewhat larger than the mean residence time of ^{10}Be in the stratosphere, generally taken to be about one or two years. From models of stratospheric dynamics, air traveling from equatorial regions towards the pole reaches high temperate latitudes within one or two years, but may take an additional year or more to cross the vortex barrier (Dunkerton, 1978; Rosenlof, 1995). This general picture suggests that is it appropriate to represent the stratosphere as two separate reservoirs, each well mixed with respect to ^{10}Be. Empirical evidence for a generally well mixed stratosphere in temperate and equatorial regions may be found in the measurements of ^{90}Sr and other nuclear bomb products released during weapons testing in the atmosphere in the 1950's and 1960's, and by recent ^{10}Be measurements (Wahlen, 1994). In the polar stratosphere, uniform concentrations of ^{10}Be can be expected regardless of mixing patterns within that reservoir because the production rate is essentially invariant of latitude poleward of 60°.

Mixing between the two stratospheric reservoirs can be parameterized in terms of the gradient $\frac{\chi^{PS} - \chi^{NS}}{L}$ where X^{PS} and X^{NS} are the average ^{10}Be concentrations in the polar and non-polar stratosphere, respectively, and L is the width of the vortex barrier:

$$\frac{\partial \chi}{\partial t} = P - v\frac{\chi^{PS}(t) - \chi^{NS}(t)}{L} - f\chi(t) \qquad (8)$$

For $(\partial\chi/\partial t = 0)$, Equation 9 reduces to

$$\chi^{PS} = \frac{1}{f}\left(P^{PS} - v\frac{\chi^{PS} - \chi^{NS}}{L}\right) \tag{9}$$

giving the steady-state concentration of ^{10}Be in the polar stratosphere.

It is useful to rewrite Equation 10 in terms of time constants for dynamics and chemistry (see e.g. Brasseur & Solomon, 1984). The characteristic timescale, τ_{dyn}, for dynamical mixing across a gradient is a function only of the advection coefficient and the length scale (cf Hartmann, 1990):

$$\tau_{dyn} = \frac{L}{v} \tag{10}$$

Defining τ^{NS} as the residence time in the non-polar stratosphere and making the substitution $P^{NS}\tau^{NS} = \chi^{NS}$, we obtain a straightforward equation for the concentration of ^{10}Be in the polar stratosphere:

$$\chi^{PS} = \frac{P^{PS}\tau_{dyn} + P^{NS}\tau^{PS}}{f\tau_{dyn} + 1} \tag{11}$$

Figure 4.4 shows the two-dimensional surface defined by Equation 12, giving the average concentration of ^{10}Be in the polar stratosphere as a function of f (the rate of loss to the polar troposphere) and τ_{dyn} (the time constant for meridional mixing). In constructing Figure 4.4 I have assumed that $\tau_{NS} = 1$

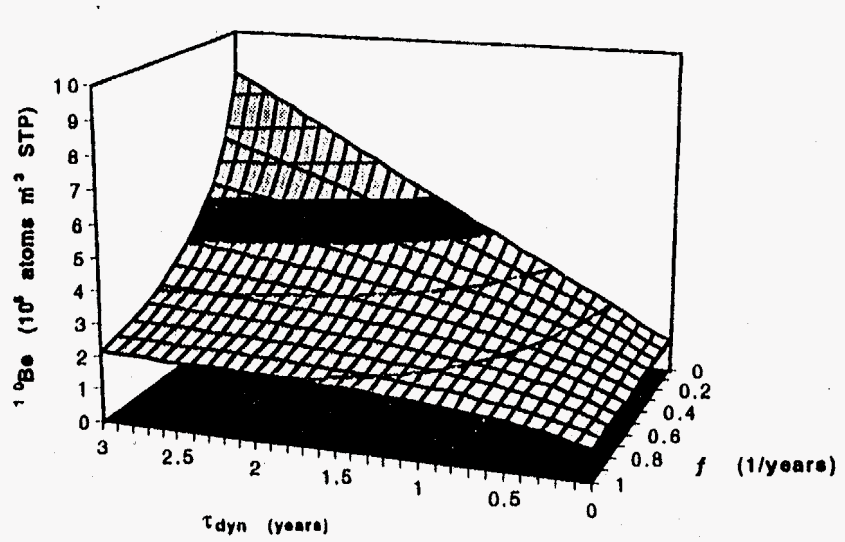

Figure 4.4 Calculated ^{10}Be concentration in the polar stratosphere as a function of f and τ_{dyn}. Dark gray band shows typical measured values at South Pole, Antarctica.

year. Also shown in Figure 4.4 is the average measured value for the concentration of ^{10}Be in the polar stratosphere (Raisbeck and Yiou, 1985).

4.4.2 *Stratosphere-troposphere exchange.*

As illustrated in Figure 4.1, the vertical gradients in ^{10}Be production are stronger than the meridional gradients, and it follows that stratosphere-troposphere exchange should be more important than meridional mixing in determining the concentration of ^{10}Be in the polar troposphere. Currently, both qualitative and quantitative understanding of stratosphere-troposphere exchange processes is undergoing considerable revision (Holton et al., 1996). For example, injection of stratospheric air into the troposphere at mid-latitudes, known as "tropopause folding," and often taken as the dominant source of stratospheric ^{10}Be to the troposphere (e.g. McHargue & Damon, 1991) may be less important than once thought. Of possibly equal importance is role of polar stratospheric clouds (PSCs) in transporting stratospheric aerosols across the tropopause. PSCs are composed primarily of nitric acid (Solomon, 1990); since beryllium forms a soluble nitrate compound, $Be(NO_3)_2$, deposition of PSCs at the ice-sheet surface should be accompanied by deposition of stratospheric ^{10}Be. At present, knowledge is limited about the relative importance of this process, in part because of the difficulty of distinguishing advective transport from diffusive settling in the motion of stratospheric aerosols (e.g. Iwasaka, 1986).

Neglecting tropospheric transport for the reasons given earlier, we can parameterize the range of plausible variations in stratosphere-troposphere

exchange processes in terms of the stratospheric sink term, $f\chi^{PS}$. The neglect of tropospheric transport is not entirely reasonable because of the possibility that stratospheric air may be mixed into the troposphere at mid-latitudes, and then mixed (meridionally) into the polar troposphere (Dibb et al., 1994). Nevertheless, this simple parameterization gives a first-order view of the influence of stratosphere-troposphere exchange on the ^{10}Be concentration in the polar troposphere. From Equation 11, we have

$$\begin{aligned}\chi^{PT} &= \tau^{PT}\left(f\chi^{PS} + P^{PT}\right) \\ &= \tau^{PT}\left(f\frac{P^{PS}\tau_{dyn} + P^{NS}\tau^{NS}}{f\tau_{dyn}+1} + P^{PT}\right)\end{aligned} \tag{12}$$

where P^{PT} is the ^{10}Be production rate, τ^{PT} is the residence time, and χ^{PT} in the concentration in the polar troposphere. Figure 4.5 shows χ^{PT} as a function of f and τ_{dyn}.

Although the full range of possible values for χ^{PT} implied in Figure 4.5 is large (about a factor of ten), it is notable that very large and probably unrealistic changes in atmospheric circulation are implied by the full domain $\{0 \le f \le 1,\ 0 \le \tau_{dyn} \le 1\}$. Both two and three-dimensional atmospheric dynamics models show that increased stratosphere-troposphere exchange, if it occurs, should be accompanied by greater meridional transport (e.g. Garcia and Solomon, 1983; K.K. Tung, pers. comm, 1995; Holton et al., 1996). As a consequence of the direction (increasing with altitude and latitude) of the production-rate gradients, the effect of atmospheric circulation changes on

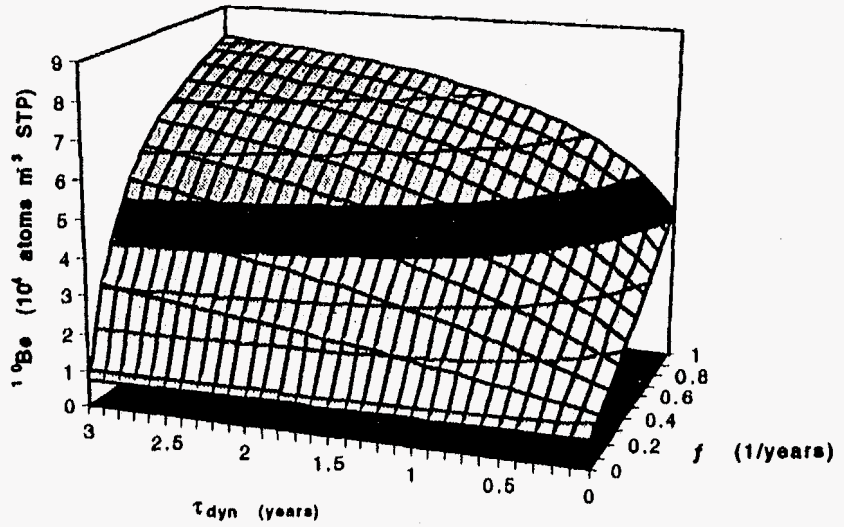

Figure 4.5 Calculated ^{10}Be concentration in the polar troposphere as a function of f and τ_{dyn}. Dark gray band shows typical measured values at South Pole, Antarctica. *Note that for clarity of presentation the f axis is reversed with respect to Figure 4.4.*

^{10}Be in the polar troposphere are thus likely to be quite small. Expressed in terms of our simple mixing model (Equation 12), increasing the strength of the general circulation is equivalent to moving roughly parallel with the f-τ_{dyn} plane in Figure 4.5.

4.5 Conclusions: how well do we know $\chi^{PT}_{^{10}Be}$?

From the foregoing discussion, we cannot, at present, specify the time-dependent concentration of ^{10}Be in the polar tropospheric to any great degree of accuracy. At best, we know absolute production rates within about a factor of two, and the importance of stratospheric input to the polar troposphere remains open to question. Changes in atmospheric circulation and production rate may account for a non-negligible fraction of the observed variability in ice-core concentrations. As Mazaud et al. (1994) have shown, it is realistic to interpret many of the fluctuations in the Vostok ice-core record in terms of changes in geomagnetic field strength.

On the other hand, we *can* place specific limits on the variability of ^{10}Be in the polar troposphere. The major features in the ice-core ^{10}Be record cannot be accounted for in terms of production rate or atmospheric mixing changes, suggesting that the concentration of ^{10}Be in the polar troposphere is not highly variable, especially when compared with other aerosol species. For example, the doubling of ^{10}Be concentrations in the Vostok core between interglacial and glacial climate regimes might be interpreted in

terms of greater input from the stratosphere. If meridional mixing were to remain constant, a doubling of ice-core concentrations would imply a five-fold increase in the fraction of stratospheric aerosol transported to the ice-sheet (assuming that, as indicated in Figure 4.2, production rates were not substantially different). If meridional mixing were to increase as well (lower τ_{dyn}) an even larger change in f required. Unless PSC scavenging of stratospheric ^{10}Be increases greatly during cold periods, such a large change seems unlikely. For the Taylor Dome ice core, in which ^{10}Be concentrations increase by a factor of five during the last glacial maximum, only an extreme combination of decreased meridional mixing, greater input from the stratosphere, and increased production rates could account for the observed changes. That explanation, of course, would be inconsistent with the Vostok record, since an increase in any of these factors would influence both sites more or less equally. A much simpler interpretation of both records is that they reflect local conditions, primarily snow accumulation rates (see Chapters 6 and 8).

The greatest contribution to uncertainty in calculated variations in $\chi^{PT}_{^{10}Be}$ lies in the importance of stratospheric input. The possibility that there is significant input from the stratosphere (in contrast to the view of Lal and Peters (1967) that such input is negligible) must be seriously considered, especially in the light of recent evidence that PSCs may act as a sink for stratospheric aerosols. While it is beyond the scope of this dissertation to fully address the role of PSCs or of atmospheric dynamics, we can use

existing ^{10}Be data to address the role of stratospheric input indirectly. This is the subject of the following chapter.

Notes to Chapter 4

10. By definition, the 'wet' and 'dry' scavenging parameters refer to the deposition of an atmospheric constituent dependent on and independent of, respectively, the rate of precipitation (see Davidson, 1989, for a review).

11. Because of the symmetry of the geomagnetic field, production of cosmogenic isotopes is independent of geomagnetic longitude. Furthermore, for time-averages greater than about 200 years, the geomagnetic and geographic latitude are essentially identical (Merrill and McElhinny, 1983). Thus, for our purposes here, cosmogenic isotope production is a two-dimensional, rather than three dimensional problem. The zonal-mean is the average in the longitudinal direction.

12. Thermal neutrons have energies below ~100 MeV.

13. An uncertainty of 20 % in the latitude scaling of star production can account for discrepancies between different estimates of ^{10}Be and ^{26}Al production as measured in terrestrial rocks at different latitudes.

14. The expected "yield per star" is defined as

$$y_{^{10}Be} = \frac{\int_0^{\infty} \sigma(E)\phi_i(E)dE}{\int_0^{\infty} \sigma_{n,d_-}(E)\phi_i(E)dE}$$

where $y_{^{10}Be}$ is the yield of ^{10}Be, σ is the production cross section (probability of producing ^{10}Be per destructive collision), $\sigma_{n.el}$ is the non-elastic cross section (fraction of collisions which are destructive) ϕ_i is the hadron energy spectrum (i = n, p, etc.), and E is energy.

15. There is some evidence for short-term variation in the galactic cosmic ray flux, possibly due to nearby supernovae (McHargue et al., 1995). There is also a small solar component which becomes important during periods of intense solar flare activity (Lal and Peters, 1967).

16. The strong 11-year cycle is, on the other hand, of some use in determining atmospheric mixing patterns, since its amplitude is dependent on latitude. See Chapter 5 and Steig et al. (1996).

17. I used the measured natural remnant magnetism (NRM) data of Tric et al (1992) combined with the data of Weeks et al. (1995) to extend the record to 140,000 years. The assumption is made that NRM is directly proportional to geomagnetic field strength. I normalized the NRM data to a modern value of M = 1, where M is the strength of the magnetic field (arbitrary units). Multiplication by the appropriate factor as determined by interpolation of O'Brien et al. data (1991) gives the relative star-production rate. For example, for a change from M = 1 to M = 0.5, the global average star production rate increases by 33%.

18. This is an extremely small gradient when compared with that of aerosol species such as SO_4, which is produced by oxidation of biologically-produced dimethyl sulfide at the ocean surface. The source term for SO_4 in equatorial regions is about twice that in temperate and polar regions, per unit area of ocean (Andreae, 1985; Charlson et al., 1987). More importantly, there is no source term for SO_4 over the land or sea ice. As a result, even a small change in atmospheric circulation patterns can greatly affect the concentration of SO_4 in polar regions. Mayewski et al. (1994) argue that the increased atmospheric loading of SO_4 and many other aerosol species over Greenland during the last glacial maximum is *primarily* a reflection of increased meridional mixing in the troposphere.

Chapter 5

ESTIMATION OF THE STRATOSPHERIC FRACTION OF ^{10}BE IN THE POLAR TROPOSPHERE

5.1 Introduction

Over the 11-year solar cycle, ^{10}Be production variations of about ±20% are predicted for the high-latitude stratosphere (Lingenfelter, 1963; Lal and Peters, 1967; O'Brien, 1979; Lal, 1988), compared with variation of <5% for the troposphere + stratosphere at the geomagnetic equator. The modulation of cosmic rays by the geomagnetic field, on the other hand, is greatest at the equator. Atmospheric mixing thus plays a critical role in determining local atmospheric ^{10}Be concentrations and the ^{10}Be flux from atmosphere to surface (Raisbeck and Yiou, 1985; Lal, 1987; Dibb et al., 1994).

A question of particular importance is whether or not there is significant deposition, at polar latitudes, of ^{10}Be produced in the low-latitude stratosphere, where modulation by the geomagnetic field is greatest. If so, then a strong geomagnetic signal is expected in the ice-core ^{10}Be record. Mazaud et al. (1994) approached this question by optimizing the fit between geomagnetic field variations estimated from ocean sediment cores (Tric et al., 1992), and ^{10}Be concentrations in the Vostok ice core (Raisbeck et al., 1987) over the last 150 ka. In this chapter, I take a similar approach to that of Mazaud et al. (1994), but compare the Antarctic

^{10}Be flux with estimates of solar, rather than geomagnetic variability, and with empirical measurements of the cosmic ray flux.[19]

5.2 ^{10}Be variations at Taylor Dome

To obtain an estimate of the amplitude of the ~11-year solar modulation cycle of ^{10}Be at Taylor Dome, I collected samples at 2 to 3-year resolution from a firn core at location 40S (see Chapter 2) and at ~0.5 year resolution in a 4-meter deep snowpit at the deep-drilling site. Dating was achieved by locating the 1954 and 1964 bomb-radioactivity horizons in the firn (Dibb et al., 1990), and assuming a constant accumulation rate corrected for the measured density of each sample. Independent dating control by seasonal oxygen isotope stratigraphy indicates that the assumption of constant accumulation rate is reasonable; based on this comparison, I estimate a dating uncertainty of ±1.5 years. Figure 5.1 shows the $\delta^{18}O$ data and the gross β radiation data used to calculate the age/depth relationship.

In Figure 5.2, Taylor Dome ^{10}Be concentrations are shown as a function of time. Also shown in Figure 5.2 is the neutron counting rate at Deep River, eastern Canada (NRC, 1994). The Deep River counter provides a convenient index; variations in counting rate at Deep River are not significantly different than at other locations worldwide. The neutron counting rate is directly related to the cosmic-ray flux, and therefore to the

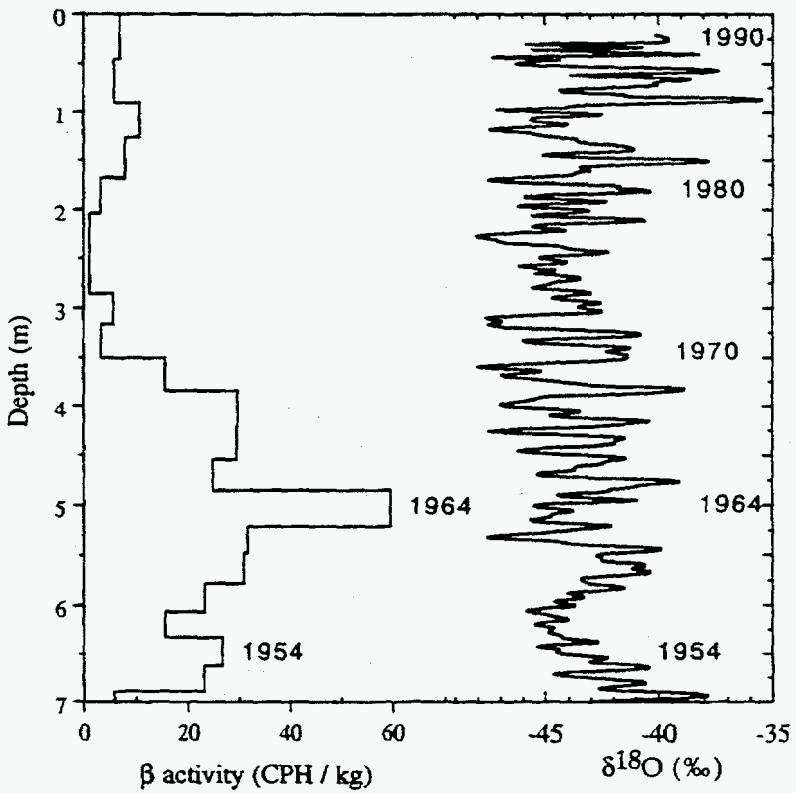

Figure 5.1 $\delta^{18}O$ and gross β radiation profiles at Taylor Dome. Numbers show dates of counted years (assuming that $\delta^{18}O$ cycles are annual) and of known bomb-radiation peaks.

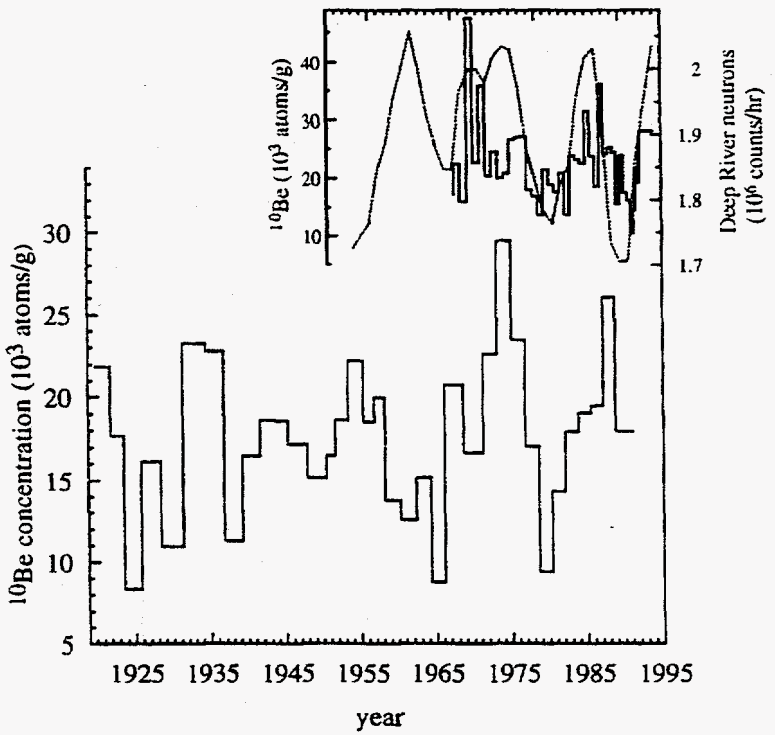

Figure 5.2 ^{10}Be concentrations at Taylor Dome from a firn core (lower) and a snow pit (upper). Dashed line shows mean-annual neutron count at Deep River, Canada, for comparison.

^{10}Be production rate at any point in the earth's atmosphere (Lingenfelter, 1963; Lal and Peters, 1967; O'Brien and Burke, 1973; O'Brien, 1979; Castagnoli and Lal, 1980; Lal, 1988; O'Brien et al., 1991).

5.3 Relationship among solar variability, ^{10}Be concentrations and atmospheric circulation

Comparison of the ^{10}Be and neutron counter data shows that there is an ~11-year periodicity common to both records. Following Beer et al. (1990), I attribute this periodicity to solar modulation of production. The ^{10}Be flux lags the neutron flux by about 1 year. This lag results from the one-to-two-year residence time of ^{10}Be in the atmosphere (Raisbeck and Yiou, 1981; Beer et al., 1990); limited ^{7}Be data from air samples (Höltz et al., 1991) show that cosmogenic isotope production is in phase with the cosmic ray flux, as expected from theory. Although correlation between ^{10}Be concentrations and neutron counting rates is relatively low ($r^2 = 0.32$, lag 1 year), it may be compromised by slight variations in snowfall rate (and associated errors in dating for the ^{10}Be profiles), and by the possibility that the atmospheric residence time is variable.

An alternate causal mechanism for the observed 11-year periodicity of ^{10}Be is solar forcing of climate. Solar forcing may cause changes in atmospheric circulation patterns or snow deposition rates, with resultant changes in ice-core ^{10}Be concentrations (Lal, 1987). Changes in

atmospheric circulation patterns may indeed be the dominant mechanism for ice-core ^{10}Be variations at some time-scales, such as the prolonged high concentration of ^{10}Be in Greenland ice during the Little Ice Age/Maunder minimum (Lal, 1987). However, although there is evidence for an approximately ~11-year periodicity in stable isotope ($\delta^{18}O$) data (Stuiver et al., 1995) from the GISP2 (Summit, Greenland) ice core, such cycles are only regional. At Taylor Dome, Fourier spectrum analysis of high-resolution $\delta^{18}O$ and electrical conductivity data yields a dominant periodicity at ~50 years, but nothing near 11 years. Thus, although long-term meteorological changes and high-frequency 'noise' may be superimposed on production-rate variations (Raisbeck et al., 1990), there is at present little evidence for a meteorological contribution to the 11-year periodicity observed for ^{10}Be at Taylor Dome.

5.4 Amplitude of the 11-year cycle at Taylor Dome

To quantify the relationship between cosmic ray flux and ^{10}Be deposition rates, I applied a 9-13 year bandpass filter to both the ^{10}Be and the neutron-counter data. Taking autocorrelation into account, comparison of the 11-year-periodic component of each data set yields a correlation coefficient of $r = 0.89$ ($n_{eff} = 49$, lag 1 year). I also filtered the data of Beer et al. (1987) using the same algorithm. Before filtering, all data were numerically re-sampled, using cubic splines (Rasmussen, 1991), to obtain

average values over identical one-year intervals. For the firn-core ^{10}Be data from Taylor Dome, which consist of 2-3 year averages, this may underestimate the 11-year amplitude, relative to the other data sets, but comparison with results from the ~0.5-year resolution snowpit data suggests that this is a relatively minor effect.

Figure 5.3 shows a comparison of the filtered ^{10}Be data from Taylor Dome (A.D. 1920 - 1994) and from Dye 3, Greenland (1860 - 1985), plotted relative to the average ^{10}Be concentration at each site. Also shown is the sunspot number and the filtered Deep River neutron counter data. The amplitude of the ^{10}Be variations at Taylor Dome is on average larger than at Dye 3. There are no variations in the entire Dye 3 data set (1875-1985) as large as the largest observed at Taylor Dome over the last 75 years. This suggests a fundamental difference between the northern (Dye 3) and southern hemisphere (Taylor Dome) sites. A likely explanation for this difference is that ^{10}Be deposition at Taylor Dome (latitude 78°50'S) reflects ^{10}Be production from a higher-latitude atmospheric reservoir than does ^{10}Be deposition at Dye 3 (65°N).

5.5 Comparison between predicted and observed ^{10}Be production variations

I used the calculations of O'Brien et al. (1979; 1991) to integrate total production over various latitude and altitude ranges as a function of the

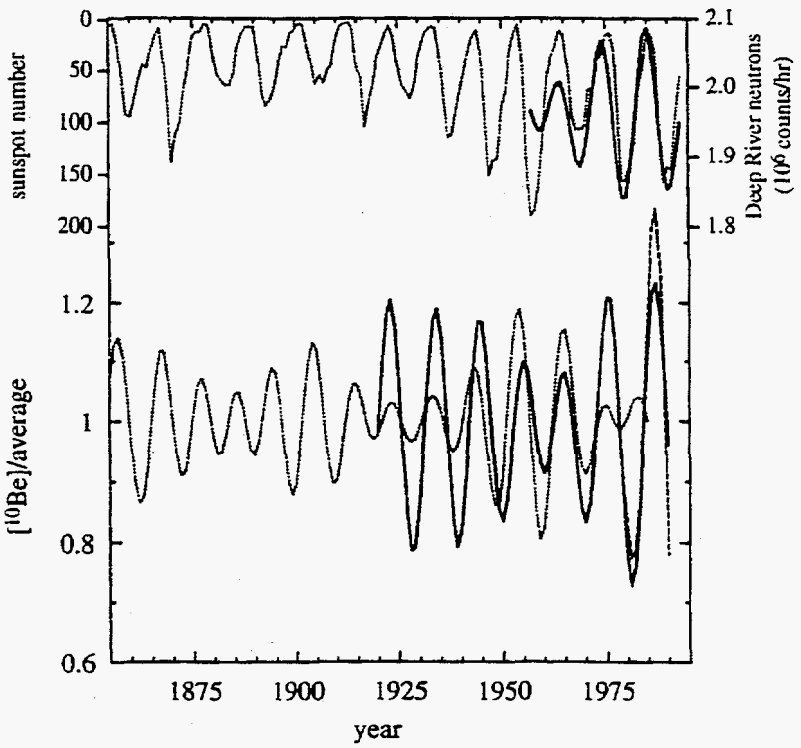

Figure 5.3 Lower: bandpass-filtered (9-13 year) ^{10}Be data from Taylor Dome (—) and Dye 3 (····, Beer et al., 1990). Dashed line shows filtered snow pit ^{10}Be data from Taylor Dome. Data are plotted relative to the average. For clarity, the Dye 3 data have been shifted forward by 0.5 years. Upper: filtered Deep River neutron counting rate (—) and smoothed mean-annual sunspot numbers (····).

Deep River neutron counting rate.[20] O'Brien et al.'s (1991) calculations agree closely with empirical observations of the neutron-flux/altitude relationship (Simpson et al., 1953), and with the earlier calculations of Lingenfelter (1963) and Lal and Peters (1967). Because I use ratios rather than absolute concentrations, the absolute production rate of ^{10}Be is not important here, although implicit in the model is that the scavenging ratio (the proportion of the atmospheric concentration of ^{10}Be that is deposited per unit time) is constant.

Figure 5.4 compares the neutron counting rate with the relative variation in ^{10}Be concentration at Taylor Dome, for the years 1958-1994, using the filtered data shown in Figure 5.3. Also shown are predicted variations integrated over 1) the whole atmosphere, 2) stratosphere only, and 3) the polar stratosphere (latitude 60° - 90°). The uncertainty in the average slopes of the theoretical curves to be ±10%, based on comparison among different calculations of cosmogenic nuclide production rates (Lingenfelter, 1963; Lal and Peters, 1967; O'Brien, 1979; Lal, 1988; O'Brien, et al., 1991). A straight or parabolic line fit to the Taylor Dome data is statistically distinct (>95% confidence) from the predicted curves for both the whole atmosphere and whole stratosphere. The discrepancy is even greater if it is taken into account that the Taylor Dome variability is probably damped by about 5% because of a 1-2 year average residence time of ^{10}Be in the stratosphere.

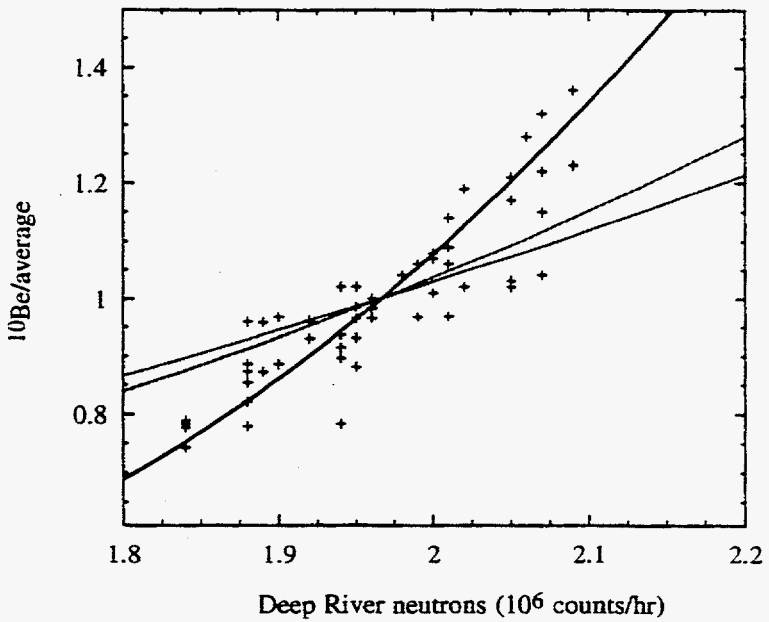

Figure 5.4 Comparison of predicted and measured ^{10}Be production as a function of counting rates at the Deep River neutron monitor, 1958-1994. Crosses show 1-year mean data from bandpass-filtered Taylor Dome data shown in Figure 5.3. Lines show predicted values for entire atmosphere (····), stratosphere only (---) and polar stratosphere only (—).

5.6 Discussion

The data suggest a significant contribution of polar stratospheric ^{10}Be to the Antarctic ^{10}Be deposition flux. This conflicts with the traditional view that, at high latitudes, there is very little input of cosmogenic isotopes produced in the stratosphere (Lal and Peters, 1967), but is consistent with observations of ozone and aerosol concentrations in the Antarctic (Maenhaut et al., 1979; Toon et al., 1986; Manney et al., 1994; Fox et al., 1995; Santee et al., 1995). The condensation of water vapor on aerosols to form polar stratospheric clouds (Crutzen and Arnold, 1986; Gobbi et al., 1991; Deshler et al., 1995) favors the advection of stratospheric aerosols into the troposphere either by direct settling of ice particles (Vömel et al., 1995), or by descent of stratospheric air (Iwasaka, 1986). Both of these mechanisms are strongest in the winter, when latitudinal mixing is severely restricted by the polar stratospheric vortex (Maenhaut, et al., 1979; Toon, et al., 1986; Shaw, 1989a, b; Manney, et al., 1994; Fox, et al., 1995; Santee, et al., 1995; Vömel, et al., 1995).

To quantify the relative contribution of non-polar ^{10}Be to the polar ^{10}Be flux, I calculate a sensitivity factor,

$$\frac{\partial(^{10}Be/^{10}Be_{mean})}{\partial\phi} \qquad (13)$$

where ϕ is the Ehmert potential, a measure of the degree of solar modulation of the cosmic ray flux (Ehmert, 1960). For a typical solar cycle, ϕ varies from 300 to 600 MV, with an average value of 450 MV (Lal, 1988); ϕ = 450 MV corresponds to a counting rate at Deep River of 1.97×10^6 neutrons/hour (O'Brien and Burke, 1973).

I divide the atmospheric ^{10}Be production into geomagnetically 'modulated' and 'unmodulated' components, corresponding to the low latitude (0° to 60°) and high-latitude (60° to 90°) atmosphere, as discussed in Chapter 4 and illustrated in Figure 4.3. The boundary at 60° corresponds to a break in slope in theoretical cosmogenic isotope production curves. The high/low-latitude division is meaningful also from the perspective of atmospheric dynamics, since 60° approximates the location of the polar vortex (Kakegawa et al., 1986). Note that although geomagnetic and geographic latitudes are different, this difference is negligible because production rates are essentially independent of latitude poleward of 60° (Lingenfelter, 1963). Averaged over just a few hundred years, the geomagnetic and geographic poles coincide closely (Merrill and McElhinny, 1983; Ohno and Hamano, 1992).

Figure 5.5 depicts the predicted sensitivity of ^{10}Be production to changes in Ehmert potential, for different mixing ratios between ^{10}Be derived from high latitudes and from the low-latitude stratosphere. I assume zero contribution from the low-latitude troposphere. Also shown in Figure 5.5 are the average sensitivities determined from ^{10}Be

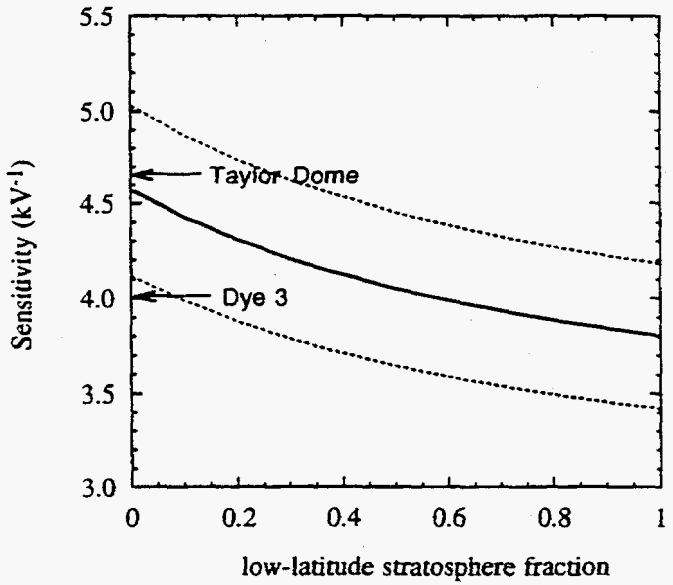

Figure 5.5 Sensitivity of the polar ^{10}Be flux to changes in the cosmic-ray flux, as characterized by the Ehmert potential, ϕ, as a function of the fraction of ^{10}Be derived from the low-latitude stratosphere. Curved lines show theoretical sensitivities near a mean value for ϕ of 450 MV; bold line is from calculations of O'Brien et al. (1991). Dotted lines denote estimated 2σ uncertainty in the calculations (see text). Arrows show mean values for Taylor Dome and Dye 3. A least squares 2nd-order polynomial fit to the data in Figure 5.4 gives 95% confidence limits of ± 0.4 kV^{-1} for the Taylor Dome value.

concentrations at Taylor Dome and Dye 3 over the same period (1920-1985), assuming average solar conditions ($300 < \phi < 600$ MV).

Comparison of the calculated and observed sensitivities shows that, in Antarctica, at most 35%, and more likely <10%, of the Antarctic ^{10}Be flux can be derived from low-latitude sources. In contrast, the amplitude of variation of ^{10}Be observed in the Dye 3 core (Beer et al., 1990) is consistent with a well-mixed stratosphere (Monaghan, 1987). This conclusion is at odds with recent work of Mazaud et. al., (1994), who were able to produce a reasonable match between the Vostok, Antarctica, ^{10}Be record and ocean-sediment proxy records of geomagnetic field strength. As has been done here, Mazaud et al. (1994) divided the atmospheric ^{10}Be sources into 'unmodulated' and 'modulated' components; they determined a value of 75% for the modulated component. The discrepancy with my value of <35% suggests several possibilities: 1) ocean-sediment geomagnetic records approximate geomagnetic field variations rather poorly (Raisbeck et al., 1994) 2) the slight adjustment made by Mazaud et al. (1994) to the accepted Vostok timescale (Jouzel et al., 1993) to achieve their best-fit match introduces errors, 3) the fraction of 'modulated' ^{10}Be in the ice core record is variable, and 4) the theoretical production rate variations are in error. The first three possibilities draw into question the validity of using ^{10}Be ice core records as proxies for the geomagnetic modulation of cosmogenic isotope production.

Conclusions

Evidently, a relatively small proportion of the Antarctic ^{10}Be flux is derived from latitudes at which variations in geomagnetic field strength are important. If my 75-year record is applicable to the distant past, then the ^{10}Be record from Antarctic ice cores should contain only a small geomagnetic signal. The global average geomagnetic modulation over the last 10 ka is on the order of ±25%; assuming a maximum 35% contribution from the low-latitude stratosphere; geomagnetic modulation accounts for variation of at most ±10%.

This conclusion is satisfying from the point of view of glaciology, because it suggests that ^{10}Be concentrations can be used to determine accumulation rates in ice cores (Yiou et al., 1985; Raisbeck, et al., 1987; Lorius et al., 1989; 1992; Steig et al., 1995). The rather minimal effect of geomagnetic modulation on the Antarctic ^{10}Be flux makes more reasonable the assumption of a "constant" ^{10}Be flux over millennial timescales, improving confidence in this approach. The effect of solar variability, of course, must still be considered, but my results suggest that comparison of ^{10}Be records among Antarctic and Greenland ice cores may allow us to separate the geomagnetic and solar contributions to changes in cosmogenic isotope production rates. It will be important to collect more profiles of ^{10}Be solar cycles in both polar and non-polar regions as a further test of these findings.

Notes to Chapter 5

19. See Steig et al. (1996) for a published version of this chapter.

20. See footnote 17 (Chapter 4).

In summary...two relatively independent procedures [^{10}Be and δD] for estimating polar precipitation, neither on a particularly solid theoretical footing, give similar and apparently reasonable results. The degree to which one is convinced by such concordance is ... a question of personal taste....

—Lorius et al., *The Environmental Record in Glaciers and Ice Sheets*, 1989, p. 351.

Chapter 6

ON THE RELATIONSHIP BETWEEN ^{10}BE CONCENTRATIONS AND ICE-ACCUMULATION RATES

6.1 Introduction

A widely-discussed application of cosmogenic isotopes in ice-core research is the use of ^{10}Be as a proxy for accumulation rate. The "^{10}Be method" is based on the assumption that the ^{10}Be flux to the ice-sheet surface is approximately constant, such that changes in ^{10}Be concentration are inversely proportional to the ice flux or accumulation rate, $\dot{b}$; that is

$$[^{10}Be] = \frac{F}{\dot{b}} \tag{14}$$

Particularly notable is the application of Equation 14 to the Vostok ice core record; Raisbeck et al. (1987) showed that accumulation rates from ^{10}Be concentrations correlate remarkably well with stable isotope (δD) values, which are also believed to closely mirror accumulation rates in that core (Figure 6.1). While more up-to-date estimates of the age-depth relationship in the Vostok core (Jouzel et al., 1993; Sowers et al., 1993) show that the

assumption of a constant ^{10}Be flux (F) is unlikely to be strictly correct, it seems clear that accumulation rate is the dominant factor affecting ^{10}Be concentrations at Vostok, and probably in most other ice cores as well. The only significant exception to this general rule is during two periods of apparently enhanced ^{10}Be production, which may relate to geomagnetic field reversals or possibly to supernovae (McHargue et al., 1995a). The periods of enhanced production occur as spikes in the Vostok records at about 37.5 ka and 64 ka on the Jouzel et al. (1993) timescale. These are correlated with similar spikes in the Taylor Dome record on the Std_Time_9507 timescale (Figure 6.2). Because these spikes are not believed to be associated with changes in accumulation rate, I have removed them for all calculations made in this chapter.

In spite of its complications, the ^{10}Be method is important because for most ice cores there is no straightforward way to determine accumulation rates independently. Indeed, even for the high-resolution cores at Summit, Greenland, where the annual layer thickness profile is known quite accurately (Alley et al., 1993), accumulation-rate estimates are dependent on knowledge of the vertical thinning rate. Inherent limitations to the accuracy of ice-dynamics models means that the annual layer thickness cannot be uniquely inverted for accumulation rate (Weertman, 1993). While the error may be insignificant for the upper few hundred meters of a typical deep ice core, it may become very large near the bed. In the Taylor Dome ice core an independent geochemical method for determining

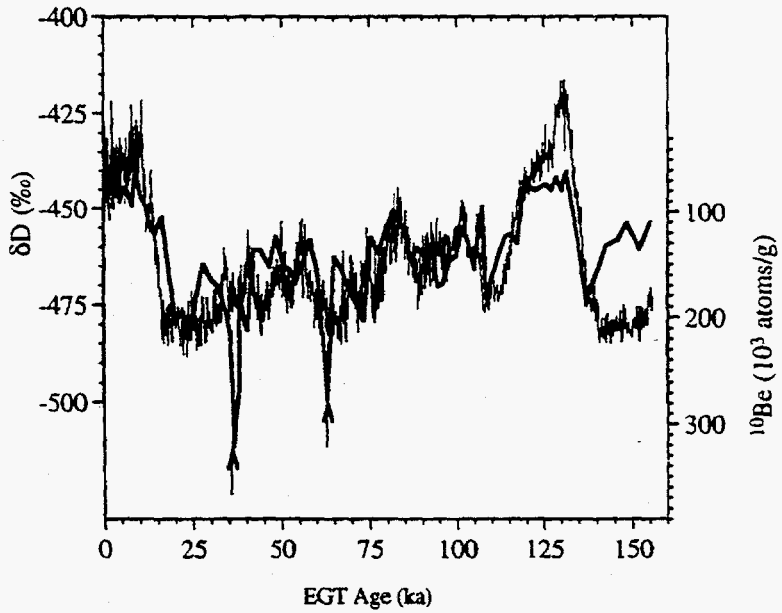

Figure 6.1 δD (Jouzel et al., 1987; light line) and ^{10}Be concentrations (Raisbeck et al., 1987; bold line) in the Vostok Core, on the EGT timescale (Jouzel et al., 1993), illustrating coherence of the two records. Higher concentrations of ^{10}Be and lower δD values are expected during times when acumulation rates are low. Arrows indicate times of apparent enhanced ^{10}Be production (see text).

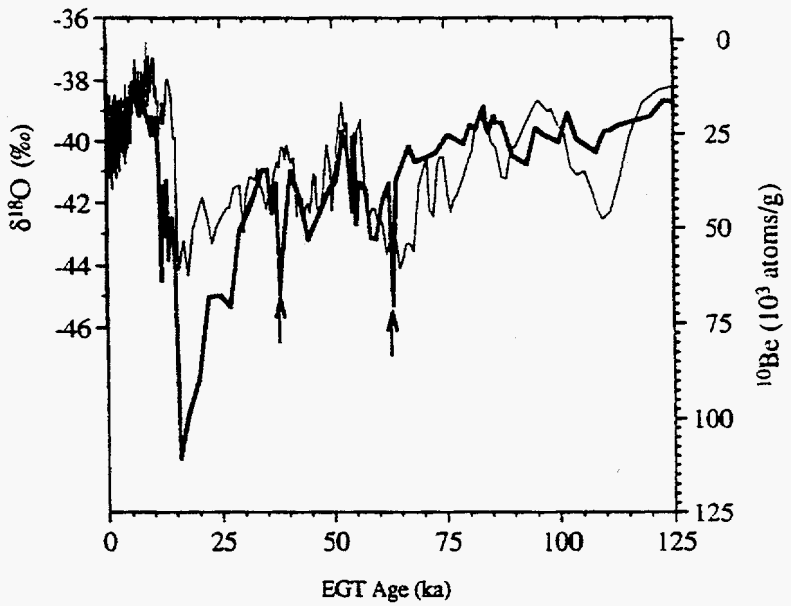

Figure 6.2 $\delta^{18}O$ (light line) and ^{10}Be concentrations (bold line) in the Taylor Dome core, on the STD_Time_9507 timescale. Arrows as in Figure 6.1.

accumulation rate is essential because most of the pre-Holocene part of the core lies within only 150 meters of the bed.

If we wish to use ^{10}Be as a proxy for accumulation rate, a more sophisticated approach is needed than the simple assumption of a constant flux. In particular, we need to consider the changing concentration of ^{10}Be in the troposphere, and to take into account both the the wet and dry deposition components of the atmosphere-to-ice-sheet flux. In this chapter, I discuss the relationship between ^{10}Be deposition mechanisms and snow accumulation rates in the context of data from snow pit and shallow firn cores at Taylor Dome. Combining these data and the model results presented in Chapters 4 and 5, I use the ^{10}Be profile from the Taylor Dome deep core to determine the accumulation-rate history. While the results cannot be considered definitive, they provide a realistic 'best estimate' which will be useful as input for ice-flow modeling efforts and in establishing an independent timescale for the core.

6.2 Relationship between accumulation rate and wet and dry flux parameters

The total flux, F of ^{10}Be to the ice sheet surface is the sum of the "wet" and "dry" fluxes

$$F = F^W + F^D \tag{15}$$

By definition, the dry flux, F^D is independent of the snow accumulation-rate, $\dot{b}$, while F^W is a linear function of $\dot{b}$. The wet and dry fluxes are related to the mixing ratio of ^{10}Be in the atmosphere by

$$F^W = W\chi\dot{b} \tag{16}$$

$$F^D = \upsilon_d \chi \rho_{air} \tag{17}$$

where υ_d is the dry deposition velocity (cm a^{-1}), W is the dimensionless wet scavenging ratio, ρ_{air} is the density of air, and χ is the mixing ratio of ^{10}Be in the atmosphere (atoms g^{-1}). From (16) and (17), the concentration of ^{10}Be in a polar ice core is related to the snow accumulation rate and the atmospheric mixing ratio by

$$\left[{}^{10}Be\right] = \chi\left(W + \frac{\upsilon\rho_{air}}{\dot{b}}\right) \tag{18}$$

To determine the value of υ_d and W, I measured ^{10}Be concentrations in a series of firn cores and snow pits at Taylor Dome. Comparison of the accumulation rate at each site with the total ^{10}Be flux allows us to estimate the dry deposition flux, if we assume that the atmospheric mixing ratio (and the dry deposition flux) is uniform over the spatial area considered.

Although Legrand (1987) has questioned the validity of this approach when applied to a large geographic area, Taylor Dome has the advantage of strong spatial gradients in meteorological conditions over a relatively small area (Waddington and Morse, 1994). Each of the snow-pit and core samples are averages over at least 20-30 years of accumulation, making it unlikely that the assumption of a uniform dry deposition flux is in error.

Snow accumulation rates range from about 15 g $cm^{-2}a^{-1}$ 10 km south of the drill site, to less than 2 g $cm^{-2}a^{-1}$ in the upper reaches of Taylor Glacier 30 km to the north (Grootes and Steig, 1992). Table 6.1 summarizes the results of ^{10}Be measurements in surface snow at Taylor Dome, along with accumulation rates from each location (see also Chapter 2).

Figure 6.3 shows the total ^{10}Be flux ($[^{10}Be] \times \dot{b}$) as a function of accumulation rate. The intercept of the regression line through the data gives $1.04 \pm 0.2 \times 10^5$ atoms $cm^{-2}a^{-1}$ for the dry deposition flux, while the slope of the regression gives the average concentration in fresh snow $[^{10}Be]_{wet} = 7.5 \pm 0.2 \times 10^3$ atoms/g. Although the correlation is not high, these values agree with previous estimates for East Antarctica, and imply that dry deposition accounts for between 50% and 75% of the total flux of $\sim 1.4 \times 10^5$ atoms $cm^{-2}a^{-1}$. A single measurement from fresh snow, which fell on blue ice on lower Taylor Glacier, and was collected within two days of having fallen, gives a value for $[^{10}Be]_{wet}$ of only 9.9×10^2 atoms/g, suggesting that the regression analysis may overestimate the importance of wet deposition.

Table 6.1 Comparison of accumulation rates and ^{10}Be concentrations at Taylor Dome.

Location	^{10}Be concentration (10^3 atoms g^{-1})	Accumulation rate (g $cm^{-2}a^{-1}$)
Taylor Dome		
20N	152.2	1.23
Taylor Mouth	28.10	2.26
10C	32.12	3.02
Drill Site	21.32	7.60
20S	26.23	7.86
20C	18.23	6.71
10S	14.32	15.0

From the given values for F^W and F^D, we can estimate v_d and W from the measured mixing ratio of ^{10}Be in the polar troposphere. Using a mean value of 5×10^4 atoms/$_{m^3\ STP}$ for χ (Raisbeck and Yiou, 1985; Harder, personal communication, 1995) and Equations 16 and 17, the regression analysis gives $v_d = 0.07$ cm/s and $W = 260$. If we assume that the lower value of 9.9×10^2 atoms/g is correct for $[^{10}Be]_{wet}$, we obtain 0.1 for v_d and ~30 for W.

6.2.1 *Comparison with values determined for sulfate and nitrate.*

Although there have been no direct measurements of wet and dry deposition parameters for ^{10}Be specifically, deposition of ^{10}Be occurs in association with the other more common aerosols. Beryllium atoms,

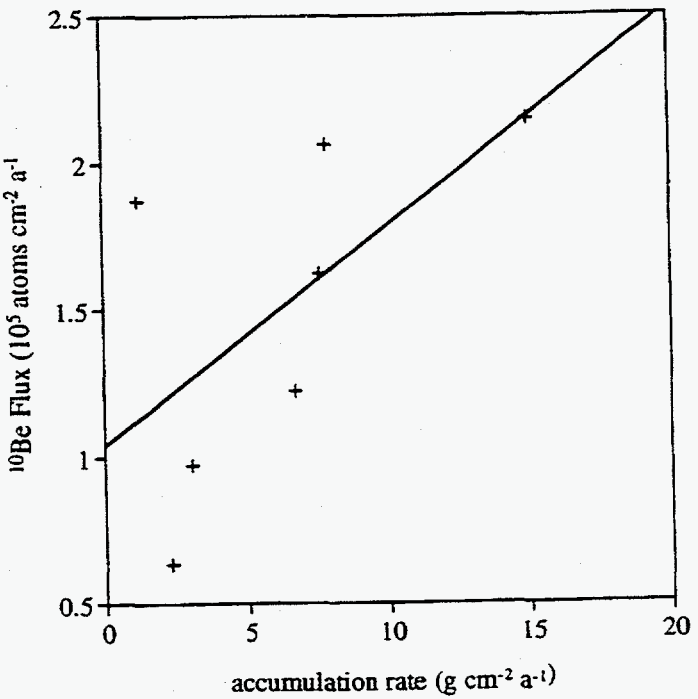

Figure 6.3 Total ^{10}Be flux at Taylor Dome, as a function of accumulation rate.
Line shows linear best-fit (F = 0.075 b + 1.04).

which have a 2+ valence state, are generally assumed to be associated with sulfate (SO_4^{2-}), which is the most common aerosol in both polar regions. It is highly probable that ^{10}Be is also associated with nitric acid (HNO_3), which is the most important cloud condensation nucleus in the polar stratosphere. The compounds $BeSO_4$ and $Be(NO_3)_2$ are both highly soluble in water (Lide, 1992). In Antarctica, sulfate and other sulfur compounds accounts for 70-80% of the aerosol mass (Shaw, 1989). A reasonable approach for determining the depositional behavior of ^{10}Be is therefore to examine the behavior of sulfate aerosol.

Davidson et al. (1985) at Dye 3, Greenland, and Ibrahim et al. (1983) in North America show that the dry deposition velocity for SO_4^{2-} is between 0.039 and 0.16 cm/s. From measurements at the ATM site in central Greenland, Bergin et al. (1994) obtained comparable values (0.027 ± 0.015 cm/s) at the low end of this range. [21] For Antarctica as a whole, Legrand (1987) used the same kind of $\dot{b}$-F plot I used for ^{10}Be, and obtained similar values for SO_4^{2-} (60 % dry deposition for $\dot{b} = 6.5$ g cm^{-2}a^{-1}). For wet deposition of SO_4^{2-} Davidson et al. (1989) report a value of 180±120 at Dye 3. For Antarctica, Legrand's $\dot{b}$-F calculation gives $F^W/F^{total} \sim 30\%$ for SO_4^{2-}, again comparing favorably with my results for ^{10}Be.

Taken together, the ^{10}Be and SO_4^{2-} are compatible. In general, the results are higher than indicated by the estimate for W suggested by the single measurement from fresh snowfall; clearly more fresh snowfall data are needed. Until such data are available, it is prudent to consider the

plausible range of values for ^{10}Be, rather than adopting a single mean value. Thus, in calculations of accumulation rate from ^{10}Be data, ranges of $\upsilon_d = 0.05 - 0.1$ and $W = 30 - 260$ seem reasonable.

6.3 Determination of accumulation rate in the Taylor Dome core.

From Equation 18, we can determine the accumulation rate an an arbitrary depth, z, in an ice core using

$$\dot{b}(z) = \dot{b}_0 \left(\frac{\chi(z)}{\chi_0} \right) \left(\frac{\upsilon(z)}{\upsilon_0} \right) \left(\frac{[^{10}Be]_0 - W_0 \chi_0}{[^{10}Be](z) - W(z)\chi(z)} \right) \qquad (19)$$

where the subscript $(_0)$ denotes measured modern (surface) values. At present, we must assume that the values of υ_d and W are temporally constant (that is, constant with depth in the core). Although this assumption may be in error (Cunningham and Waddington, 1993; Harder et al., 1996), our current knowledge of these parameters is too limited to justify a more sophisticated analysis. Furthermore, there is some empirical evidence for the validity of this assumption, at least for ^{10}Be if not for other chemical constituents in the atmosphere (Alley et al., 1996).

Initially, I assume also that χ is temporally constant, as supported by evidence that geomagnetic field variations and atmospheric circulation

change should not impart large fluctuations to the mixing ratio of ^{10}Be in the polar troposphere (Chapters 4 and 5). Equation 19 thus reduces to

$$\dot{b}(t) = \dot{b}_0 \frac{\left[{}^{10}Be\right]_0 - W\chi}{\left[{}^{10}Be\right](t) - W\chi} \tag{20}$$

Note that the assumption that W and v_d are constant allows us to eliminate v_d, but not W, from Equation 19.

Figure 6.4 shows the accumulation rate at Taylor Dome as determined from Equation 20 using values of 30 and 265 for W. For comparison, the $\delta^{18}O$ profile is also shown. Figure 6.4 suggests that the ^{10}Be profile at Taylor Dome is a fairly robust indicator of accumulation rates, given the assumed range of values for W. This is a rather fortuitous result; during the Holocene, where the calculated accumulation rate is relatively sensitive to W, the ^{10}Be concentration does not change by more than 20 % during most of this time period. On the other hand, during the cold, dry conditions prior to the Holocene, accumulation rates are so low that the effect of wet deposition is almost negligible. The only significant exception is over the depth range 250-270 m. There, very low ^{10}Be concentrations (10^4 atoms/g) imply particularly high accumulation rates, especially for the larger value of W.

The $\delta^{18}O$ profile provides a qualitative test of the accumulation-rate calculations. Making the reasonable assumption that $\delta^{18}O$ is correlated with temperature and accumulation rate, we find that the general decline

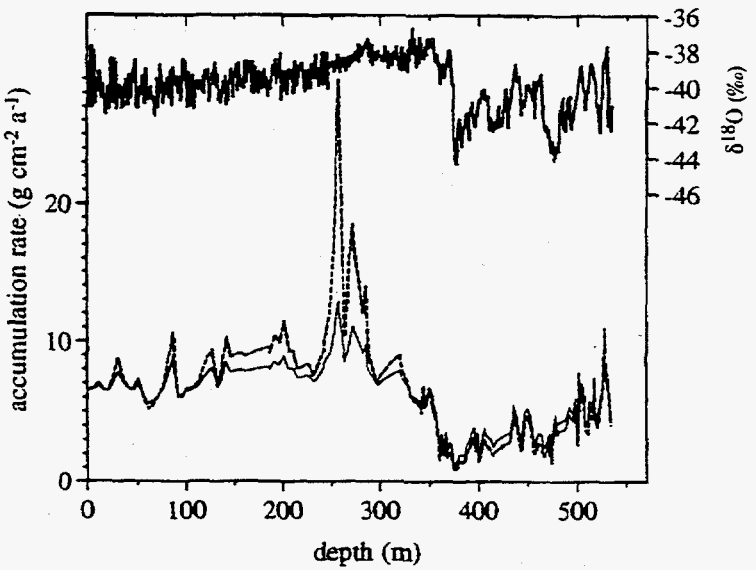

Figure 6.4 Accumulation rates at Taylor Dome as calculated from Equation 6 for different values of the wet deposition scavenging ratio, *W*. *Dashed line: W =260; solid line W = 30.* Uppermost curve shows $\delta^{18}O$ profile for comparison.

in $\delta^{18}O$ values since the early Holocene is consistent with the parallel decline in calculated accumulation rates. Note, however, that the correlation is not high enough to warrant the kind of comparison made by Lorius et al. (1989), who assumed that stable isotope (δD) values in the Vostok core *directly* reflect accumulation rate via the saturation vapor pressure relationship discussed by Robin (1977). Notably, $\delta^{18}O$ shows no marked change during the 250-270 meter interval, suggesting that the accumulation rates calculated for $W = 265$ are probably unrealistically high and that a lower value for W may be more reasonable. At present, we cannot completely rule out the possibility that either (1) accumulation rates at 250-270 meters were actually very high or (2) the low ^{10}Be concentrations at this depth interval reflect atmospheric circulation or production-rate variations. Detailed comparison with other ice-core ^{10}Be records may offer a way to address this question.

6.3.1 *Accounting for changes in* χ

Accounting for production rate and atmospheric circulation change in the accumulation-rate calculation is problematic. To first order, it is probably quite reasonable to ignore such effects when considering Antarctic ice cores. As discussed in the previous chapter, there is some evidence that geomagnetic field strength varations should introduce variability of only a few percent to the concentration of ^{10}Be in the polar atmosphere (Steig et al., 1996). Because of the relative isolation of Antarctica from the rest of the

global atmosphere, we also do not expect atmospheric circulation changes to have a large effect. Finally, while the effect of solar variability on the polar ^{10}Be flux is large over short time scales, averages over a few centuries should eliminate both of the dominant known periodicities in solar modulation, the 11-year Schwabe and 88-year Gleissberg cycles. While longer-period variations cannot be ruled out, there is at present no evidence to suggest that this is a significant concern. On the other hand, it is precisely during times of major climate change, such as the glacial-interglacial transitions, when possible small changes in the atmospheric concentration of ^{10}Be become important. For example, Sowers et al. (1993) provide evidence from time-scale correlation arguments that the ^{10}Be flux at Vostok was 20% higher at about 15 ka, a time period corresponding both to greatly reduced accumulation rates and to increased global production of ^{10}Be.

A conservative approach then, is to include a maximum and minimum plausible estimate of χ in our calculation of accumulation rate. To do so, I combined geomagnetic field variation data (Figure 4.2) with the given range of plausible values for W and v_d, using Equation 19. Although atmospheric circulation changes are not explicity taken into account, they are implicit in the consideration of both the maximum and minimum expected effects of geomagnetic field strength, since atmospheric circulation determines the contribution of low-latitude (geomagnetically

modulated) ^{10}Be to the total ^{10}Be flux. The resulting envelope of plausible accumulation-rate values is shown in Figure 6.5.

Comparison of Figures 6.4 and 6.5 suggests that production-rate variation does not introduce as much uncertainty to the ^{10}Be method as does the sensitivity to the values adopted for W and v_d. Although the Tric et al. (1992) geomagnetic record is just one of several production-rate proxies that could have been used, the coherence of the geomagnetic signal in many sediment cores suggests that the accuracy of the approach I use here is reasonable, and that it can be improved as the geomagnetic record becomes better defined (Weeks et al., 1995).

6.4 Discussion: reliability of the ^{10}Be method

The extent to which we can use the ^{10}Be method to determine accumulation rates depends on the reliability of our independent records of geomagnetic field strength and solar variability, and our knowledge of atmospheric circulation processes. As discussed in Chapter 4, atmospheric circulation changes are unlikely to have had a significant effect during the Holocene (i.e. the last ~10 ka) but could have sizeable effect during major shifts in climate. This, and the possibility that increased wind speeds could greatly enhance dry deposition velocities, are probably the largest sources of uncertainty in the method (Harder et al., 1996).

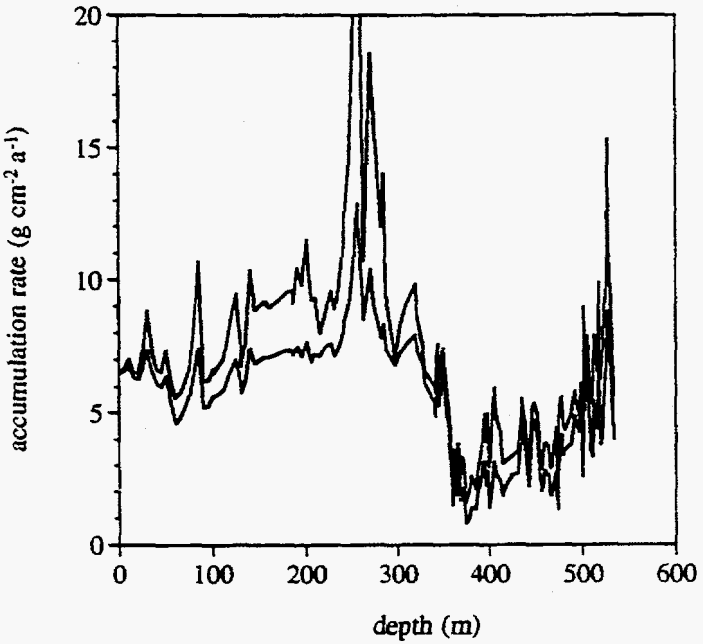

Figure 6.5 Maximum and minimum envelope of plausible values for accumulation rates at Taylor Dome, assuming that υ_d is constant, but that$W$ can vary between 260 and 30, and χ varies within maximum bounds given by the global average ^{10}Be production rate (cf. Figure 4.2).

The calculations presented in this chapter suggest that under favorable circumstances the ^{10}Be method yields reliable determinations of accumulation rate, particularly if good estimates are available of the wet-deposition scavenging ratio. For ice-core drilling sites such as Vostok, or during cold climatic periods at locations such as Taylor Dome, the very low accumulation rates actually enhance the reliability of the method because the wet deposition flux becomes less important. Moreover, their is evidence that production-rate variability should not introduce large errors to Antarctic ice-core records (Steig et al., 1996; Raisbeck et al., 1987). Comparison among different ice-core records of ^{10}Be, the explicit incorporation of ^{10}Be in atmsopheric general circulation models, and continued measurement of ^{10}Be concentrations in surface snow and air in Antarctica, should permit us to improve considerably the reliability of the ^{10}Be method. It should be reiterated that the ^{10}Be method provides an independent check on ice-flow modeling estimates of accumulation rate and, as such, is useful even for high-resolution cores where annual layer thicknesses can be determined directly from annual $\delta^{18}O$ or 11-year ^{10}Be cycles.

Notes to Chapter 6

21. At GISP2, Bergin et al. (1994) found that fog deposition accounts for a significant amount of the total flux during summer. Because the water deposited during evening fog events frequently re-evaporates quantitatively the following day, the fog flux would be considered as part of the "dry" flux on an accumulation rate vs. total flux plot such as Figure 6.2. Bergin et al.'s calculations of dry flux are empirical, and not taken from a *b*-F plot. In Antarctica, fog deposition is not expected to be significant.

Chapter 7

ON THE USE OF ^{10}BE TO DETERMINE ANNUAL-LAYER THICKNESSES IN ICE CORES

7.1 Introduction

Accurate dating of ice cores is one of the fundamental problems in ice-core research. In favorable cases, high accumulation rates have enabled researchers to determine ages to high precision, using direct counting of visible annual layers (Alley et al., 1993) or seasonal $\delta^{18}O$ cycles (Hammer et al., 1986). For many ice cores, however, low snow-accumulation rates preclude the preservation of the seasonal patterns that permit annual layer counting. In these cases, age control is usually achieved by correlation with other better-dated ice cores or through numerical ice-flow models. Both of these approaches, however, are limited in accuracy. The most rigorous correlation method uses the global signature of gas concentrations, but such correlations are unlikely to resolve differences smaller than about 1500 years, largely because of uncertainty in the age difference between the ice and the air that is trapped in it (Sowers and Bender, 1995). For ice-flow models, results are sensitive to boundary conditions such as accumulation rate and ice-sheet configuration in the past (Reeh, 1989). It would be useful, therefore, from the point of view of ice-core dating, to develop an alternate method for determining annual layer thickness. In this chapter, I present a novel approach to this problem: I suggest that in place of the high-frequency

(seasonal) variability of ice-core chemistry, we can take advantage of the low-frequency periodicities present in the production of cosmogenic isotopes in the atmosphere. In particular, I propose that the 11-year solar modulation cycle in ^{10}Be production can be used to determine layer thickness directly, even for ice cores where the accumulation rate is too low to preserve annual layering.

7.2 Principles of the method

Essentially, the proposed method assumes that the well-known Schwabe sunspot cycle has persisted over long periods of time, and is reflected in the deposition rate of ^{10}Be at the earth's surface. On average, the Schwabe cycle is 10.8 years in length, but may vary by ±1 year, placing a practical limit of ~10% on the precision of the method. Having established the '11-year thickness' at various depths in an ice core, one can interpolate the data to obtain an estimate of the layer thickness at arbitrary depths in the core. If ^{10}Be is measured continuously and at high resolution along the core, this method is independent of ice-flow and accumulation rate estimates. However, the amount of ice needed per sample (about 500 g) is likely to be prohibitive; in practice, ^{10}Be measurements must be used in concert with, and as a refinement to, independent determinations of vertical strain-rate conditions and of the accumulation-rate history of the ice core.

For the proposed method to work, the 11-year solar cycle must have existed throughout the time period of interest in ice-core research, that is the last 10^3 to 10^5 years. The existence of the 11-year cycle is known from historical records of aurora observations and sunspots to have existed for the last several hundred years (Stephenson and Clark, 1978; Eddy, 1988). A strong apparent 11-year cycle in pre-Cambrian rhythmites was at one time thought to have been proof of the long-term stability of solar periodicities (Williams, 1981), but it has since been shown that the rhythmites are not annual and that the cyclicity is of tidal (lunar) origin (Sonett et al., 1988, G.E. Williams, pers. comm., 1995). While a near-constant length solar cycle is expected from theoretical considerations in astrophysics, it has not been demonstrated convincingly (Soderblom, 1988). For periods prior to the last few centuries, the assumption of 'solar uniformitarianism' (Eddy, 1988) must therefore be considered a working model.

If the assumption of a persistent 11-year cycle is correct, then we can rely on the well-established anti-correlation between solar activity and the production of ^{10}Be in the atmosphere. Over a typical 11-year cycle, solar modulation of the cosmic-ray flux results in a global average variation in ^{10}Be production of ±10 %, with a larger variation (±30%) in polar regions. This periodicity is reflected in deposition of ^{10}Be at the earth's surface which occurs within one or two years following production. In Greenland, ^{10}Be deposition appears to reflect global average production-rate variations (Beer et al., 1990); in Antarctica, the deposition-rate signal has a larger amplitude,

probably reflecting the greater isolation of polar air masses in the southern versus northern hemispheres (Chapter 5). From high-resolution measurements in the Dye 3 (Greenland) ice core, we know that ^{10}Be deposition has followed an 11-year cycle for at least the last 250 years (Attolini et al., 1988; Beer, et al., 1990).

7.3 Detection of the 11-year cycle in ^{10}Be data at Taylor Dome

I measured ^{10}Be in detail to establish the 11-year layer thickness at three depth intervals in the Taylor Dome core: 49.12-51.25, 298.5-300.6 and 340.5-341.5 meters, in a 4-m-deep snow pit within 100 m of the drill site, and in a firn core 20 km from the drill site (*40S* in Figure 2.2). As discussed in Chapter 5, the data from the 4-m snow pit agree well with the data from the firn core; here I discuss only the results from the firn core, which cover a greater period of time (about 75 years). The Wisconsin-Holocene transition occurs at a depth of 374 m in the Taylor Dome core. All of the measured sections fall within the Holocene, during which the accumulation rate is expected to have changed little.

Each section was analyzed at a resolution of ~10 samples/meter, except the 340.5-341.5 meter section which is at 20 samples/meter. For simplicity I have converted all depths to ice-equivalent using the measured ice-core density profile (Table 2.1). I refer to each section for which ^{10}Be was analyzed

by its nominal ice-equivalent depth: "surface," "33" "278," and "320." Figure 7.1 shows the results; as expected from thinning due to ice flow, there is an increase in the wave number for ^{10}Be variation from about 1 cycle per meter in the upper two sections to multiple cycles per meter at greater depth.

As a statistical method for determining a "best estimate" of the 11-year thickness, I applied spectral analysis in the depth domain to the ^{10}Be data in Figure 7.1. To identify spectral peaks, I use the maximum entropy method (M.E.M, Burg, 1967) with a constant auto-regressive (AR) order of 9. Use of a relatively high AR order (slightly less than $1/2$ the number of data points in the 33, 278 and 320 meter sections) is appropriate because it tightly constrains the frequency, which is of primary interest. The amplitude of spectral peaks determined in this way is not a reliable indicator of significance (compared with, for example, the conventional Fourier-transform approach; Jenkins and Watts, 1968); however, we assume *a priori* that there is no other production-rate frequency near 0.09 a^{-1} (i.e. the 11-year cycle) so that identification of the 'correct' wave number should be unambiguous unless there are confounding meteorological factors affecting the ^{10}Be deposition rate.

For the surface measurements we can translate the depth domain to the time domain, using the 1954 and 1964 ß-decay bomb horizons peaks for a timescale (Chapter 5) and assuming that the accumulation rate is constant. The resulting time series has an average sampling frequency of 0.7 a^{-1}; it displays a clear 11-year periodicity (Figure 7.2) with a strong 0.09 a^{-1} peak.

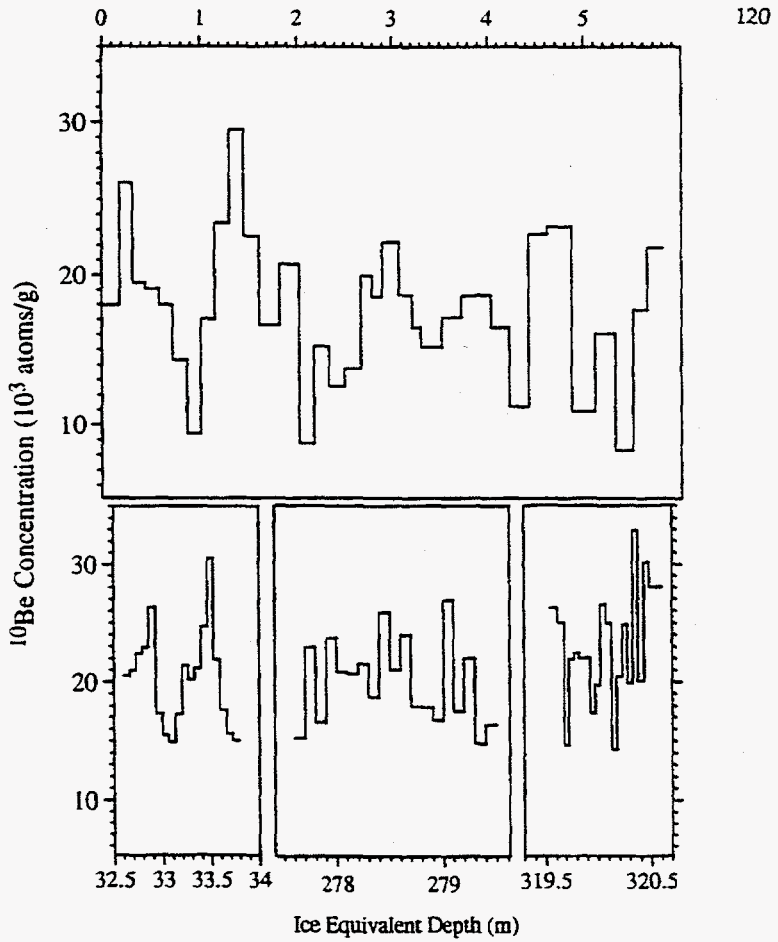

Figure 7.1 ^{10}Be data from firn and ice cores at Taylor Dome vs. ice-equivalent depth. Bold labels refer to the nominal depths referred to in the text.

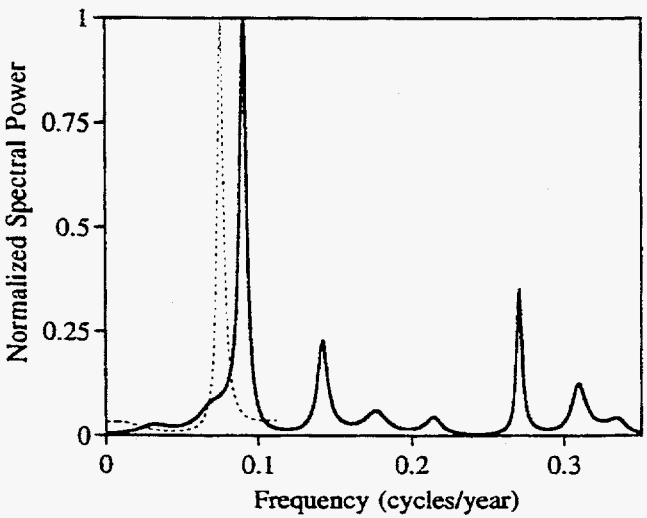

Figure 7.2 Frequency spectrum of the surface interval ^{10}Be data. Dotted line shows results obtained when data is re-sampled at low resolution (see text for details).

Note that because the samples represent continuous averages, rather than discrete points, aliasing of higher frequencies is reduced and the spectral estimate is quite reliable. For example, if we re-sample the data numerically at lower resolution (0.25 a^{-1}), the 11-year cycle can be identified even very close to the Nyquist frequency although the analysis underestimates the frequency by about 7 %. This observation is important because it turns out that layer thinning in the lower part of the core is so great that the 278 and 320 meter sections were analyzed at quite low time- resolution.[22]

Figure 7.3 shows the MEM results for all sections measured, normalized to ice-equivalent thicknesses and depths. As already noted above, the surface section yields a peak in the data at ~1.3 m^{-1}, corresponding to the 11-year solar cycle. At 33 meters, there is a sharp spectral peak at 1.4 m^{-1}; the absence of low wave numbers in this section is in part a result of the short interval analyzed (about 20 years). For the 278 and 320 meter sections, interpretation is not as straightforward because both data sets yield several spectral peaks. It is tempting to associate the highest-wave-number peak in each case with the 11-year cycle because doing so yields an increasing wave number with depth that is in general agreement with expectations from ice-flow modeling; this association yields 4.7 and 8.2 m^{-1} at 278 and 320 meters respectively.

If we assume that we have correctly identified the 11-year cycle for each section, we can calculate the annual-layer thickness λ, from

$$\lambda(z) = \frac{1}{11 f(z)} \qquad (21)$$

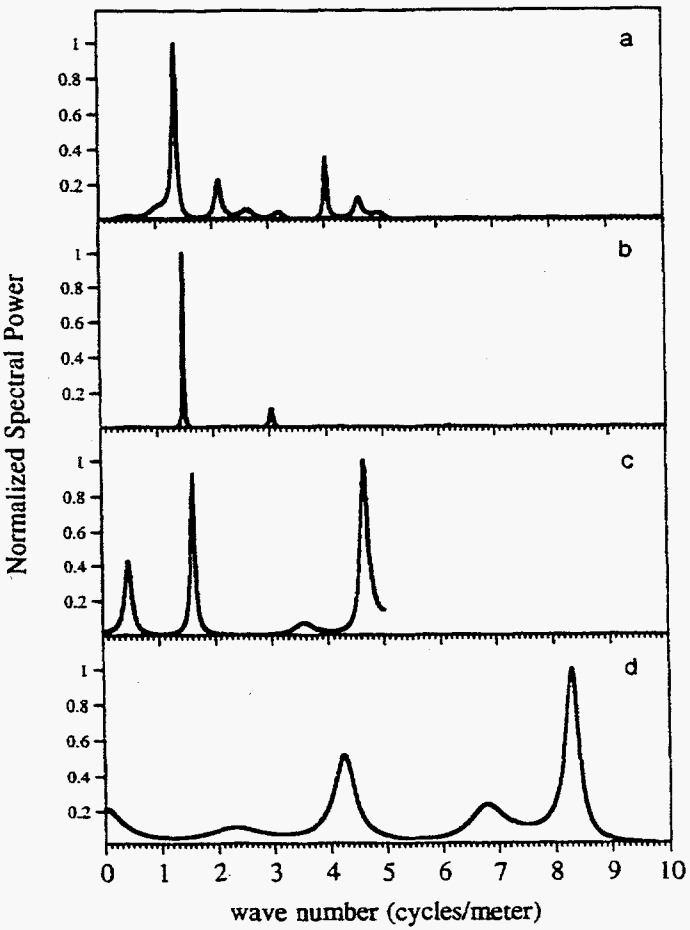

Figure 7.3 Wave numbers for the ^{10}Be data in Figure 7.1. Nominal depth intervals are a) surface, b) 33, c) 278 and d) 320 meters.

where f is the cycle wave number (m^{-1}) and z is depth, and where it is assumed that 1) the 11-year cycle is identified by the mid-point wave number of the chosen spectral peaks, 2) the cycle has a fixed length of exactly 11 years. Figure 7.4 shows the annual-layer thickness determined from Equation 21 as a function of depth in the Taylor Dome core, under the assumptions noted. Also shown are annual-layer thicknesses predicted from two simple flow models, which both assume a constant accumulation rate. The simplest model, often referred to as the Nye model, additionally assumes that the vertical strain rate is constant with depth. At an ice divide, the vertical strain-rate may be assumed to decrease nearly linearly with depth (Raymond, 1983); I refer to this assumed strain-rate curve as the "Raymond" model. It is expected that the Taylor Dome drilling site, located about 1 ice-thickness from the ice divide, should fall between these two models.

From Figure 7.4, it is readily apparent that assignment of the lower-wave-number spectral peaks in Figure 7.3 to the 11-year cycle gives unreasonable results. For example, selection of the second-largest peak at 278 meters would imply that almost no thinning has occurred between 33 meters (6 % of the total ice thickness) and 278 meters (53 %), unless the original layer thickness was about five times greater for the section at 278 meters; such a large change in accumulation rate is unlikely because all the measured sections are in Holocene ice (Chapter 2, 4, 6).

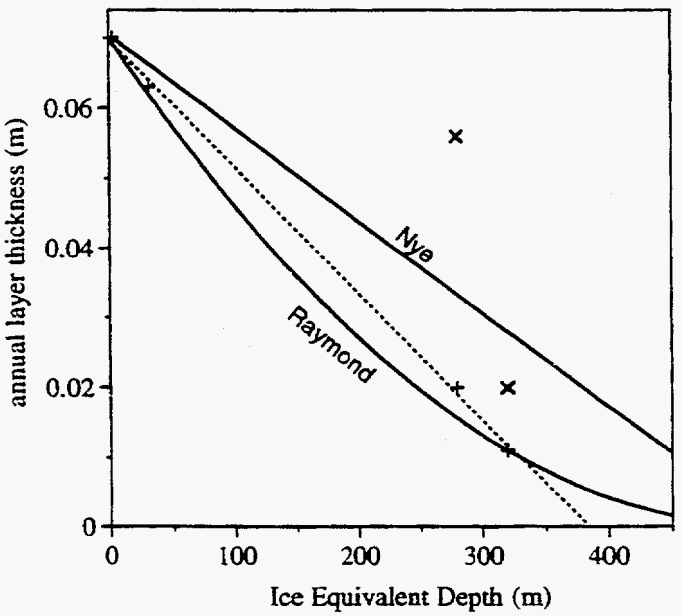

Figure 7.4 Estimates of annual layer thickness as a function of depth in the Taylor Dome core. "Raymond" and "Nye" refer to end-member models (see text). Crosses and plus-signs show maximum and minimum estimates, respectively, from spectral analysis of the ^{10}Be data.

7.4 Validation of the method: comparison with other proxy data

If the annual-layer thicknesses calculated above are correct, then we should be able to make certain predictions about the spectral behavior of other properties measured in the Taylor Dome core. First, we postulate that periodicities in the ^{10}Be data that are *not* associated with known solar cycles probably reflect meteorological variability, and should therefore appear in the spectra of accepted "climate" proxy data such as $\delta^{18}O$. Second, if there are any characteristic periodicities in the climate proxies, these should appear as spectral peaks at a constant frequency (in the time domain). The corollary to these predictions is that the 11-year cycle should not appear in the climate proxy data if, as I assume, it actually reflects production rate variations.

At present, the only properties which have been measured in the Taylor Dome core at comparable resolution to ^{10}Be are electrical conductivity (ECM) and, for the upper section only, $\delta^{18}O$ (see Chapter 2). Figure 7.5 shows the $\delta^{18}O$ and ECM spectra compared with those of ^{10}Be, both as functions of the cycle length in years, where I have assumed that the 11-year cycles have been correctly identified as described above. In constructing this graph, I numerically re-sampled the 5-mm-resolution ECM data at the same sampling frequency as the ^{10}Be data (i.e. 0.10 and 0.05 m averages). The sampling interval for $\delta^{18}O$ is 0.10 m, as for ^{10}Be. The MEM routine was applied over 20-meter intervals centered on the depth of interest. Note that

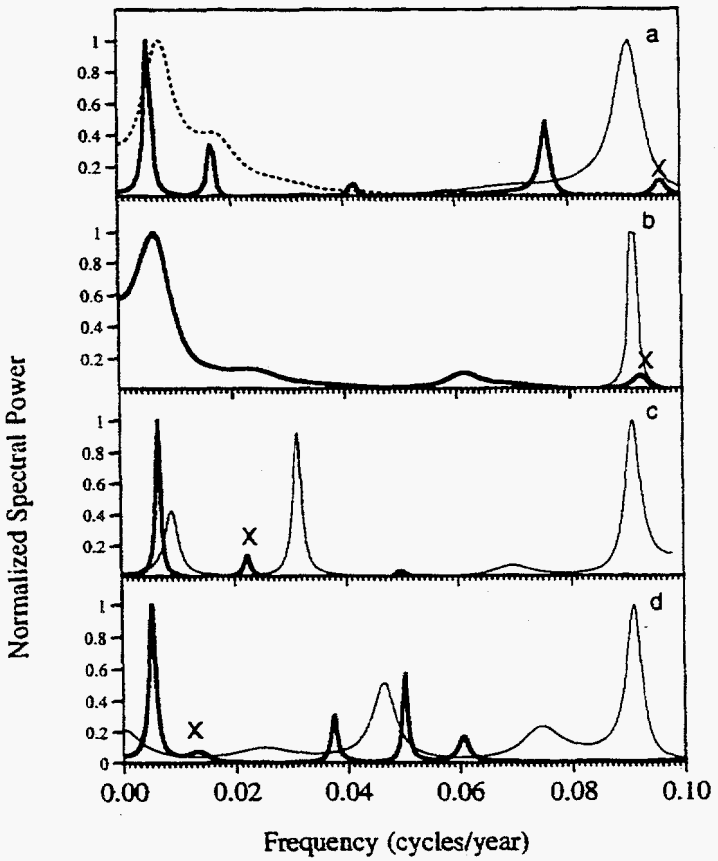

Figure 7.5 Frequency spectra for ^{10}Be (bold) and ECM (thin) for each of the depth intervals discussed in the text. Dashed line shows spectrum for $\delta^{18}O$ in the surface interval. Small x's denote frequencies in the ECM spectra that are artefacts of the 1-meter sampling interval. Nominal depths are a) surface, b) 33, c) 278 and d) 320.

some of the spectral peaks in the ECM data are artifacts of the ECM analysis, which is sensitive to the temperature of the ice core at the time of measurement. These peaks, which coincide to a wave number of 1.0 m^{-1} (the length of a core section) are marked with a small "x" in Figure 7.5.

The MEM analysis of the climate proxy data appears to support the first prediction, that 'spurious' periodicities in the ^{10}Be spectra should coincide with periodicity in the climate proxy data. Although not all ^{10}Be frequencies can be accounted for, there is an arguably correspondence between the 0.04 a^{-1} frequency in the ^{10}Be at 320 meters and the clustering of spectral peaks in the ECM data.

The second prediction, that translation to the time domain should yield peaks of constant frequency in climate proxy data, also appears to be supported. There is a low-frequency peak in ECM at all depths, with an average frequency of 0.006 a^{-1} and a small standard deviation of ±12%. The large low-frequency peak, in contrast, appears also in the $\delta^{18}O$ data, showing that it is not an artifact of the ECM analysis, but reflects a real periodicity of climate.

At Taylor Dome, neither the $\delta^{18}O$ nor the ECM data show a spectral peak with a period at or near 11 years. This contrasts with recent evidence in the northern hemisphere: analyses of both $\delta^{18}O$ (Stuiver et al., 1995) and soluble ions (P. Mayewski, pers. comm., 1995) in the GISP2 core show that a strong 9–12 year periodicity exists in Greenland ice-core climate data, apparently in phase with, or slightly leading, the 11-year solar cycle.

7.5 Validation of the method: comparison with ice-flow modeling results

As a first-order model for glacier flow, I assume that horizontal flow deformation is confined to a lower layer, below some characteristic height, h, above the bed, and that the horizontal strain rate, $\frac{\partial u}{\partial y}$, in this layer is constant. If the ice is frozen to the bed, the horizontal velocity increases linearly from 0 at the bed to some value u_s at height h. Above this layer, which deforms by *simple shear*, the ice experiences plug flow such that $\frac{\partial u}{\partial y} = 0$, $u = u_s$ and there is *pure shear* only (vertical compression of layers). This 2-D approximation (Figure 7.6) was used to determine the age-depth relationship in the Dye 3 core, southern Greenland (Dansgaard and Johnsen, 1969), and is known as the Dansgaard-Johnsen model; it is probably the most appropriate model to use in the absence of contradictory evidence (Reeh 1989). If the accumulation rate is constant, we can use the horizontal velocity profile to calculate annual layer thickness:

$$\lambda(y) = \frac{1}{\bar{u}} \int_0^y u dy \qquad (22)$$

Note that by convention (e.g. Paterson, 1983) y denotes height (positive upward) above the glacier bed; I use it here also to distinguish from depth, z

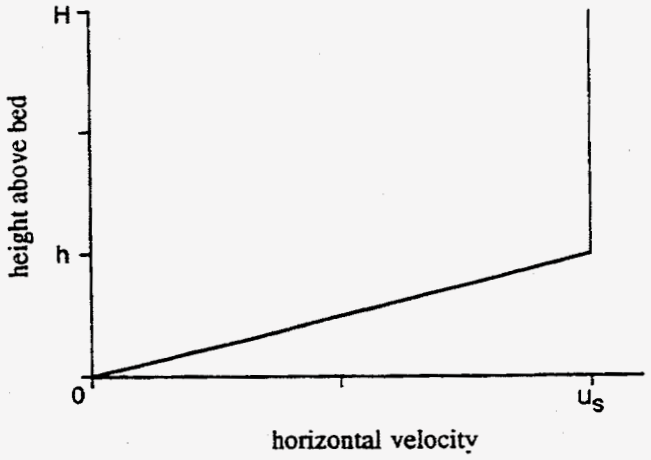

Fig 7.6 Schematic representation of Dansgaard-Johnsen flow model.

(positive downward). The integral (Eq. 22) is easily calculated from the geometry of the model.

To constrain the value of h, I use least-squares minimization to fit the flow model to the layer-thickness data obtained from the ^{10}Be spectra. The minimization consists of two parts:

$$f_y = \frac{u_s}{\bar{u}}\left(\frac{y}{2}\right) - \lambda_{^{10}Be}(y) \qquad y < h$$
$$g_y = \frac{u_s}{\bar{u}}\left(\frac{h}{2} + (y-h)\right) - \lambda_{^{10}Be}(y) \qquad y \geq h \tag{23}$$

where we minimize the sum

$$\sum (f_y^2 + g_y^2) \tag{24}$$

with respect to h. Recognizing that at the surface the layer thickness is equivalent to the accumulation rate, we determine u_s from

$$\lambda(H) = \frac{u_s h}{2} + u_s(H-h)$$
$$u_s = \frac{\lambda(H)}{\frac{h}{2} + (H-h)} \tag{25}$$

Applying the least-squares minimization to the layer-thickness data determined from the ^{10}Be spectra, we obtain h = 320 ± 15 meters.

We are now in a position to compare these results with those from an independent glacier flow model. To do this, it is convenient first to convert the measured layer thicknesses, λ_z, to relative layer thicknesses:

$$\lambda_z^R(z) = \frac{\lambda_z(z)}{\lambda_z(0)} \tag{26}$$

where $\lambda_z(0)$ is the original layer thickness at the surface. Assuming the accumulation rate to be the same for each section analyzed, $\lambda_z(0)$ is just the surface accumulation rate (0.07 m/a ice equivalent). The depth distribution of λ_z^R is independent of accumulation rate if the changes are small enough that ice-sheet configuration remains constant; λ_z^R essentially describes the vertical velocity distribution in the ice core.

Waddington et al. (1993) describe the application of a two-dimensional finite-element glacier flow model (Raymond, 1983) to the Taylor Dome core. More up-to-date results are those of Morse (Morse, 1996), who uses a more realistic ice-sheet configuration, based on an airborne radar profile along the main direction of ice flow. While ongoing geophysical analyses—particularly vertical strain-rate measurements—are expected to improve these results, the preliminary model is probably reasonable to a depth of about 400 meters (Morse, personal communication, 1995), covering the entire Holocene period of the core.

Figure 7.7 shows layer thicknesses calculated with the finite element flow-model, here referred to as the "Morse-Waddington model," compared

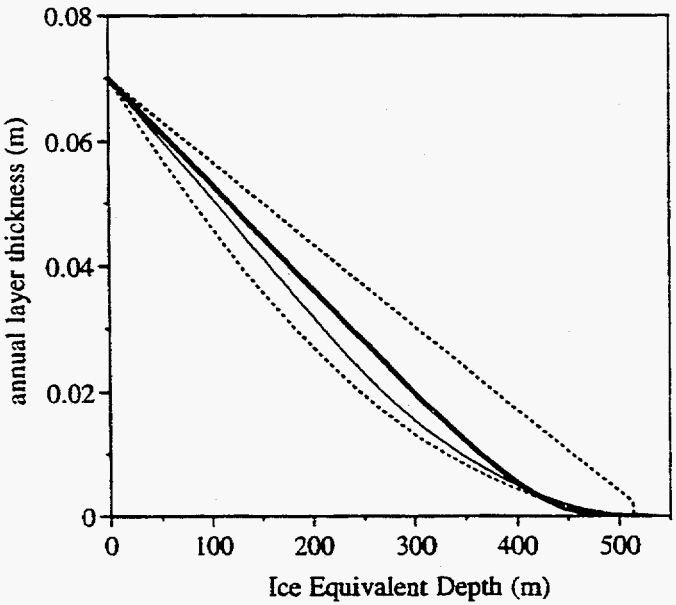

Figure 7.7 Estimates of layer thickness as a function of depth in the Taylor Dome core, assuming accumulation rate is consant. Dashed lines: Raymond (lower) and Nye (upper) models. Bold line: Morse-Waddington model. Thin line: best fit Dansgaard-Johnsen model to the ^{10}Be spectra.

with the best-fit Dansgaard-Johnsen model constrained by the ^{10}Be data. Also shown are the Nye and Raymond "end-member" models, which are equivalent to Dansgaard-Johnsen models with h = 0 and h = H, respectively. The ^{10}Be data show a remarkably good correspondence with the Morse-Waddington model, at least down to 400 meters, although the constrained Dansgaard-Johnsen model under-predicts λ_z^R relative to the Morse-Waddington model by up to 15%. In principle, we should be able to constrain the layer thicknesses at Taylor Dome further by making ^{10}Be 11-year cycle determinations over additional depth intervals.

7.6 Refinements

In the preceding section, I assumed that the accumulation rate was the same for each analyzed section of the core. In fact, the different average concentration of ^{10}Be in each section suggests that accumulation rates vary somewhat. In particular, the ^{10}Be concentration in the 320 m section is about 20% higher than in the other sections, suggesting that the accumulation rate may have been as much as 20% lower. This assumption gives a minimum estimate of the accumulation rate at 320 m, since the ^{10}Be production may have been slightly higher (though not by 20%) during the time-period represented by this section (~9 ka).[23]

As described in Chapter 6, the accumulation rate, $\dot{b}$, can be determined from the measured ^{10}Be concentrations, [^{10}Be], from the relationship

$$\chi\left(\frac{\upsilon_d}{\dot{b}} + W\right) = [^{10}Be] \tag{27}$$

where χ is the concentration in air, and υ_d and W are the wet and dry scavenging coefficients, assumed to be constant. Assuming that χ remains constant throughout the Holocene, we can then calculate relative layer thickness from

$$\lambda_z^{rel} = \frac{\lambda_z(z)}{\lambda_z(0)} = \frac{\lambda_z}{\dot{b}_0}\left(\frac{[^{10}Be]_0 - W\chi}{[^{10}Be]_z - W\chi}\right) \tag{28}$$

where the term $W\chi \sim 10^2$ atoms/g is just the concentration of ^{10}Be in precipitation.

Applying Equation 8 to the ^{10}Be data, we find that some improvement is made to the match between the Morse-Waddington flow model and the ^{10}Be-constrained Dansgaard-Johnsen model. As shown in Figure 7.8, the least-squares minimization (Eq. 5) now gives h = 280 m; the Morse-Waddington model is closely approximated by h = 220, which suggests that the latter slightly overestimates the λ_z^{rel} between 200 and 300 meters.

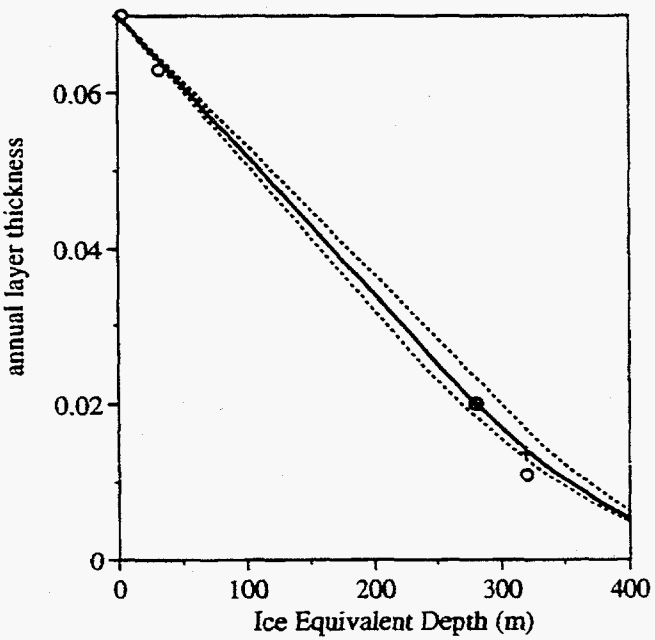

Figure 7.8 Layer thickness profiles at Taylor Dome calculated from the Dansgaard-Johnsen model, assuming constant accumulation rate, for h = 220 (upper dashed line), 280 (middle) and 320 (lower dashed)meters. Circles shows estimates from the raw ^{10}Be spectra; crosses show data after correction for accumulation rates determined from average ^{10}Be concentrations.

7.7 Discussion

The proposed method—using the solar-modulation cycle in ^{10}Be production to determine the 11-year layer thickness in ice cores—depends on two critical assumptions. First, the 11-year cycle period must remain constant with time. Second, this cycle must be reflected in the deposition of cosmogenic ^{10}Be at the earth's surface. The results from the Taylor Dome core presented in this paper suggest that these assumptions are valid. Furthermore, both assumptions could be tested with ^{10}Be measurements in the GRIP or GISP2 ice cores from central Greenland, which have excellent age control and discernible annual layers. At this writing, the necessary high-resolution measurements have not been made at these sites.

At present, the limited amount of data and the preliminary nature of the ice-flow modeling results preclude us from stating with certainty that the proposed method has been validated. It is promising, however, that the measured layer thicknesses using the ^{10}Be data agree closely with those predicted from an independent ice-flow model, and that they correctly predict the spectral characteristics of the ECM and $\delta^{18}O$ climate-proxy data. On the other hand, the *discrepancy* between the ice-flow modeling results and the ^{10}Be results serve to illustrate the potential utility of the method. In particular, it may be important for refining estimates of layer thicknesses for ice cores where the accumulation rate is too low to preserve discernible annual layers.

Notes to Chapter 7

22. The low-resolution (~ .2 a^{-1}) sampling is a consequence of the Taylor Dome core being much older at the bottom than was originally predicted by Waddington et al. (1994). There is probably enough ice available to repeat this experiment at 2-3 times greater resolution.

23. The global average production of ^{10}Be at 9 ka may have been about 5% higher than today (Fig. 4.2) because of a lower geomagnetic field strength. Production rates may also change because of changes in solar modulation. This may be a source of error particularly for the 33 m section, because the time-period measured (~22 years) is shorter than the Gleissberg solar cycle, which has a period of about 88 years. The amplitude of the Gleissberg cycle, however, is small, resulting in a variation of less than 10% in ^{10}Be production (Beer et al., 1988).

Chapter 8

A PRELIMINARY PALEOCLIMATIC INTEPRETION OF THE ^{10}BE RECORD AT TAYLOR DOME

In spite of nearly a century of research, the configuration of the Antarctic ice sheet under different climate regimes is a topic of considerable controversy (Kennet and Hodell, 1995). A long-standing question is the contribution of Antarctic ice volume change to eustatic sea-level variation, which depends on the relative magnitude of ice-sheet expansion at the margin and ice-sheet thinning in the interior (Meier, 1993). As discussed in Chapter 2, the Taylor Dome ice core project was originally inspired by the need for a local climate record to complement the terrestrial and marine geologic record (Stuiver et al., 1981; CLIMAP, 1984) in the Western portion of the Ross ice drainage system. The Ross Drainage accounts for about 25% of the surface area of the Antarctic ice sheet (Drewry and Robin, 1983) and from the point of view of global paleoclimate, is probably the most important area in the Antarctic. While it is premature to consider a comprehensive analysis of the paleoclimatic significance of the Taylor Dome record—given that there is potential for improved dating control and higher-resolution geochemical analysis—the ^{10}Be and δ^{18}O records presented in this dissertation do permit a preliminary interpretation. Of particular interest is whether the inferences made from the glacial-geologic record of past climate conditions in the Dry Valleys and Transantarctic Mountains are borne out in the Taylor Dome record.

According to the terrestrial glacial-geologic record, during the sea-level low-stand of the last glacial maximum, about 20,000 years ago, the Ross Ice Shelf expanded and became grounded in the lower Dry Valleys. During the same period, many Dry Valleys glaciers remained stationary or retreated (Stuiver et al., 1981, Denton et al., 1989a, b, Marchant et al., 1994). A strong inference of this out-of-phase relationship is that there is increased aridity on the polar plateau during times of ice-sheet expansion. Thus, the ice-volume increase associated with expansion of the Antarctic ice sheet onto the greater land area available during sea level low-stands may be partly offset by lower accumulation rates and ice-sheet thinning.

As illustrated in Figure 8.1, the accumulation-rate history inferred from East Antarctic cores such as Vostok (Raisbeck et al, 1987; Jouzel et al., 1989) is generally consistent with the glacial-geologic record, with lower accumulation rates corresponding to times of Ross Ice Shelf expansion and retreat of alpine and outlet glaciers in the Dry Valleys. Here, I calculate accumulation rate by assuming that the ^{10}Be flux (F) is constant:

$$accum.\ rate = \frac{F}{[^{10}Be]}$$

Although changes in atmospheric circulation, ^{10}Be production, and the relative importance of wet and dry deposition processes introduce some error to the calculation, the required corrections are small relative to the

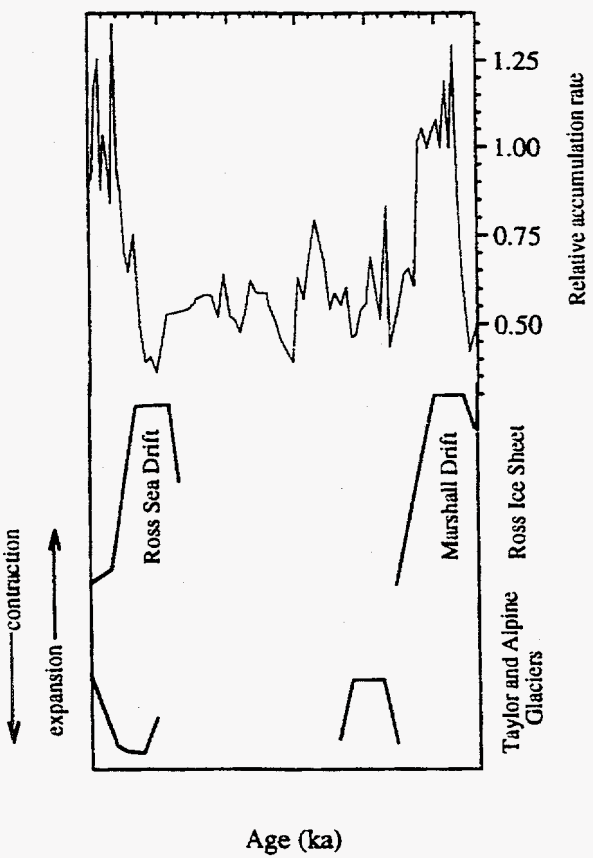

Figure 8.1 Top) Accumulation rate at Vostok, as determined from ^{10}Be concentrations (after Raisbeck et al., 1987). Bottom) Schematic representation of the glacial-geologic record from the Dry Valleys and McMurdo Sound (after Denton et al., 1989a).

large changes in accumulation associated with major climate events such as glacial-interglacial shifts (Chapter 6).

A reduction in accumulation during times of ice-sheet expansion is expected from the colder temperatures associated with glacial periods (Denton et al., 1989a; Jouzel et al., 1989). However, temperature cannot be the only determining factor at Taylor Dome: although the stable isotope records at Vostok and Taylor Dome are similar in their overall features (Figure 2.8), the accumulation rate histories inferred from ^{10}Be concentrations are quite different. As shown in Figure 8.2, accumulation rates at Taylor Dome during marine isotope stage 2 were about 20% of Holocene values, compared with a lowering of 50% in the Antarctic interior. During the prominent "Antarctic Cold Reversal" (ACR: Jouzel et al., 1995) accumulation rates at Taylor Dome were about 50% of the present value; this is a larger change than has been observed elsewhere in Antarctica for that period (Lorius et al., 1979; Jouzel, et al., 1995).

The large variations in accumulation rate recorded in the Taylor Dome core suggest that during times of ice-sheet expansion, aridity may have been locally enhanced by the orographic effects of a grounded ice sheet and/or the increased distance to open water. If this interpretation is correct, it implies that there should be a delayed response in the Taylor Dome record, relative to Vostok, because of the time required for sea level and ice-sheet configuration to respond to changing climate conditions.

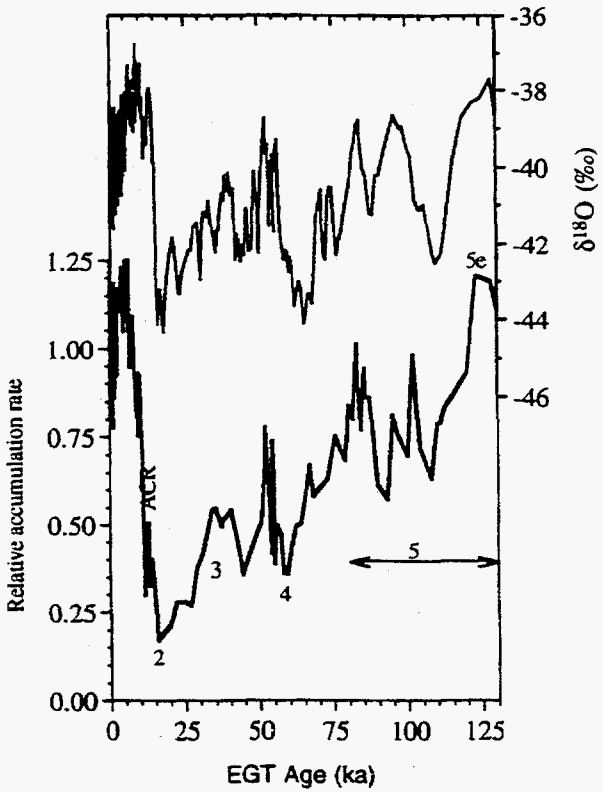

Figure 8.2 $\delta^{18}O$ (upper) and accumulation rate (lower, relative to the average Holocene value) at Taylor Dome. Numbers show approximate mid-points of marine isotope stages and the Antarctic Cold Reversal (ACR) mentioned in the text.

Specifically, we expect accumulation rates at Taylor Dome to reflect fluctuations in global sea level as well as in temperature.

Figure 8.3 compares the Vostok and Taylor Dome ^{10}Be profiles with the Taylor Dome $\delta^{18}O$ record and the SPECMAP record of average sea-water $\delta^{18}O$ (Pisias et al., 1984; Martinson et al., 1987). The SPECMAP record, derived from benthic foraminifera $\delta^{18}O$ measurements on multiple deep-sea cores, is an accepted proxy for global sea level (Chappell and Shackleton, 1986). Sowers et al. (1993) used the $\delta^{18}O$ of O_2 in air bubbles in the Vostok ice core to place the core on the SPECMAP timescale; they found that sea level, as recorded in SPECMAP lags global temperature, as recorded at Vostok, by several thousand years. In constructing Figure 8.3, I have calculated a preliminary SPECMAP timescale for the Taylor Dome core, following the relationship between the SPECMAP and EGT timescales for Vostok (Sowers et al., (1993) and Jouzel et al., (1993) respectively). This timescale is in good agreement with that from preliminary $\delta^{18}O$ of O_2 and CH_4 results at Taylor Dome (E. J. Brook, personal communication). Also shown in Figure 8.3 is the ratio of ^{10}Be concentrations at Vostok and Taylor Dome, which is essentially the Taylor Dome/Vostok ratio of accumulation rates. An advantage to using this ratio is that it normalizes out changes in ^{10}Be production that should be common to both the Vostok and Taylor Dome records, thereby reducing the error in the assumption that ^{10}Be concentrations directly reflect accumulation rates. Because of possible remaining errors in the

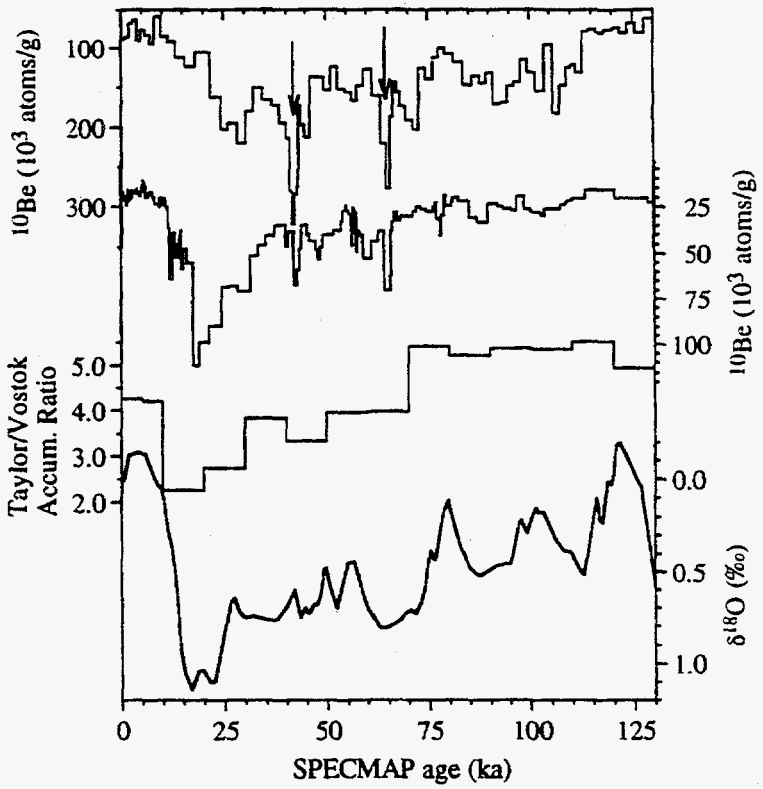

Figure 8.3 ^{10}Be at a) Voststok and b) Taylor Dome on the SPECMAP timescale, compared with c) the ratio of accumulation (Taylor Dome/Vostok) and d) the SPECMAP global sea-level (δ^{18}O) curve. Numbers on bottom graph denote marine isotope stages referred to in the text. Arrows show ^{10}Be "spikes."

preliminary Taylor Dome SPECMAP timescale, 5000-year average ratios only are shown.

Particulary notable in Figure 8.3 is the difference in timing between the beginning of isotope stage 4 at about 75 ka, as defined by the SPECMAP record, and the increase in ^{10}Be concentrations (decrease in accumulation rates) at Taylor Dome and at Vostok, respectively. Although the Taylor Dome timescale is at present less accurate than that of Vostok, the relative timing of events around the beginning of isotope stage 4 is unequivocal because of the ^{10}Be spike which is present in both records at about 64 ka (see Chapter 6). At Vostok, ^{10}Be concentrations increase (i.e. accumulation rates decrease) at about 70 ka, *prior* to the 64 ka ^{10}Be spike, while at Taylor Dome, this increase is delayed until after the 64 ka spike. There is a similar offset between the beginning of the last glaciation as defined by the ^{10}Be record; although ^{10}Be concentrations increase at both Taylor Dome and Vostok at about 32 ka, prior to the marine isotope stage 2 sea-level drop, ^{10}Be concentrations continue to increase at Taylor Dome—but not at Vostok—through about 18 ka. The implication is that accumulation rates at Taylor Dome are driven in part by sea-level fluctuations, presumably through changes in conditions in the Ross Sea.

Comparison between the SPECMAP marine $\delta^{18}O$ curve and the ratio of accumulation rates between Taylor Dome and Vostok further supports the idea that the Taylor Dome record reflects Ross Sea conditions. While the accumulation rate at Taylor Dome leads the stage 2 sea-level minimum,

the Taylor Dome/Vostok ratio appears to lag it slightly, with the minimum ratio occuring after 20 ka. It is further notable that the ratio between accumulation rates at Taylor Dome and Vostok ratio remains relatively constant throughout all of marine isotope stage 5, suggesting that there was no significant change in configuration of the Ross Ice Shelf following stage 5e, in spite of the large drop in temperature and sea level. This in turn implies that the Ross Ice Shelf was not substantially more retreated during the last integlacial maximum than it is today, in spite of the slightly higher sea levels at that time (Chappell and Shackleton, 1986). If correct, this is an important result because the behavior of the Ross Ice Shelf during marine isotope stage 5e is often treated as an anolog for West Antarctic ice-sheet behavior—including possible collapse—under future anthropogenic climate warming scencarios (CLIMAP, 1984; MacAyeal, 1995).

In summary, it appears that the Taylor Dome record supports the inferences of Denton and others (1989a; Stuiver et al., 1981; Marchant et al., 1994) as to the climatic conditions in the Dry Valleys/McMurdo Sound region during the Quaternary. It further appears that there is promise for using the Taylor Dome record as a proxy for sea-surface conditions and/or Ross Sea ice-sheet configuration. It will be particularly interesting to examine the Holocene portion of the record in some detail, as radiocarbon control on glacier and ice-shelf marginal positions over the last 10,000

years continues to improve (C. Hart, pers. comm., 1996; B. Hall, pers. comm., 1995; Licht et al., 1996).

Whether the Taylor Dome accumulation record is a purely local signal, reflecting changes in accumulation patterns for a small geographic area, or is indicative of regional conditions in the western Ross Drainage remains open to question. During the last glacial period, accumulation rates at Taylor Dome were almost as low as at Vostok, possibly reflecting greater continentality throughout the Transantarctic Mountains at that time. Certainly, retreat of Taylor Glacier and Transantarctic outlet glaciers during times of ice-sheet expansion in the Ross Sea (Denton et al., 1989b; Bockheim et al., 1989) is consistent with the Taylor Dome accumulation rate record, as is evidence for an advance of Taylor Glacier during marine isotope stage 5e (Brook et al., 1993; Marchant et al., 1994), when high sea level would have precluded ice-sheet expansion. On the other hand, the lower accumulation rates expected from lowered temperatures alone may be sufficient to account for these observations. Further work at Taylor Dome, particularly interpretation of the high-resolution ice-penetrating radar profiles in terms of the spatial variability of accumulation rates (Morse, 1996), refinement of the timescale through high-resolution trace gas analysis (Sowers and Bender, 1995; Malaize et al., 1995), and ^{10}Be-based layer thickness measurements, may shed further light on this question. Finally, determination of the deuterium excess parameter, a measurement of the difference between $\delta^{18}O$ and δD stable isotope values (Merlivat and

Jouzel, 1979), may provide an independent way to discern changes in sea-surface conditions affecting accumulation at Taylor Dome.

REFERENCES CITED

Anderson, E. C., W. F. Libby, S. Weinhouse, A. F. Reid, A. D. Kirshenbaum and A. V. Grosse. 1947. Natural radiocarbon from cosmic radiation. *Physics Reviews* **72**, 931-936.

Andreae, M. O. 1985. *In* J. N. Galloway, R. J. Charlson, M. O. Andreae and H. Rodhe (eds.), *The Role of Air-Sea Exchange in Geochemical Cycling*. Dordrecht, Reidel, 5-25.

Alley, R. B., D. A. Meese, C. A. Shuman, A. J. Gow, K. C. Taylor, P. M. Grootes, J. W. C. White, M. Ram, E. D. Waddington, P. Mayewski and G. A. Zielinski. 1993. Abrupt increase in Greenland snow accumulation at the end of the Younger Dryas event. *Nature* **362**, 527-529.

Alley, R. B., R. C. Finkel, K Nishiizumi, S. Anandakrishnan, C. A. Shuman, G. R. Merson, G. A. Zielinski and P. A. Mayewski. 1996. Changes in continental and sea-salt atmospheric loadings in central Greenland during the most recent deglaciation: model-based estimates. *Journal of Glaciology*, in press.

Attolini, M. R., S. Cecchini, G. C. Castagnoli, M. Galli and T. Nanni. 1987. Cosmic-ray ^{10}Be biennial data and their relationship to aurorae and sunspots. *Proceedings of the International Cosmic Ray Conference* **19**, 1-3.

Attolini, M. R., M. Galli and T. Nanni. 1988. Long and short cycles in solar activity during the last millenia. *In* F. R. Stephenson and A. W. Wolfendale (eds.), *Secular Solar and Geomagnetic Variations in the Last 10,000 years*. London, Kluwer Academic Publishers, 49-53.

Beer, J., G. Bonani, H. F. Hofmann, M. Suter, A. Synal, W. Wölfli, H. Oeschger, U. Siegenthaler and R. C. Finkel. 1987. ^{10}Be measurements on polar ice: comparison of arctic and antarctic records. *Nuclear Instruments and Methods in Physics Research* **B29**, 203-206.

Beer, J., U. Siegenthaler, G. Bonani, R. C. Finkel, O. H., M. Suter and W. Wölfli. 1988. Information on past solar activity and geomagnetism from ^{10}Be in the Camp Century ice core. *Nature* **331**, 675-679.

Beer, J., A. Blinov, G. Bonani, R. C. Finkel, H. J. Hofmann, B. Lehmann, H. Oeschger, A. Sigg, J. Schwander, T. Staffelback, B. Stauffer, M. Suter and W. Wölfli. 1990. Use of ^{10}Be in polar ice to trace the 11-year cycle of solar activity. *Nature* **347**, 164-166.

Beer, J., F. Joos, C. Lukasczyk, W. Mende, J. Rodriguez, U. Siegenthaler and R. Stellmacher. 1994. ^{10}Be as an indicator of solar variability and climate. *In* E. Nesme-Ribes (ed.), *The Solar Engine and Its Influence on Terrestrial Atmosphere and Climate*. Berlin, Springer-Verlag, 221-233.

Benioff, P. A. 1956. Cosmic-ray production rate and mean removal time of beryllium-7 from the atmosphere. *Physics Reviews* **104**, 1122-1165.

Bergin, M. H. 1994. Fluxes of chemical species to the Greenland ice sheet at Summit by fog and dry deposition. *Geochimica et Cosmochimica Acta* **58**, 3207-3215.

Bockheim, J. G., S. C. Wilson, G. H. Denton, B. G. Andersen and M. Stuiver. 1989. Late Quaternary ice-surface fluctuations of Hatherton Glacier, Transantarctic Mountains. *Quaternary Research* **31**, 229-245.

Brasseur, G. and S. Solomon. 1984. *Aeronomy of the Middle Atmosphere*. Dordrecht, The Netherlands, D. Reidel.

Bromwich, D. H. and C. R. Stearns (eds.). 1993. *Antarctic Meteorology and Climatology: Studies based on Automatic Weather Stations.* Washington, D. C., American Geophysical Union.

Brook, E. J., M. Kurz, R. P. Ackert, G. H. Denton, E. T. Brown, G. M. Raisbeck and F. Yiou. 1993. Chronology of Taylor Glacier advances in Arena Valley, Antarctica, using in situ cosmogenic ^{3}He and ^{10}Be. *Quaternary Research* **39**, 11-23.

Burg. J. P. 1967. Maximum entropy spectral analysis. 37th Meeting of the Scoiety of Exploration Geophysicists, Oklahoma City.

Castagnoli, G. and D. Lal. 1980. Solar modulation effects in terrestrial production of carbon-14. *Radiocarbon* **22**, 133-158.

Chappell, J. and N. J. Shackleton. 1986. Oxygen isotopes and sea level. *Nature* **324**, 137-140.

Charlson, R. J., J. E. Lovelock, M. O. Andreae and S. G. Warren. 1987. Oceanic phytoplankton, atmospheric sulphur, cloud alebdo and climate. *Nature* **326**, 655-661.

CLIMAP Project Members. 1984. The last integlacial ocean. *Quaternary Research* **21**, 123-224.

Crutzen, P. J. and F. Arnold. 1986. Nitric acid cloud formation in the cold Antarctic stratosphere: a major cause for the springtime ozone hole. *Nature* **324**, 651-654.

Cunningham, J. and E. D. Waddington. 1993. Air flow and dry deposition of non-sea salt sulfate in polar firn: paleoclimatic implications. *Atmospheric Environment* **27A**, 2943-2956.

Damon, P. E. 1988. Production and decay of radiocarbon and its modulation by geomagnetic field-solar activity changes with possible implications for global environment. *In* F. R. Stephenson and A. W. Wolfendale (eds.),

Secular Solar and Geomagnetic Variations in the Last 10,000 Years. Kluwer Academic Publishers, 267-285.

Dansgaard, W. and S. J. Johnsen. 1969. A flow model and a time scale for the ice core from Camp Century, Greenland. *Journal of Glaciology* **8**, 215-223.

Davidson, C. I., S. Santhanam, R. C. Fortmann and M. P. Olson. 1985. Atmospheric transport and deposition of trace elements onto the Greenland ice sheet. *Atmospheric Environment* **19**, 2065-2081.

Davidson, C. I. 1989. Mechanisms of wet and dry deposition of atmospheric contaminants to snow surfaces. In H. Oeschger and C. C. Langway (eds.), *The Environmental Record in Glaciers and Ice Sheets*. New York, John Wiley & Sons.

Davis, J. C., I. D. Proctor, J. R. Southon, M. W. Caffee, D. W. Heikkinen, M. L. Roberts, T. L. Moore, K. W. Turteltaub, D. e. Nelson, D. H. Loyd and J. S. Vogel. 1990. LLNL/UC AMS facility and research program. *Nuclear Instruments and Methods in Physics Research* **B52**, 269-272.

Denton G. H. and T. J. Hughes (eds). 1981. *The Last Great Ice Sheets*. New York, John Wiley & Sons.

Denton, G. H., J. G. Bockheim, S. C. Wilson and M. Stuiver. 1989a. Late Wisconsin and Early Holocene Glacial History, Inner Ross Embayment, Antarctica. *Quaternary Research* **31**, 151-182.

Denton, G. H., J. G. Bockheim, S. C. Wilson, J. E. Leide and B. G. Anderson. 1989b. Late Quaternary ice-surface fluctuations of Beardmore Glacier, Transantarctic Mountains. *Quaternary Research* **31**, 183-209.

Denton, G. H., M. L. Prentice and L. H. Burckle. 1991. Cainozoic history of the Antarctic ice sheet. *In* R. J. Tingey (ed.), *The Geology of Antarctica*. Oxford, Clarendon Press, 365-433.

Deshler, T., A. Adriani, G. P. Gobbi, D. J. Hofmann, G. Di Donfrancesco and B. J. Johnsen. 1995. Volcanic aerosol and ozone depletion within the

antarctic polar vortex during the austral spring of 1991. *Geophysical Research Letters* **19**, 1819-1822.

Dibb, J. E., P. A. Mayewski, C. S. Buck and S. M. Drummey. 1990. Beta radiation from snow. *Nature* **345**, 25.

Dibb, J. E., L. D. Meeker, R. C. Finkel, J. R. Southon and M. W. Caffee. 1994. Estimation of stratospheric input to the Arctic troposphere: ^{7}Be and ^{10}Be in aerosols at Alert, Canada. *Journal of Geophysical Research* **99**, 12855-12864.

Drewry, D. J. 1980. Pleistocene bimodal response of Antarctic ice. *Nature* **287**, 214-216.

Drewry, D. J. 1982. Ice flow, bedrock and geothermal studies from radio-echo sounding inland of McMurdo Sound, Antarctica. *In* C. Craddock (ed.), *Antarctic Geoscience*. Madison, University of Wisconsin, in press, 977-983.

Drewry, D. J. and G. Robin. 1983. Form and flow of the Antarctic ice sheet during the last million years. *In* G. Robin (ed.), *The Climatic Record in Polar Ice Sheets*. Cambridge, Cambridge University Press, 28-38.

Dunkerton, T. 1978. On the mean meridional mass motions of the stratosphere and mesosphere. *Journal of the Atmospheric Sciences* **35**, 2325-2333.

Eddy, J. A. 1988. Variability of the present and ancient sun: a test of solar uniformitarianism. *In* F. R. Stephenson and A. W. Wolfendale (eds.), *Secular Solar and Geomagnetic Variations in the Last 10,000 Years*. Boston, Kluwer Academic Publishers, 1-23.

Ehmert, A. 1960. On the modulation of the primary spectrum of cosmic rays from solar activity. *Proceedings of the International Conference on Cosmic Rays* **4**, 140-152.

Fox, L. E., D. R. Worsnop, M. S. Zahniser and S. C. Wofsy. 1995. Metastable phases in polar stratospheric aerosols. Science **267**, 351-355.

Garcia, R. R. and S. Solomon. 1983. A numerical model of the zonally averaged dynamical and chemical structure of the middle atmosphere. *Journal of Geophysical Research* **88**, 1379.

Gobbi, G. P., T. Deshler, A. Adriani and D. J. Hofmann. 1991. Evidence for denitrification in the 1990 Antarctic spring stratosphere: I Lidar and temperature measurements. *Geophysical Research Letters* **18**, 1995-1998.

Grootes, P. M. and E. J. Steig. 1992. Taylor Dome ice core study. *Antarctic Journal of the United States* **27**, 57-58.

Grootes, P. M., E. J. Steig and M. Stuiver. 1994. Taylor Ice Dome study 1993-1994: An ice core to bedrock. *Antarctic Journal of the United States* **29**, 79-81.

Hammer, C. U., H. B. Clausen and H. Tauber. 1986. Ice-core dating of the Pleistocene/Holcene boundary applied to a calibration of the ^{14}C timescale. *Radiocarbon* **28**, 284-291.

Harder, S. L. et al. 1996. Filtering of air through snow as a mechanism for aerosol deposition to the Antarctic ice sheet. *Journal of Geophysical Research* , in press.

Hartmann, D. L. 1990. Dynamical properties of the Antarctic circumpolar vortex inferred from aircraft observations. *In* A. O'Neill (ed.), *Dynamics, transport and photchemistry in the middle atmosphere of the southern hemisphere.* Boston, Kluwer Academic Publishers, 117-134.

Holton, J. R., P. H. Haynes, M. E. McIntyre, A. R. Douglass, R. B. Rood and L. Pfister. 1996. Stratosphere-troposphere exchange. *Reviews of Geophysics* , in press.

Höltz, H., G. Rosner and R. Winkler. 1991. Correlation of ^{7}Be concentrations in surface air and precipitation with the solar cycle. *Naturwissenschaften* **78**, 215-217.

Ibrahim M., L. A. Barrie and F. Fanaki. 1983. An experimental and theoretical investigation of the dry deposition of particles to snow, pine trees, and artificial collectors. *Atmospheric Environment* **17**, 781-788.

Iwasaka, Y. 1986. Descending motion of antarctic stratospheric aerosol layer in winter: possible effect on stratospheric water vapor budget. *Memoir of the National Institute for Polar Research* **45**, 13-18.

Jenkins, G. M. and D. G. Watts. 1968. *Spectral Analysis and Its Applications*. San Francisco, Holden-Day.

Jouzel, J., L. Merlivat and C. Lorius. 1982. Deuterium excess in an East Antarctic ice core suggests higher relative humidity at the oceanic surface during the last glacial maximum. *Nature* **299**, 688-691.

Jouzel, J., C. Lorius, J. R. Petit, C. Genthon, N. I. Barkov, V. M. Kotlyakov and V. M. Petrov. 1987. Vostok ice core: a continuous isotope temperature record over the last climatic cycle (160,000 years). *Nature* **329**, 403-407.

Jouzel, J., G. Raisbeck, J. P. Benoist, F. Yiou, C. Lorius, D. Raynaud, J. R. Petit, N. I. Barkov, Y. S. Korotkevitch and V. M. Kotlyakov. 1989. A comparison of deep Antarctic ice cores and their implications for climate between 65,000 and 15,000 years ago. *Quat. Res.* **31**, 135-150.

Jouzel, J., N. I. Barkov, J. M. Barnola, M. Bender, J. Chappellaz, C. Genthon, V. M. Kotlyakov, V. Lipenkov, L. C, J. R. Petit, D. Raynaud, G. Raisbeck, C. Ritz, T. Sowers, M. Stievenard, F. Yiou and P. Yiou. 1993. Extending the Vostok ice-core record of palaeoclimate to the penulitmate glacial period. *Nature* **364**, 407-412.

Jouzel, J., R. Vaikmae, J. R. Petit, M. Martin, D. Y, M. Stievenard, C. Lorius, M. Toots, M. A. Mélières, L. H. Burckle, N. I. Barkov and V. M. Kotlyakov. 1995. The two-step shape and timing of the last deglaciation in Antarctica. *Climate Dynamics* **11**, 151-161.

Kakegawa, H., T. Yasunari and T. Kawamura. 1986. Seasonal and intra-seasonal fluctuations of polar anticyclone and circumpolar vortex over Antarctica. *Memoir of the National Institute for Polar Research* **45**, 19-29.

Kennet, J. P. and D. A. Hodell. 1995. Stability or instability of Antarctic Ice sheets during warm climates of the Pliocene? *GSA Today* **5**, 1-22.

Lal, D. and B. Peters. 1962. Cosmic ray produced isotopes and their application to problem in geophysics. *In* J. G. Wilson and S. A. Wouthuysen (eds.), *Progress in Elementary Particle and Cosmic Ray Physics*. Amsterdam, North-Holland, 1-74.

Lal, D. and B. Peters. 1967. Cosmic ray produced radioactivity on the earth. *Handbuch der Physik* **46**, 551-612.

Lal, D. 1987. ^{10}Be in polar ice: data reflect changes in cosmic ray flux or polar meteorology. *Geophysical Research Letters* **14**, 785-788.

Lal, D. 1988. Theoretically expected variations in the terrestrial cosmic-ray production rates of isotopes. *In* G. C. Castagnoli (ed.), *International School of Physics "Enrico Fermi"*. Varenna sul Lago di Como, North-Holland, 216-233.

Legrand, M. 1987. Chemistry of Antarctic Snow and Ice. *Journal de Physique, Colloque C1* **48**, 77-86.

Libby, W. F. 1946. Atmospheric helium three and radiocarbon from cosmic radiation. *Physics Reviews* **69**, 671-672.

Licht, K. J., A. E. Jennings, J. T. Andrews and K. M. Williams. 1996. Chronology of the late Wisconsin ice retreat from the western Ross Sea, Antarctica. *Geology*, in press.

Lide, D. R. (ed.). 1992. *Handbook of Chemistry and Physics*. Boca Raton, Florida, CRC Press.

Lingenfelter, R. E. 1963. Production of carbon 14 by cosmic-ray neutrons. *Reviews of Geophysics* **1**, 35-55.

Lorius, C., L. Merlivat, J. Jouzel and M. Pourchet. 1979. A 30,000 yr isotope climatic record from Antarctic ice. *Nature* **280**, 644-648.

Lorius, C., G. Raisbeck, J. Jouzel and D. Raynaud. 1989. Long-term environmental records from Antarctic ice cores. In H. Oeschger and C. C. Langway (eds.), *The Environmental Record in Glaciers and Ice Sheets*. New York, John Wiley & Sons.

MacAyeal, D. R. 1992. Irregular oscillationsof the West Antarctic ice sheet. *Nature* **359**, 29-32.

Maenhaut, W., W. H. Zoller and D. G. Coles. 1979. Radionuclides in the South Pole atmosphere. *Journal of Geophysical Research* **84**, 3131-3137.

Malaize, B., M. L. Bender, L. B., C. Sucher, P. M. Grootes and E. J. Steig. 1994. Chronology of the Taylor Dome ice core based on the $\delta^{18}O$ of O_2 in trapped air. *Eos Transactions* **75**, 226.

Manney, G. L., L. Froidevaux, J. W. Waters, R. W. Zurek, W. G. Read, L. S. Elson, J. B. Kumer, J. L. Mergenthaler, A. E. Roche, A. O'Neill, R. S. Harwood, I. MacKenzie and R. Swinbank. 1994. Chemical depletion of ozone in the Arctic lower stratosphere during winter 1992-93. *Nature* **370**, 429-433.

Marchant, D. R., G. H. Denton, J. G. Bockheim, W. S. C. and A. R. Kerr. 1994. Quaternary changes in level of the upper Taylor Glacier, Antarctica: implications for paleoclimate and East Antarctic Ice sheet dynamics. *Boreas* **23**, 29-43.

Martinson, D. G., N. G. Pisias, J. D. Hays, J. Imbrie, T. C. Moore Jr. and N. J. Shackleton. 1987. Age dating and the orbital theory of the ice ages: development of a high-resolution 0 to 300,000-year chronostratigraphy. *Quat. Res.* **27**, 1-27.

Mayewski, P. A., L. D. Meeker, S. Whitlow, M. S. Twickler, M. C. Morrisos, P. Bloomfield, G. C. Bond, R. B. Alley, A. J. Gow, P. M. Grootes, D. A. Mees, M. Ram, K. C. Taylor, W. Wumkes. 1994. Changes in atmospheric circulation and ocean ice cover over the North Atlantic during the last 41,000 years. *Science* **263**, 1747-1751

Mazaud, A., C. Laj and M. Bender. 1994. A geomagnetic chronology for Antarctic ice accumulation. *Geophysical Research Letters* **21**, 337-340.

McCorkell, R., E. L. Fireman and C. C. Langway Jr. 1967. Aluminum-26 and beryllium-10 in Greenland ice. *Science* **158**, 1690-1692.

McHargue, L. R. and P. E. Damon. 1991. The global beryllium-10 cycle. *Reviews of Geophysics* **29**, 141-158.

McHargue, L. R., P. E. Damon and D. J. Donahue. 1995a. Enhanced cosmic-ray production of ^{10}Be coincident with the Mono Lake and Laschamp geomagnetic excursions. *Geophysical Research Letters* **22**, 659-662.

McHargue, L. R., P. E. Damon and D. J. Donahue. 1995a. Confirmation of the ca. 60 kyr beryllium-10 anomoly? *EOS Transactions* **76**, F686.

Meier, M. F. 1993. Ice, climate and sea level; do we know what is happening? *In* W. R. Peltier (ed.), *Ice in the Climate System*. Berlin, Springer-Verlag, 141-160.

Merlivat, L. and J. Jouzel. 1979. Global climatic interpretation of the deuterium-oxygen 18 relationship for precipitation. *Journal of Geophysical Research* **84**, 5029-5033.

Merrill, R. T. and M. W. McElhinny. 1983. *The Earth's Magnetic Field: Its History, Origin, and Planetary Perspective*. London, Academic Press.

Meyer, P. and J. A. Simpson. 1955. Changes in the low-energy particle cutoff and primary spectrum of cosmic radiation. *Physics Reviews* **99**, 1517-1523.

Middleton, R., L. Brown, D. Dezfouly-Arjomandy and J. Klein. 1993. On ^{10}Be standards and the half-life of ^{10}Be. *Nuclear Instruments and Methods in Physics Research* **B82**, 399-403.

Monaghan, M. C. 1987. Greenland ice ^{10}Be concentrations and average precipitation rates north of 40°N to 45°N. *Earth and Planetary Science Letters* **84**, 197-203.

Morse, D. L. and E. D. Waddington. 1992. Glacier geophysical studies for an ice-core site at Taylor Dome: Year two. *Antarctic Journal of the United States* **27**, 59-61.

Morse, D. L. 1996. University of Washington Ph.D. thesis, in preparation.

Nilsson, E. 1961. The Younger Dryas age. *Uppsala University Geological Institute* **B 40**, 375-383.

NRC. 1994. *Cosmic Ray NM-64 Neutron Monitor Data*. Ottawa, Herzberg Institute of Astrophyics, National Research Council of Canada (NRC).

O'Brien, K. and G. Burke. 1973. Calculated cosmic ray neutron monitor response to solar modulation of galactic cosmic rays. *Journal of Geophysical Research* **78**, 3013-3019.

O'Brien, K. 1979. Secular variations in the production of cosmogenic isotopes in the Earth's atmosphere. *Journal of Geophysical Research* **84**, 423-431.

O'Brien, K., A. Lerner, M. A. Shea and D. F. Smart. 1991. The production of cosmogenic isotopes in the Earth's atmosphere and their inventories. *In* C. P. Sonnet, M. S. Giampapa and M. S. Matthews (eds.), *The Sun in Time*. Tucson, University of Arizona Press.

Oeschger, H. and J. Beer. 1990. The past 5000 years history of solar modulation of cosmic radiation from ^{10}Be and ^{14}C studies. *Philosophical Transactions of the Royal Society of London* **A 330**, 471-480.

Oeschger, H., J. Beer and M. Andree. 1987. ^{10}Be and ^{14}C in the earth system. *Philosophical Transactions of the Royal Society of London* **A 323**, 45-56.

Ohno, M. and Y. Hamano. 1992. Geomagnetic poles over the past 10,000 years. *Geophysical Research Letters* **19**, 1715-1718.

Olson, I. U. 1970. *Radiocabron variations and absolute chronology*. New York, John Wiley & Sons.

Paterson, W. S. B. 1983. *The Physics of Glaciers*. New York, Permagon Press.

Pavich, M. P., L. Brown, J. Klein and R. Middleton. 1984. ^{10}Be accumulation in a soil chronosequence. *Earth and Planetary Science Letters* **68**, 198-204.

Pearson, G. W. and M. Stuiver. 1986. High-precision calibration of the radiocarbon time scale, 500-2500 BC. *Radiocarbon* **28**, 839-862.

Pearson, G. W., J. R. Pilcher, M. L. Baillie, D. M. Corbett and F. Qua. 1986. High-precision 14 C measurement of Irish oaks to show the natural 14 C variations from AD 1840-5210 BC. *Radiocarbon* **28**, 911-934.

Pisias, N. G., D. G. Martinson, T. C. Moore, N. J. Shackleton, W. Prell, H. J. and B. Boden. 1984. High resolution stratigraphic correlation of benthic oxygen isotopic records spanning the last 300,000 years. *Mar. Geol.* **56**, 119-136.

Polissar, P. 1995. *10-Be and 36-Cl in the Taylor Dome Ice Core: Clues to Antarctic Glacier and Climate Dynamics*. Hampshire College. B.A. Thesis.

Raisbeck, G. M., F. Yiou, M. Fruneau and J. M. Loiseaux. 1978. Beryllium-10 mass spectrometry with a cyclotron. *Science* **202**, 215-217.

Raisbeck, G. M. and F. Yiou. 1981. Cosmogenic $^{10}Be/^{7}Be$ as a probe of atmospheric transport processes. *Geophysical Research Letters* **8**, 1015-1018.

Raisbeck, G. M., F. Yiou, M. Fruneau, J. M. Loiseaux, M. Liuevin, J. C. Ravel and C. Lorius. 1981. Cosmogenic ^{10}Be concentrations in Antarctic ice during the past 30,000 years. *Nature* **292**, 825-826.

Raisbeck, G. M. and F. Yiou. 1985. ^{10}Be in polar ice and atmospheres. *Annals of Glaciology* **7**, 138-140.

Raisbeck, G. M., F. Yiou, D. Bourles, C. Lorius, J. Jouzel and N. I. Barkov. 1987. Evidence for two intervals of enhanced ^{10}Be deposition in Antarctic ice during the last glacial period. *Nature* **326**, 273 - 277.

Raisbeck, G. M., F. Yiou, J. Jouzel and J. R. Petit. 1990. ^{10}Be and $\delta^{2}H$ in polar ice cores as a probe of the solar variability's influence on climate. *Philosophical Transactions of the Royal Society of London* **A330**, 463-470.

Raisbeck, G. M., F. Yiou, J. Jouzel, J. R. Petit, N. I. Barkov and E. Bard. 1992. ^{10}Be deposition at Vostok, Antarctica, during the last 50,000 years and its relationship to possible cosmogenic production variations during this period. *In* E. Bard and W. S. Broecker (eds.), *The Last Deglaciation: Absolute and Radiocarbon Chronologies*. Berlin, Springer-Verlag, 127-139.

Raisbeck, G. M., F. Yiou and S. Z. Zhou. 1994. Palaeointensity puzzle. *Nature* **371**, 207-208.

Rasmussen, A. 1991. Piecewise integral splines of low degree. *Computers & Geosciences* **17**, 1255-1263.

Raymond, C. 1983. Deformation in the vicinity of ice divides. *Journal of Glaciology* **29**, 357-373.

Reeh, N. 1989. Dating by ice flow modeling: a useful tool or an exercise in applied mathematics? *In* H. Oeschger and C. C. Langway (eds.), *The Environmental Record in Glaciers and Ice Sheets*. New York, John Wiley, 141-159.

Robin, G. de Q. 1977. Ice cores and climatic changes. *Philos. Transactions of the R. Society of London, Ser. B* **280**, 143-168.

Rosenlof, K. H. 1995. Seasonal cycle of the residual mean meridional circulation in the stratosphere. *Journal of Geophysical Research* **100**, 5173-5191.

Rudstam, G. 1966. Systematics of spallation yields. *Z. Naturforsch A* **21**, 1027-1030.

Santee, M. L., W. G. Read, J. W. Waters, L. Froidevaux, G. L. Manney, D. A. Flower, R. F. Jarnot, R. S. Harword and G. E. Peckham. 1995. Interhemispheric differences in polar stratospheric HNO_3, H_2O, ClO, and O_3. *Science* **267**, 849-852.

Shackleton, N. J. and N. D. Opdyke. 1973. Oxygen isotope and paleomagnetic stratigraphy of equatorial Pacific core V28-238: oxygen isotope temperatures and ice volumes on a 10^5 and 10^6 year scale. *Quaternary Reserach* **3**, 39-55.

Shaw, G. E. 1989a. Aerosol transport from sources to ice sheets. *In* H. Oeschger and C. C. Langway (eds.), *The Environmental Record in Glaciers and Ice Sheets*. New York, John Wiley & Sons, 13-27.

Shaw, G. E. 1989b. Antarctic aerosols: a review. *Reviews of Geophysics* **26**, 89-112.

Silberberg, R. and C. H. Tsao. 1973. Partial cross sections in high-energy nuclear reactions, and astrophysical applications, I. Targets with Z<=28. *Astrophysical Journal Supplement Series* **25**, 315-330.

Simpson, J. A. and W. C. Fagot. 1953. Properties of the low-energy nucleaonic component at large atmospheric depths. *Physics Reviews* **90**, 1068-1072.

Simpson, J. A., W. Fonger and S. B. Treiman. 1953. Cosmic radiation intensity-time variations and their origin. 1. Neutron intensity variation method and meteorological factors. *Physics Reviews* **90**, 934-950.

Soberman, R. K. 1953. High altitude cosmic ray neutron intensity variations. *Physics Reviews* **102**, 1399-1409.

Soderblom, D. R. 1988. The sun among the stars: what stars indicate about solar variability. *In* F. R. Stephenson and A. W. Wolfendale (eds.), *Secular Solar and Geomagnetic Variations in the Last 10,000 Years*. Boston, Kluwer Academic Publishers, 25-48.

Solomon, S. 1990. Nitrogen chemistry in Antarctica: A brief review. *In* A. O'Neill (ed.), *Dynamics, Transport and Photochemistry in the Middle Atmosphere of the Southern Hemisphere*. London, Kluwer Academic Publishers, 191-201.

Somayajulu, B. L. K., P. Sharma, J. Beer, G. Bonani, H. J. Hofmann, E. Morenzoni, M. Nessi, M. Suter and W. Wolfli. 1984. ^{10}Be annual fallout in rains in India. *Nuclear Instruments and Methods in Physics Research* **B5**, 398-403.

Sonett, C. P., S. A. Finney and C. R. Williams. 1988. The lunar orbit in the late Precambrian and the Elatina sandstone laminae. *Nature* **335**, 806-808.

Southon, J. R., M. W. Caffee, J. C. Davis, T. L. Moore, I. D. Proctor, B. Schumacher and J. S. Vogel. 1990. The new LLNL AMS spectrometer. *Nuclear Instruments and Methods in Physics Research* **B52**, 301-305.

Sowers, T. and M. Bender. 1995. Climate records covering the last deglaciation. *Science*, **289**, 210-214.

Sowers, T., M. Bender, L. Labeyrie, D. Martinson, J. Jouzel, D. Raynaud, J. J. Pichon and Y. S. Korotkevich. 1993. A 135,000-year Vostok-SPECMAP common temporal framework. *Paleoceanography* **8**, 737-766.

Steig, E. J., P. J. Polissar and M. Stuiver. 1995. Cosmogenic isotope concentrations at Taylor Dome, Antarctica. *Antarctic Journal of the United States* , in press.

Steig, E. J., P. J. Polissar, M. Stuiver, P. M. Grootes and R. C. Finkel. 1996. Large amplitude solar modulation cycles of ^{10}Be in Antarctica: implications for atmospheric mixing processes and interpretation of the ice core record. *Geophysical Research Letters* , in press.

Stephenson, F. R. and D. H. Clark. 1978. *Applications of Early Astronomical Records*. Bristol, U. K., A. Hilger.

Stuiver, M. and G. W. Pearson. 1986. High-precision calibration of the radiocarbon time scale , AD 1950-500 BC. *Radiocarbon* **28**, 805-838.

Stuiver, M., G. H. Denton, T. J. Hughes and J. L. Fastook. 1981. History of the marine ice sheet in West Antarctica during the last glaciation, a working hypothesis. *In* G. H. Denton and T. H. Hughes (eds.), *The Last Great Ice Sheets*. New York, Wiley-Interscience, 319-436.

Stuiver, M., T. F. Braziunas, B. Becker and B. Kromer. 1991. Climatic, solar, oceanic, and geomagnetic influences on Late-glacial and Holocene atmospheric $^{14}C/^{12}C$ change. *Quaternary Research* **35**, 1-24.

Stuiver, M., T. Braziunas and P. Grootes. 1995. The GISP2 $\delta^{18}O$ climate record of the past 16,500 years and the role of the sun, ocean, and volcanoes. *Quaternary Research* **44**, 341-354.

Thompson, L. G. and E. Mosley-Thompson. 1982. Spatial distribution of microparticles within Antarctic snow-fall. *Annals of Glaciology* **3**, 300-373.

Toon, O. B., P. Hamill, R. P. Turco and J. Pinto. 1986. Condensation of HNO_3 and HCl in the winter polar stratospheres. *Geophysical Research Letters* **13**, 1284-1287.

Tric, E., J. -P. Valet, P. Tucholka, M. Paterne, L. Labeyrie, F. Guichard, L. Tauxe and M. Fontugne. 1992. Paleointensity of the geomagnetic field during the last 80,000 years. *Journal of Geophysical Research* **97**, 9337-9351.

Vömel, H., S. J. Oltmans, D. J. Hofman, T. Deshler and J. M. Rosen. 1995. The evolution of the dehydration in the Antarctic stratospheric vortex. *Journal of Geophysical Research* **100**, 13,919-13,926.

Waddington, E. D., D. L. Morse, P. M. Grootes and E. J. Steig. 1993. The connection between ice dynamics and paleoclimate from ice cores: a study of Taylor Dome, Antarctica. *In* W. R. Peltier (ed.), *Ice in the Climate System*. Berlin, Springer-Verlag, 499-516.

Waddington, E. D. and D. L. Morse. 1994. Spatial variations of local climate at Taylor Dome: implications for paleoclimate from ice cores. *Annals of Glaciology* **20**, 219-225.

Waddington, E. D. Where are we going? The ice-core paleoclimate inverse problem. In Wolff, E. W. and R. C. Bales (eds.), *Processes of chemical exchange between the atmosphere and polar snow*. Springer-Verlag, Berlin, in press.

Wahlen, M. 1994. ^{7}Be and ^{10}Be in filters from stratospheric air and in mid-latitudes. Upublished manuscript.

Wayne, R. P. 1991. *Chemistry of atmospheres*. Oxford, Claredon Press.

Weeks, R. J., C. Laj, L. Endignoux, A. Mazaud, L. Labeyrie, A. P. Robers, C. Kissel, E. Blanchard. 1995. Normalized natural remanent magnetisation intesity during the last 240,000 years in piston cores from the central North Atlantic Ocean; geomagnetic field intesnsity or environmental signal? Physics of the Earth and Planetary Interiors, **87**, 213-229.

Weertman, B. R. 1993. *Interpretation of ice sheet stratigraphy: a radar-echo sounding study of the Dyer Plateau, Antarctica.* University of Washington Ph.D. thesis.

Williams, G. E. 1981. Sunspot periods in the late Precambrian glacial climate and solar-planetary relations. *Nature* **291**, 624-628.

Yasyulenis, R., V. Yu, L. Yu and B. I. Styro. 1974. Argon spallation yields of cosmogenic radioisotopes. *In* ed. *Proceeding of the All-Union Conference on Nuclear Meteorology, Olminsk.*

Yiou, F., G. M. Raisbeck, D. Bourles, C. Lorius and N. I. Barkov. 1985. ^{10}Be in ice at Vostok Antarctica during the last climatic cycle. *Nature* **316**, 616-617.

VITA

Eric J. Steig

M.S. 1992. University of Washington, Seattle, WA
Measurement of Carbon Isotopes in Ice Cores
Minze Stuiver (advisor)

B.A. 1988. Hampshire College, Amherst, MA
Reconstructing the Granite Question
John B. Reid, Jr. (advisor)